

**UNIVERSITY OF CAMERINO**  
**School of Science and Technology Geology Division**  
Master of Science (M.Sc.)  
Degree in  
Geoenvironmental Resources and Risks  
(Classe LM74)



**Hydrogeological Variations Induced by the 2016  
Seismic Sequence in the South-Eastern Sibillini  
Mountains**

**Experimental Thesis in Groundwater Resources and  
Hydrogeological Hazard**

Student: Francesco Lampa

Supervisor: Prof. Pietro Paolo Pierantoni

Co-supervisor: Prof. Marco Materazzi

Academic year: 2018-2019

## SUMMARY

<b>1. INTRODUCTION</b>	<b>1</b>
<b>2. GEOGRAPHIC FRAMING</b>	<b>1</b>
<b>3. REGIONAL GEOLOGICAL AND STRUCTURAL FEATURES</b>	<b>2</b>
3.1. Stratigraphy	4
3.2. The geology of the studied area	10
<b>4. HYDROGEOLOGICAL SETTING</b>	<b>13</b>
4.1. Detailed hydrogeological framework	14
4.2. Geostructural data	16
<b>5. THE 2016-2017 SEISMIC SEQUENCE</b>	<b>16</b>
5.1. Hystorical earthquakes	22
<b>6. THE BASAL AQUIFER ANALYSIS</b>	<b>23</b>
6.1. Work planning	23
6.2. Methodology	23
6.2.1. Flow rate measurements	24
6.2.2. The hydrographs rebuilding	27
6.3. The pre-earthquake state	29
6.3.1. Stream hydrographs and yielded volumes	30
6.4. The post-earthquake state	35
6.4.1. Stream hydrographs and yielded volumes	35
6.5. The pre/post-earthquake comparison	38
6.6. The river first-emergence evolution	40
6.7. Considerations	42
<b>7. THE SPRINGS</b>	<b>47</b>
7.1. Work planning	50
7.1.1. The interpretation criterion and a general Total Dissolved Solids analysis	52
7.2. Fonte delle Ciaule	54
7.2.1. Detailed features and geological setting	54
7.2.2. Physical and chemical data	57
7.2.3. Data analysis	59
7.3. Fonte SN delle Ciaule	66
7.3.1. Detailed features and geological setting	66
7.3.2. Physical and chemical data	70
7.3.3. Data analysis	72
7.4. Fonte Casale Fiori	77
7.4.1. Detailed features and geological setting	77
7.4.2. Physical and chemical data	82
7.4.3. Data analysis	86
7.5. Fonte delle Cacere	93
7.5.1. Detailed features and geological setting	93

7.5.2. Physical and chemical data	97
7.5.3. Data analysis	101
7.6. Fonte dei Mietitori	106
7.6.1. Detailed features and geological setting	106
7.6.2. Physical and chemical data	110
7.6.3. Data analysis	114
7.7. Springs general observations	120
<b>8. CONCLUSIONS</b>	<b>122</b>
<b>9. BIBLIOGRAPHY</b>	<b>123</b>

## 1. INTRODUCTION

The 2016-2017 seismic sequence has affected the Sibillini Mountains (S.M.) area belonging to four regions (Marche, Umbria, Abruzzo and Lazio) and, in addition to the man-made structure damages, it led to remarkable morphologic modifications such as many terrain fractures, landslides (the most important was the Valnerina rockfall) and the Monte Vettore fault footwall exhumation along its scarp.

However, other effects have been observed. In particular those related the underground hydraulic transmission. Shortly after the October 2016 shocks, it was noticed that the Nera river flow was strongly increased in the spring sector. Furthermore, other rivers not far from Norcia, that before the earthquake were dry for tens of years, are reactivated after the shocks.

The University of Camerino has started a research project including all the high-altitude springs and those feeding directly the rivers originating in the M.S. National Park. Our study, being part of it, tries to understand the possible effects of the 2016-2017 seismic sequence on the south-eastern S.M.

The Regional Section of C.A.I. (Club Alpino Italiano), in order to provide a basic geological/geochemical knowledge about the Monti Sibillini high-altitude springs, during a three-years period (2009-2011) had performed physical and chemical analysis on water samples. The results, reported into Aringoli et al. (2017), can be considered the starting point of the whole study.

The thesis was performed by means of:

- the comparison of physical and chemical data collected during 2009-2011 and 2018-2019 survey campaigns on high-altitude springs;
- Aso river flow measurements made before and after the seismic events.

We have focused onto the high-altitude springs in the south-eastern slopes of Monte Vettore and on the initial spring-segment of Aso river, near the village of Foce di Montemonaco.

## 2. GEOGRAPHIC FRAMING

The S.M. belong to the Apennines chain. They are located in central Italy, on the border between Marche, Umbria, Abruzzo and Lazio, however the wider part of the M.S. National Park lies in the first two regions.

The area under study is sited in the SE sector of the S.M. (Fig. 2.1.). In detail:

- Aso river originates near Foce di Montemonaco (Montemonaco municipality) and, for its early kilometers, flows northwards. Shortly after it turns to ENE up to the outlet in the Adriatic Sea, close to Pedaso.

The initial part of the Aso river valley is confined by high mountain ridges: Monte Sibilla – Monte Porche ridge to the north, Monte Porche – Monte Vettoretto ridge to the west, Monte Vettore to the south and Monte Banditello – Monte Vettore to the east.

How to arrive? There are two ways: the first, from Amandola, following the signs for Montemonaco and then for Tofe. The second, from Comunanza, travelling the road that runs along Lago di Gerosa until Tofe, where you can see the signs for Foce.

- High altitude springs falls into the Tronto river hydrographic basin and all are located on the hydrographic left. The river flows easternward into the Adriatic Sea, near San Benedetto del Tronto. Springs are located on the SE slope of Monte Vettore (2476 m a.s.l.), overlooking the villages of Pescara

del Tronto and Pretare, under the municipality of Arquata del Tronto, to which belongs the whole springs area.

You can arrive here from Ascoli Piceno or Rome, by means of the SS4 (Salaria) until Trisungo, where you have to take the signs for Forca di Presta. Another way to come here is from Norcia following the signs for Castelluccio di Norcia and then for Forca di Presta.

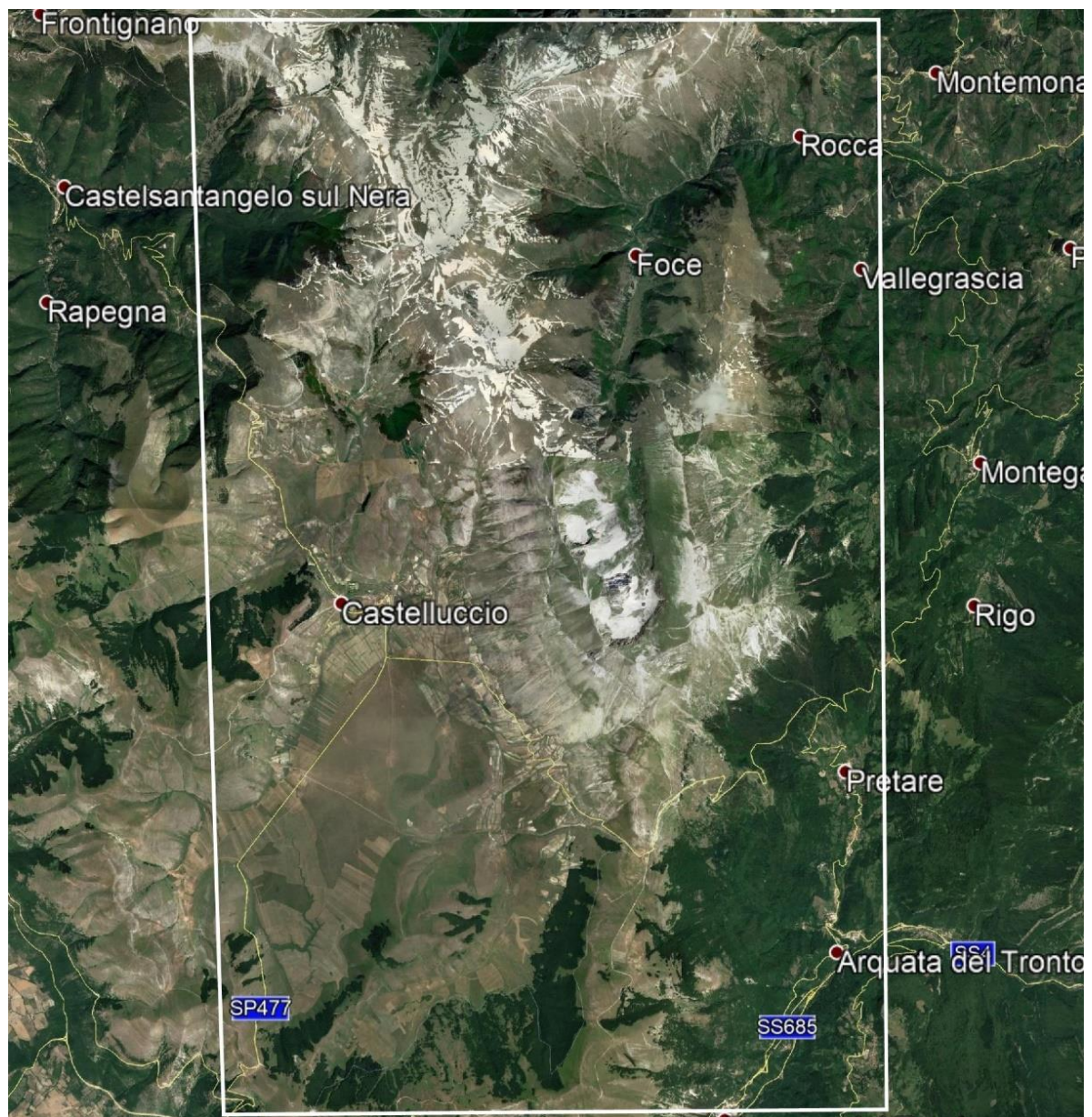


Fig. 2.1. The study area. ©Google Earth view modified with ©ArcMap 10.2

### 3. REGIONAL GEOLOGICAL AND STRUCTURAL FEATURES

The Umbria-Marche and Lazio-Abruzzo Apennines chain is a fold and thrust belt developed from the neogenic deformation of the southern boundary of the Neotetide during the Mesozoic – low Tertiary. The area was characterized by two paleogeographic domains: a carbonatic platform in the south-western sector (*Piattaforma carbonatica laziale-abruzzese*) surrounded by a wide basinal area to the north, west and east (*Bacino umbro-marchigiano-sabino*), passing towards south-east to *Bacino molisano* (Fig. 3.1.). This environment differentiation is the consequence of the fragmentation and sinking (triggered by an extensional tectonic phase during the early middle Lias) of parts of the carbonatic-evaporitic platform that, during the upper Trias – lower Lias, covered most of the Apennines areas.

Therefore, there were two different sedimentation environments, separated by steep Jurassic normal faults:

- the carbonatic platform, characterized by shallow sea sedimentation;
- the basinal areas, characterized by pelagic and hemipelagic sedimentation.

This situation persisted until middle-upper Miocene, when it turned to a siliciclastic-turbiditic deposition.

Jurassic normal faults controlled the paleoenvironments, but also the lithologies and thickness variations of the coeval sedimentary successions (Pierantoni et al., 2013).

The compressive regime, started in the Oligocene, with a SW-NE vergence (from the current Tuscany towards the eastern side of the Apennines), generated folds and thrusts. It was triggered by the subduction of African plate (Adria promontory) below Eurasian one (Pierantoni et al., 2013). The thrust displays a NNW-SSE direction in the southern area, while, in the umbro-marche-sabine area, it has an arcuate trend, with eastern convexity (in particular NW-SE, N-S and NNE-SSW from N to S). The compressive structures are NE verging, therefore towards the foreland. The Sibillini thrust determined the overriding of the carbonate units over the more recent eastern units of the foothills. This is proved because all the units from *Calcare massiccio* to *Scaglia cinerea* (the whole *Umbria-Marche Sedimentary Succession*) crop out in the inner part of the Apennines (Umbria – Marche ridge and Marche ridge), while the more recent ones (*Formazione della Laga* and *Quaternary deposits*) crop out in the foothill areas.

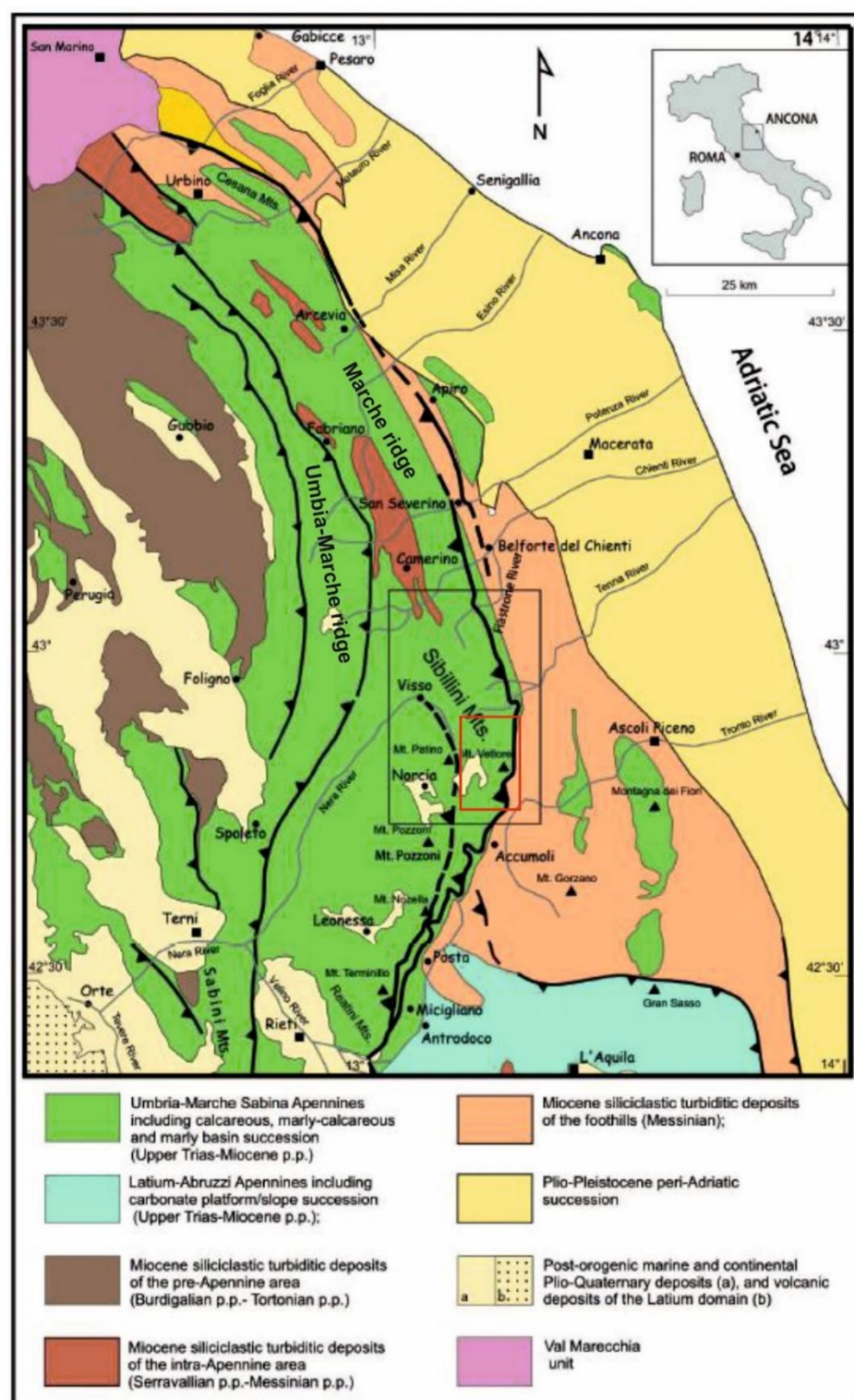


Fig. 3.1. Geological sketch map of the Umbria-Marche Apennines. The study area is indicated with the red box. Modified with  
©CorelDRAW 2018 after Pierantoni et al. (2013)

During the Pliocene – Quaternary, a tectonic inversion occurred: a post-orogenic extensive phase cuts the axial sectors, mainly by normal (but also transtensive and strike-slip) faults with NNW-SSE direction. Their progressive reactivation generates the intramontane basins (such as Castelluccio, Norcia, Cascia, Colfiorito basins). These faults (many of which still active) led to series of earthquakes of moderate magnitude, registered since historical times, consistent with the measured NE-trending extension of the Apennines at a rate of 3 mm/yr (Serpelloni et al., 2005). The extension has also reactivated some the Jurassic normal faults. Therefore, the total estimated slip (of several hundreds of meters) is the result of two separate tectonic phases. The resulting morphostructural setting is a stepped arrangement of faulted blocks.

### 3.1. Stratigraphy

The deepest wells performed in these areas (Pierantoni et al., 2013) reached the crystalline basement. It is covered by the siliciclastic continental deposits of *Verrucano group* (Permian-Trias), topped by *Anidriti di Burano* marking the base of the carbonate-dominated continental margin succession.

*Anidriti di Burano* (age: upper Trias): is composed dolomitic limestones alternating with dolomites and anhydrites. It does not crop out in the study area.

In the early Lias an extensional tectonic phase occurred, subdividing by normal faults the carbonatic platform into structural highs (footwalls) and basinal areas (hangingwalls), with different sedimentation regimes.

Above the structural highs there was a pelagic, calcareous and discontinuous sequence with a maximum thickness of 40 m, called ***condensed sequence***. Into the depressed areas a ***complete sequence*** of calcareous-siliceous material was deposited, with a maximum thickness of 400 m.

In the transition zones, between high and low structural areas, the ***composite sequence*** was deposited. It consists of lithotypes of the *condensed sequence*, followed upwards by units of the *complete sequence* (Centamore et al., 1971).

It follows a description of the units belonging to the so-called **Umbria-Marche Sedimentary Succession** which includes all the formations from *Calcare massiccio* to *Scaglia cinerea* (Fig. 3.1.1.).

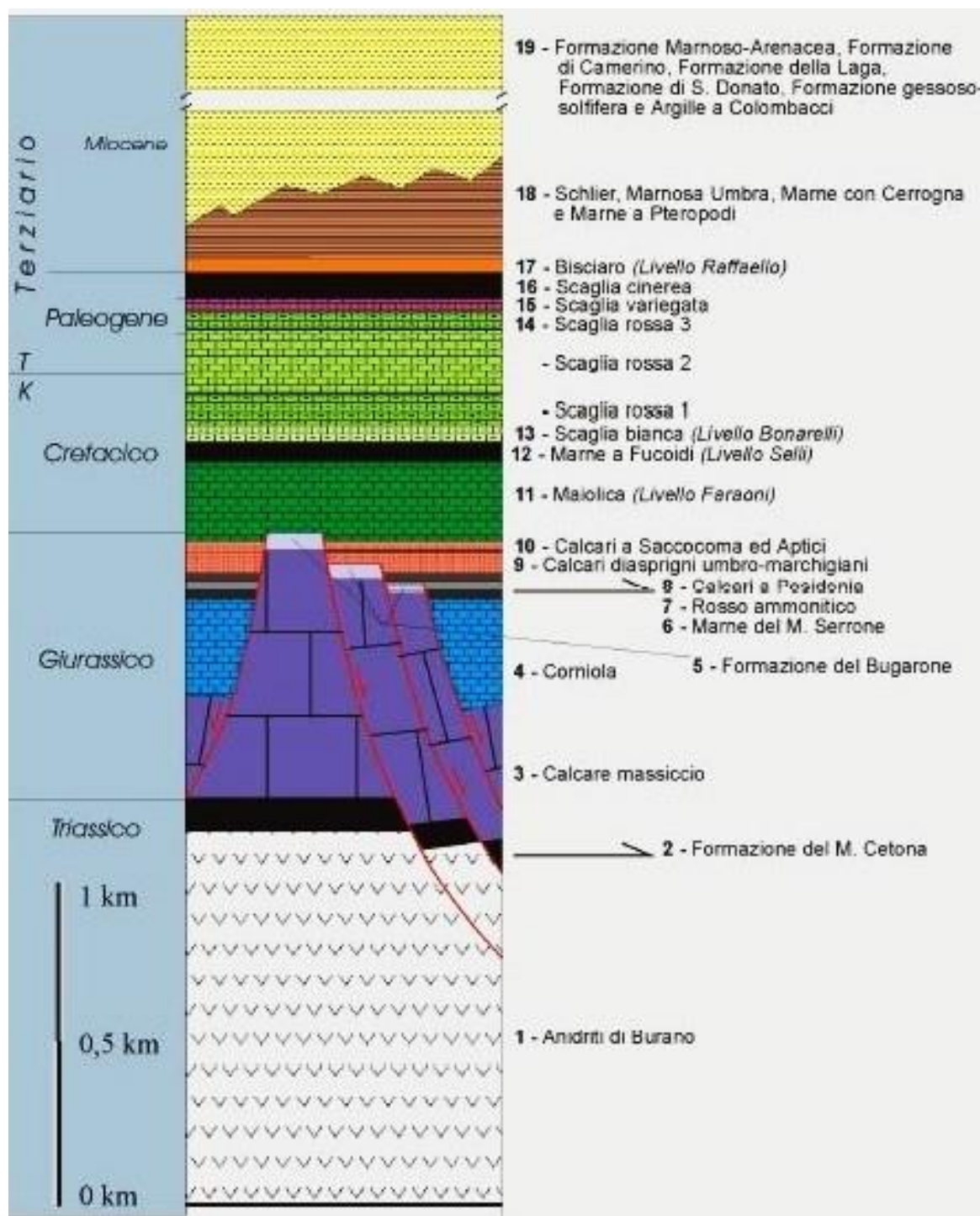


Fig 3.1.1. Stratigraphic column of Umbria-Marche Sedimentary Succession

## JURASSIC

*Calcare massiccio* (age: Hettangian – Sinemurian)

It corresponds to the *Calcare massiccio del Monte Nerone* and is composed of three members:

- *Calcare massiccio a ciclotemi*, with a maximum thickness of 700 m, consisting of white, grey and pale-brown limestones, locally with intercalations of dolomitic limestones. This unit, massive or coarsely bedded, is organized in several m-thick cyclothsems, indicating a peritidal depositional environment, ranging from subtidal to supratidal conditions.
- *Calcare massiccio B* is made of white or brown limestones of bioclastic and ooid grainstones organized in medium beds. This member was formed over the previous one, at the top of structural highs, is representative of structural drowning of the footwall blocks.
- *Calcare massiccio c* is at the base of the complete succession, but it does not crop out in this area. It is made of subtidal sediments and represents the drowning of the hangingwall blocks.

### ***Condensed sequence***

*Formazione del Bugarone* (age: Lower Pliensbachian – Lower Tithonian)

It consists of grey, brown or pink nodular limestones and marly limestones, in medium and thick beds, which are often associated, in the middle part, with green marls. The bedding planes are wavy or stylolitic. The basal part is rich in macrofossils, such as ammonites. Close to the upper contact with *Maiolica*, it can display widespread dolomitization and silicified levels.

### ***Complete sequence***

The units of the *Complete sequence* have an onlap – type contact with *Calcare massiccio* (Fig. 3.1.1.).

*Corniola* (age: Lower Sinemurian p.p. – Lower Toarcian p.p.)

It consists of grey or dark-brown mictitic limestones arranged in medium-thick beds, with nodules of white and grey chert, and thin shaly-marly levels more abundant in the upper part. The bottom can be characterized by dolomitization processes. Calcareous turbidites from structural highs, can be present, determining thickness variations: in fact, *Corniola* can reach 500-600 m, such as in the studied area. The top of the unit can be replaced by the *Marne del Monte Serrone*.

*Rosso ammonitico* (age: Toarcian p.p.)

It consists of dark red, pink, sometimes grey-green nodular limestones and marly limestones with red marls and shaly marls, everything organized in regular medium-to-thin beds. Ammonites are present. The thickness is about 25-40 m and it can be partly or totally replaced by the *Marne del Monte Serrone*.

*Marne del Monte Serrone* (age: Pliensbachian p.p. – Toarcian p.p.)

It is composed of greenish marly limestone, organized in beds of various thickness, alternated with medium to thick beds of marls and clastic limestones. The thickness varies from few meters to about 150 m in the studied area, due to the sea floor morphology and the supply of calcareous clastic material.

*Calcare a Posidonia* (age: Upper Toarcian p.p. – Lower Bojocian)

It consists of whitish or brown limestones and marly limestones, sometimes nodular, stratified in medium beds, with *Posidonia* filaments and cherts more concentrated in the upper part. Also, clastic and bioclastic limestones can be present, organized in medium-thick beds. Its thickness ranges from a few tens of meters to 100-200 m, depending on the supply of clastic material.

*Calcare diasprigni* (age: Upper Bojocian – Lower Tithonian)

It is divided in two members:

- the lower one, called *Membro selcifero*, consists of grey-greenish or reddish, finely bedded, siliceous calcilutites, alternating with green, red or greyish cherts and some marly levels. Silica content is higher in the upper part. The thickness varies from few tens of meters to over 100 m.
- the upper one, called *Calcare a Saccocoma e Aptici*, is made of grey, green, and sometimes red chert, locally by biodetritic limestones, in medium to thin beds, frequently rich in apytychi. Thickness: 30-40 m.

*Marne del Monte Serrone*, *Calcari a Posidonia* and *Calcari diasprigni* together form the so-called calcareous-silicic-marly complex.

### **Composite sequence**

It is typically composed of basinal units, generally *Calcari diasprigni*, covered by the units of the *condensed sequence* (*Formazione del Bugarone*). It was deposited above the Jurassic fault scarps, connecting the structural highs to the basins, or onto erosional depression steps lying along these escarpments. This is why the beds thickness has a minimum at the fault contact and increases towards the external part. The total thickness of the succession depends on the subduction rate of the hangingwall blocks, on the pelagic sedimentation rate and on the supply of calcareous turbidites coming from the highs.

## **CRETACEOUS – PALEOGENE**

*Maiolica* (age: Upper Tithonian – Lower Aptian p.p.)

It is characterized by white and ivory micrites, with concoidal fracture, arranged in thin and medium beds with chert (black and grey in the upper and lower part of the formation respectively) organized in nodules or lenses. There are interbedded calcarenitic and calciruditic layers. Near the boundary with *Marne a Fucoidi*, limestones become darker and they alternate with blackish pelitic levels. In the lower part, there are lithological and thickness differences between *Maiolica* deposited over *condensed* and *complete sequences*:

- nodular and dolomitic yellowish-brown colored lithofacies above the former and greenish-white limestones in medium and thick beds on the latter;
- above the *condensed sequences* the thickness is 150-200 m and over the *complete* ones it can reach values of 350-400 m.

*Marne a Fucoidi* (age: Lower Aptian p.p. – Upper Albian p.p.)

They are made of grey, green and red marls, clayey marls and marly limestones. The marl content increases downwards. In the upper part green chert beds and nodules are present. Bituminous levels, like *Livello Selli* (a regional marker 2 m thick), are present. Due to their ductility, *Marne a Fucoidi* acted as a detachment level during the compressive tectonic regime. The thickness ranges from 40-50 m to 80-100 m.

*Scaglia bianca* (age: Upper Albian p.p. – Lower Turonian p.p.)

It is composed by whitish limestones and marly limestones organized in middle beds and ribbons. Near the contact with *Scaglia rossa* there is a black anoxic bituminous level: *Livello Bonarelli*, 1.5 m thick. The total thickness of the unit is 60-70 m.

*Scaglia rossa* (age: Lower Turonian p.p. – Lutetian p.p.)

It is composed by three members. From the bottom to the top:

- *Scaglia rossa 1*: is made up by pinkish marly limestones, in medium beds, and chert nodules and ribbons.  
Thickness: 80-150 m
- *Scaglia rossa 2*: is made up by red and brown limestones, sometimes with whitish bands and marly levels. Thickness: 100-250 m
- *Scaglia rossa 3*: consists of reddish limestones and marly limestones with red chert nodules and ribbons.  
Thickness: 5-40 m

*Scaglia rossa* has thick grey or white calcareous-clastic levels interbedded with the pelagic deposits, whose spatial distribution is uneven.

*Scaglia variegata* (age: Lutetian p.p. – Bartonian p.p.)

It is made of red, grey and green limestone and marly limestone organized in thin and medium beds. These alternate with grey and red marls and calcareous marls. Close to the limits, there are red and dark cherts respectively. The total thickness varies from 10 to 50 m.

*Scaglia cinerea* (age: Bartonian p.p. – Aquitanian p.p.)

It is composed of calcareous marls, marls and clayey marls, in medium and thin beds. Limestone levels with chert can be present in the lower part. The color is green-grey to cinder-grey.

Thickness: 150-200 m.

The *Scaglia cinerea/Bisciaro* stratigraphic boundary represents the termination of the *Umbria-Marche Sedimentary Succession* carbonatic-pelagic deposition. Hereafter the sedimentation was characterized by detrital contributions of different nature.

## MIOCENE

*Bisciaro* (age: Aquitanian p.p. – Burdigalian p.p.)

This unit is made of dark-grey marly and siliceous limestones, limestones in medium to thick beds, with black cherts, alternated with grey calcareous marls and clayey marls and sometimes detrital limestones. In the lower part thin altered volcanoclastites occurs. The thickness varies from 50-60 m to 100-150 m depending on the paleomorphology.

Henceforth the sedimentation occurs in two distinct basins (Fig. 3.1.2.): the Camerino Basin, included between the Umbria-Marche ridge, and the Marche ridge and the Laga Basin, in the eastern side of the latter ridge. The study area belongs to the latter.

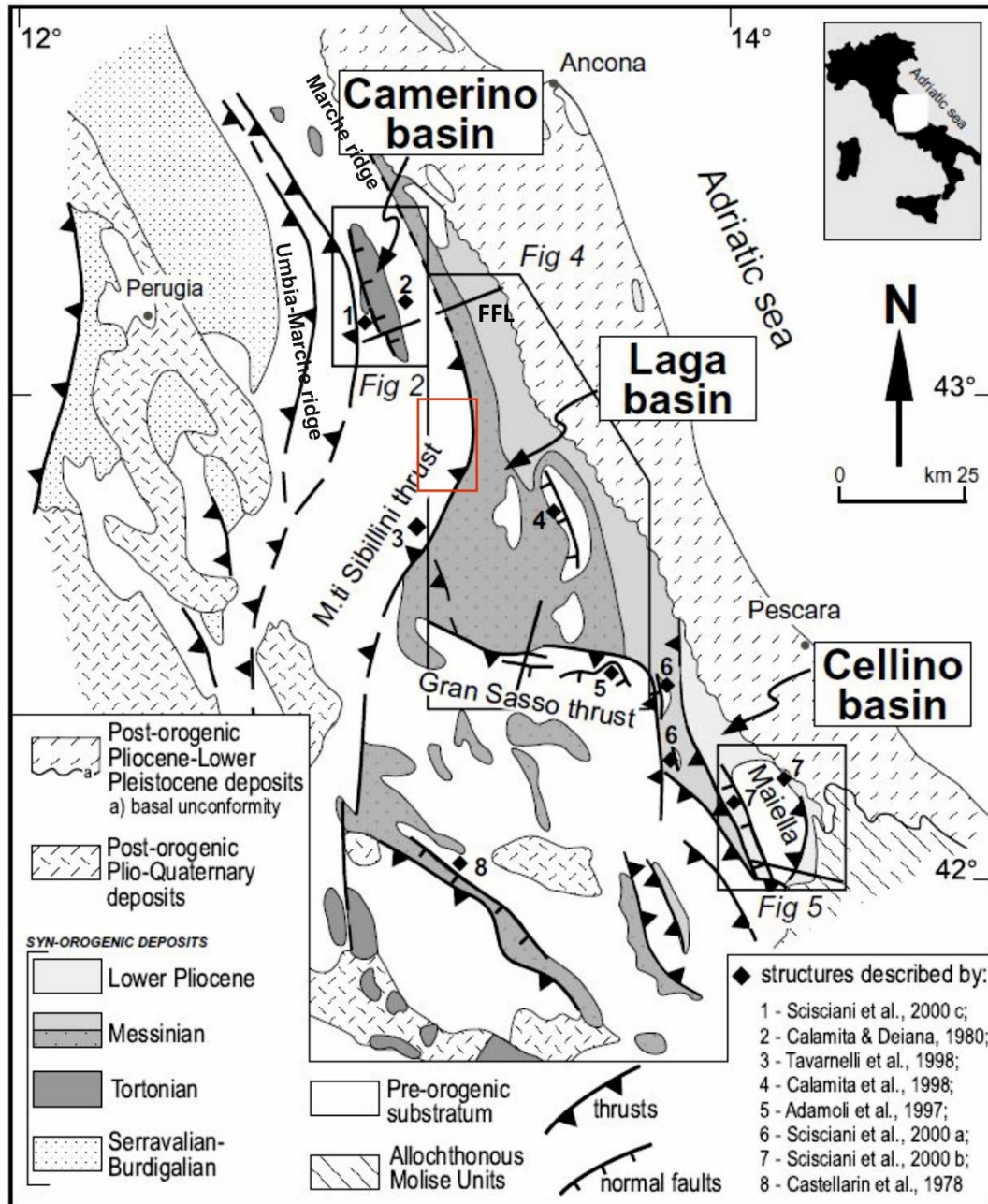


Fig. 3.1.2. Tectonic sketch map of the Central Apennines of Italy, with location of the foredeep basins. The study area is indicated with the red box. Modified with ©CorelDRAW 2018 after Scisciani et al. (2002)

The Laga Basin is part of the large peri-adriatic Miocene foredeep. It is divided by a transverse synsedimentary south-dipping normal fault: the “Fiastrone-Fiastrella line” (FFL) (Fig. 3.1.2.).

The different areas show distinctive sequences:

- in the northern sector: *Schlier*, pre-evaporitic member of *Formazione della Laga*, *Formazione Gessoso-solfifera*, post-evaporitic member of *Formazione della Laga*.

*Schlier* (age: Burdigalian p.p. – Tortonian p.p.)

It consists of alternating grey marls, clayey-silty marls, whitish calcareous marls and calcarenitic levels. Thickness: 80-250 m on the base of the sea-floor paleomorphology and gravitational-flow induced erosion.

- In the southern sector: *Marne con cerroga*, *Marne a Pteropodi*, pre-evaporitic member of *Formazione della Laga*, evaporitic member and post-evaporitic member. Monte Vettore area belongs to this one.

#### *Marne con cerroga* (age: Upper Burdigalian – Tortonian p.p.)

It consists of light grey marls, calcareous marls and clayey marls with medium to thick bedded calcareous turbidites from the Latium-Abruzzi carbonate platform. Thickness: 80-300 m.

#### *Marne a Pteropodi* (age: Tortonian p.p. – Early Messinian)

It is made of grey-green marls and clayey marls, bituminous and laminated in the upper part. Thickness: 30-40 m.

*Formazione della Laga* is divided in three members (age: Messinian)

- *Pre-evaporitic member*: turbidite deposits that fill the NNW-SSE oriented longitudinal depressions. It is characterized by vertically alternating lithofacies with also lateral transitions: arenaceous (prevailing), arenaceous-pelitic and pelitic-arenaceous. Thickness: about 800 m.
- *Evaporitic member*: arenaceous lithofacies with an anoxic bituminous marl and a gessarenitic bed. Thickness: about 500 m.
- *Post-evaporitic member*: pelitic-arenaceous lithofacies with abundant intercalations of arenaceous-pelitic and arenaceous levels. A volcanoclastic key-bed is present in the upper part. Thickness: 900 m.

The thickness of *Formazione della Laga* is about 2200 m sedimented in more or less 2 Myrs, characterized by a huge deposition rate compared to the one of the carbonatic/pelagic sequence.

The most recent units are the Quaternary deposits (Pierantoni et al., 2013) including:

- Eluvio-colluvial deposits: silty-clay sediments with sand fraction;
- Slope deposits: scree heterometric or well sorted sediments, unconsolidated or poorly cemented;
- Landslide deposits: chaotic heterometric sediments emplaced due to gravity processes;
- Alluvial deposits: fluvial deposits made of calcareous gravels along river beds, alluvial fans consisting of conglomerates, sands and silty-clay layers with or without lamination;
- Fluvial-lacustrine deposits: fine-grained sediments and peat levels mixed with coarser elements;
- Moraine deposits: heterometric chaotic sediments with a silty matrix.

### 3.2. The geology of the studied area

The Monte Vettore (Fig. 3.2.1.) represents the most elevated structural area of the Marche-Abruzzo-Lazio thrusts system and also the eastern part of the latter that includes the *Belforte-Urbino thrust* and the *OAMS (Olevano-Antrodoco-Monti Sibillini) thrust*, from N to S respectively. The two segments have a right en-echelon relationship (Pierantoni et al., 2005 & 2013).

In this area, the *OAMS thrust* hangingwall is represented by an anticlinal N-S oriented with a box-fold geometry. The anticlinal axis dips northwards of about 10°, giving to the fold a periclinal termination. The fold core consists of *Calcare massiccio* (which constrains the box-fold geometry), while the most recent formation is *Scaglia rosata* (including *Scaglia bianca* and *Scaglia rossa*), outcropping on the sides of the anticlinal. The eastern side often results vertical or reverse, whereas the western one is gently inclined (Pierantoni et al., 2005 & 2013).

In the south-eastern S.M., the *Monti Sibillini thrust* is N-S trending from the Aso river valley to the Monte Vettore slopes and then it arranges ENE-WSW up close to Monte Vettoretto. Further south it turns N-S again. The thrust has overlapped carbonatic units onto *Scaglia cinerea*, *Bisciaro*, *Marne con Cerroga* and *Formazione della Laga*. All these latter formations, outcropping in the foothills area, display a different structural framework, consisting

of broad/continuous folds but also less developed ones. The *Monti Sibillini thrust* has ENE to NE direction of tectonic transport.

The overlapping area geometry is influenced by the presence of *splay thrusts* (secondary thrust planes enucleating from the major one). They border an intermediate tectonic element, called *tectonic-chip* representing a detached section of thrust hangingwall. Then the chip was dragged by the thrust propagation.

The total measured slip ranges between 8 and 10 kms and has been partially transferred to the decollement layers located in the pre-turbiditic hemipelagites (*Marne con Cerrognia*).

As mentioned in the regional geological description, the structural setting of the study area is characterized by Jurassic normal faults (the oldest recognizable tectonic elements) that conditioned the sedimentation and the propagation paths of the folding structures, hence the whole orogenetic process. On the base of bedding relationships, lithological features of the successions overlying *Calcare massiccio* and structural framework of the whole S.M. area, two main trends of Jurassic normal faults have been recognized: the main oriented NNW-SSE and another one oriented WSW-ENE.

A Jurassic normal fault, oriented WSW-ENE, separates the Palazzo Borghese structural high (characterized by *condensed sequence*) from the Monte Porche – Monte Sibilla basinal area (*complete sequence*). A wide N-S oriented paleobasin (delimited by structural highs to the N) extends in the western sector of the map. Other normal faults have been reactivated as inverse faults during the Neogene.

Quaternary normal faults displaced the hangingwall units for about 1.5 km. The trend is NNW-SSE; however, the single structures can have variable directions (from NW-SE to N-S). They dip SW-WSW. In the study area, this tectonic phase is mainly represented by the *Monte Vettore – Monte Bove Fault System*, consisting of faults organized into a right en-echelon geometry. On the western slopes of Monte Redentore, two of these faults, with a sharp fault scarp, stand out to the eye crosscutting the *Corniola* limestones and joining near Scoglio del Lago. The main fault, delimiting the Castelluccio basin, runs through the western slopes of Monte Vettoretto, Monte Argentella, Monte Porche and Monte Bove from S to N respectively. This fault has a total slip exceeding 1000 m. Antithetical faults are present W of Monte Prata and E of Monte Lieto. Also, the E sector of the area is characterized by extensive structures but with much smaller slips. The E slopes of Monte Cima della Prata and Monte Banditello are characterized by normal faults, oriented NNW-SSE and NW-SE (Pierantoni et al., 2005 & 2013).

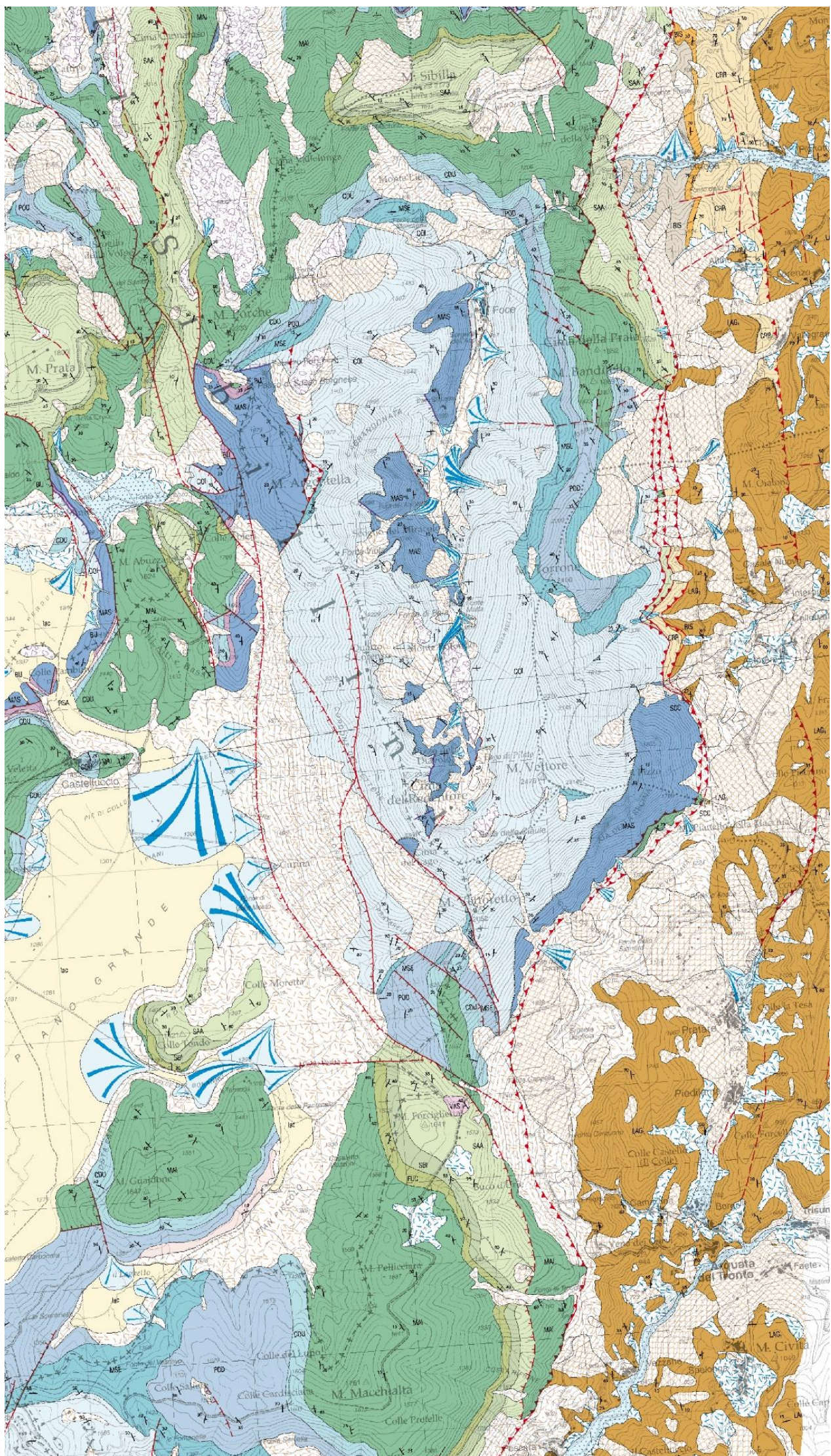


Fig. 3.2.1. Geological map of the studied area. Pierantoni et al. (2013)

#### 4. HYDROGEOLOGICAL SETTING

The S.M. belong to the *carbonatic domain of the umbria-marche ridge* characterized by three superimposed hydrogeological complexes (Fig. 4.1.), separated by aquiclude/aquitard formations. The potential hydraulic interconnections among these complexes depend on the aquiclude/aquitard effectiveness of the impermeable formations, with extremely variable geo-structural characteristics.

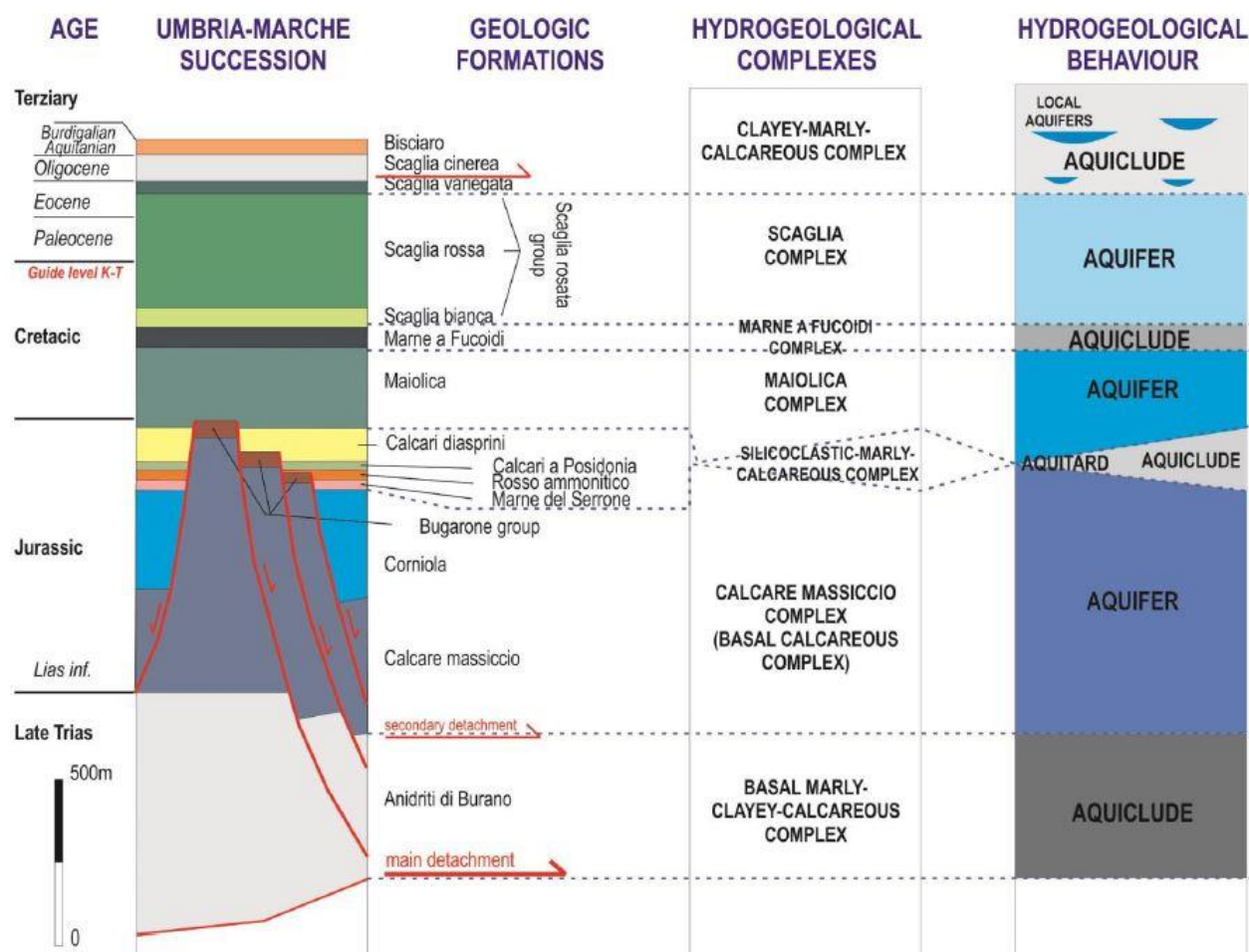


Fig. 4.1. Hydrogeological complexes of the Umbria-Marche Sedimentary Succession

**Massiccio complex (holding the Basal aquifer)** is located in the basal calcareous group composed of *Calcare massiccio*, *Corniola* and *Formazione del Bugarone*. *Calcare massiccio* is characterized by a high permeability thanks to the primary (diffused karst phenomena) and secondary porosity (lithoclasia), while in *Corniola* and in *Formazione del Bugarone* the porous space is essentially linked to the secondary porosity (Nanni T., 1991). The total thickness of the complex can reach 1000 m.

In terms of hydraulic reservoir, it is the most important because **it holds the regional base flow**. The Basal aquifer is fed by the meteoric water but also by the water of the overlying aquifers flowing thanks to fracture zones, fault hydraulic contacts or karst phenomena.

The primary porosity plays a key role, favoring the development of a system of capillary channels which permeate the whole rock volume, promoting the water storage and the slow percolation. On the other hand, a well-developed channel network led to a rapid outflow.

The Basal aquifer is supported at the bottom by the *Anidriti di Burano* and at the top by the calcareous-silicic-marly complex in case of *complete* or *composite sequence*. This aquifer can be connected with the Maiolica complex in case of:

- *condensed sequence*: *Formazione del Bugarone* has a good permeability;
- a calcareous-silicic-marly complex not enough thick or overly fractured to behave as hydraulic barrier.

Generally, Basal aquifer springs display a weak seasonal signal on temperature and discharges. In fact, the renewal times sometimes exceed 10 years, therefore the regulatory reserves must be abundant. A high stability

characterizes the chemical parameters. However, the Basal aquifer sustains several high-altitude springs with lower flow rates (< 5 l/s), with a stronger seasonal signal, especially during dry season.

**Maiolica complex (holding the Maiolica aquifer)** is included between the calcareous-silicic-marly complex and *Marne a Fucoidi* sill. The canalization depends primarily on the lithoclasis and interbeds (Nanni T., 1991). Therefore, the water transmission is strictly linked to the tectonic setting. The presence of low-fractured volumes can lead to suspended aquifers. Also, micro-karst features are present, but they are less developed respect within *Calcare massiccio*. Often springs emerge at the contact with aquiclude formations near the boundaries.

**Scaglia calcarea complex (holding the Scaglia calcarea aquifer)** is composed by *Scaglia bianca*, *Scaglia rossa* and *Scaglia variegata* (only the limestone-rich portion), for a total thickness that ranges between 200 and 400 m. The aquifer at the base is bounded by *Marne a Fucoidi* and at the top by *Scaglia cinerea*. The marl concentration is higher with respect to the previous complexes and this might suggest that it is not suitable for the storage. However, the low primary porosity is compensated by the high fracturing degree, ensuring a rapid groundwater outflow. The broad cropping area with many springs, makes the Scaglia calcarea aquifer essential for the water supply of many villages.

Maiolica and Scaglia calcarea aquifers, suspended on the Basal one, are commonly characterized by strong seasonal flow rate variations and high temperature annual excursions. In fact, residence times, at least for the less broad aquifers, are not much longer than 1 hydrologic year. The seasonal signal is also highlighted by the chemical composition variability (Nanni T., 1991).

#### 4.1. Detailed hydrogeological framework

Recent studies performed on the hydrogeology of the S.M. have concluded that the uppermost carbonatic segment of the Aso river and the Foce di Montemonaco spring are fed by the Eastern S.M. Aquifers (Nanni & Petitta, 2010). **It is crucial to point up that the following considerations were reliable before the 2016-2017 seismic sequence, that could have strongly altered the local hydrogeological setting.**

The *Hydrogeological Model of the Eastern Sibillini Mountains* covers an area 120 km<sup>2</sup> wide from Bolognola to the Monte Vettore (Nanni & Petitta, 2010). It provides a single deep hydraulic circulation in the Basal aquifer feeding the springs in the uppermost parts of the Fiastrone, Tennacola, Ambro, Tenna, Aso and Fluvione rivers, for a total average flow of 3240 l/s (data representative of April 2007). The recharge area corresponds primarily of the broad Maiolica complex outcrops, but also to those of Scaglia calcarea and Calcare massiccio complexes. **About the half of the whole volume of the considered system emerges at the Aso river springs.** In the uppermost part of the valley, near the village of Foce, the hydrographic pattern has deeply incised the morphostructures, reaching the piezometric level of the aquifer. **As a consequence, the aquifer directly feeds the river by means of a series of linear springs.** In particular, the Foce spring belongs to a complex system of natural and man-made emergences sited in the uppermost part of the Aso riverbed and partially in the draining tunnel of the collection system managed by CIIP SpA (Cicli Integrati Impianti Primari). The model proposed by Boni & Petitta (2007) does not suggest the presence of a possible hydrogeological underground watershed, bordering the Aso river (with respect to the Eastern S.M. ridge) feeding area, that could differentiate the main directions of the local underground flow. In this sector of the S.M. the aquifers are locally separated; Nanni & Petitta (2010) demonstrated this through chemical water analysis.

In the map below (Fig. 4.4.1.) are reported the hydrogeological basin (red) and the hydrological basin (blue) of the upstream carbonatic sector of the Aso river, on the base of the study Nanni & Petitta (2010). The red-dashed line borders a second smaller hypothesis for the hydrogeological basin.

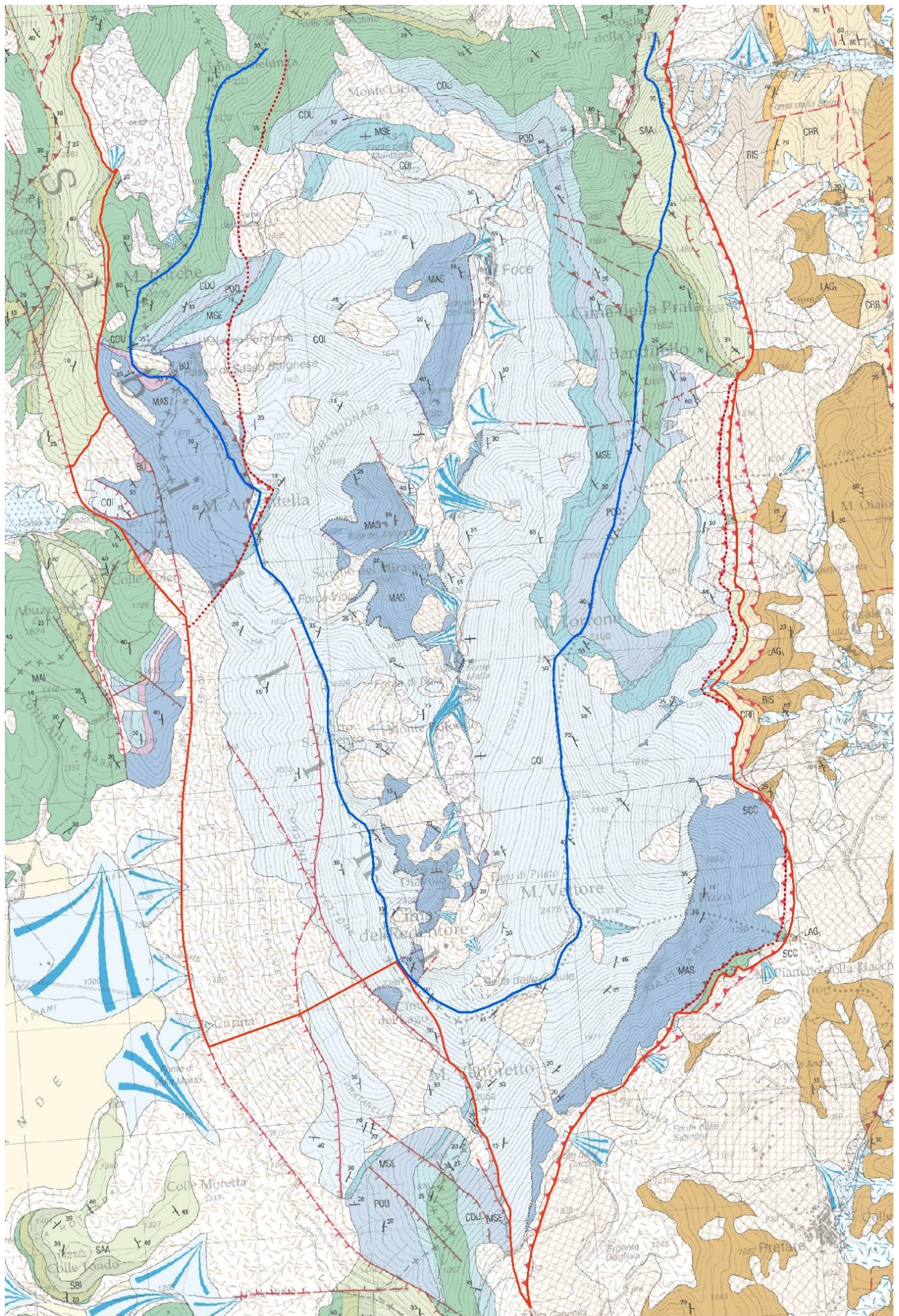


Fig. 4.1.1. Hydrological (blue) and hydrogeological basins (red and red-dashed). Basemap: modified with ©ArcMap 10.2 after Pierantoni et al. (2013)

The two hydrogeological basins have coincident watersheds in the W area, delimited by the fracture zone that winds along the W slopes of Monte Redentore up to Monte Argentella. Here they separate, isolating a *Calcare massiccio* core, that in the more restrictive case, is not considered as a feeding aquifer for the focused area. Southwards the hydrogeological boundary continues, crossing the Monte Redentore massif, probably constrained by an E-W trending pre-orogenetic structure. Then it connects, buffered by the tectonic contact with

lower permeability formations, with the *Monti Sibillini thrust* that defines the bottom permeability border. In the E sector, the basin is buffered by the *Monti Sibillini thrust*. In this late part the two hydrogeologic watersheds display the same trend, although the larger one includes some *Maiolica* fragments belonging to tectonic chips trapped among the several splay-thrust segments. In the N-W sector, the watersheds diverge due to a permeability barrier, represented by a thrust inside the macro-structure, which from the Monte Argentella propagates up to the E slope of Monte Porche (Nanni & Petitta, 2010).

#### 4.2. Geostructural data

For an improved knowledge of the underground discharge direction, a geostructural work is necessary. Nanni & Petitta (2010) has performed several geostructural stations identifying the following fracture sets:

- the first oriented N220/70° (dip/inclination) and N40/70° (NNW-SSE);
- the second oriented N320/70° and N130/60° (ENE-WSW).

Four systems have been identified with alternating dipping directions.

### 5. THE 2016-2017 SEISMIC SEQUENCE

The aim of the project is to understand the effects of the seismic sequence on the aquifers, therefore referable as a secondary coseismic effect (i.e. those attributable to the shaking of the seismic waves, such as liquefactions and landslides). Below we provide a geological description of the 2016-2017 earthquake mainshocks, implemented with some historical seismic data of the region.

The 2016-2017 central Italy seismic sequence consists of a series of moderate-to-large earthquakes, since August 2016 to January 2017, occurred on the Apennine-trending Monte Vettore-Monte Bove fault system (Chiaraluce et al., 2017).

The sequence started with the Amatrice earthquake (Mw 6.0) and the strong aftershock (Mw 5.4), occurred on August, 24<sup>th</sup> 2016, in the southern part of the fault system. Centimeters-scale fault ruptures were notable along the Monte Vettore fault escarpment outcrop. Regrettably, the high vulnerability of the local infrastructure and the shallowness of this event (depth around 8 km) resulted in 299 causalities (Chiaraluce et al., 2017).

Subsequently, it has been characterized by other strong earthquakes: on October, 26<sup>th</sup> two events of Mw 5.4 and 5.9 happened at the northernmost area, near Visso. The shocks activate another fault segment approximately located on the along-strike continuation of the structure responsible of the first shock.

In the morning of October, 30<sup>th</sup>, a shock of **Mw 6.5** occurred in the middle part of the fault system with epicenter not far from Norcia. Because of the hypocenter shallowness, the event generated new larger ruptures at the surface, sometimes exceeding those activated by the August, 24<sup>th</sup> shock. This is evidence that the event was nucleate on the same fault system, presently reaching about 60 km in length. The Mw 6.5 earthquake is the largest event to strike Italy since the 1980 Irpinia earthquake (Mw 6.9), so it was fortunate there were no fatalities because the disaster happened after the residents had already abandoned the previously damaged buildings. However, more than 20'000 people lost their home and with few hundreds of thousands of houses needing inspection within the provinces of Marche, Umbria, Lazio and Abruzzo regions (Chiaraluce et al., 2017).

Almost 5 months from the start of the seismic emergency, on January, 18<sup>th</sup> four seismic events of Mw  $\geq$  5.0 happened in the southern area of the seismic sequence.

The central Italy 2016-2017 seismicity affects the area comprised between the 1997 sequence (Colfiorito Mw 6.0, Umbria-Marche) to the north and the 2009 sequence (L'Aquila Mw 6.1, Abruzzo) to the south, as shown in the Fig. 5.1. (INGV, 2017).

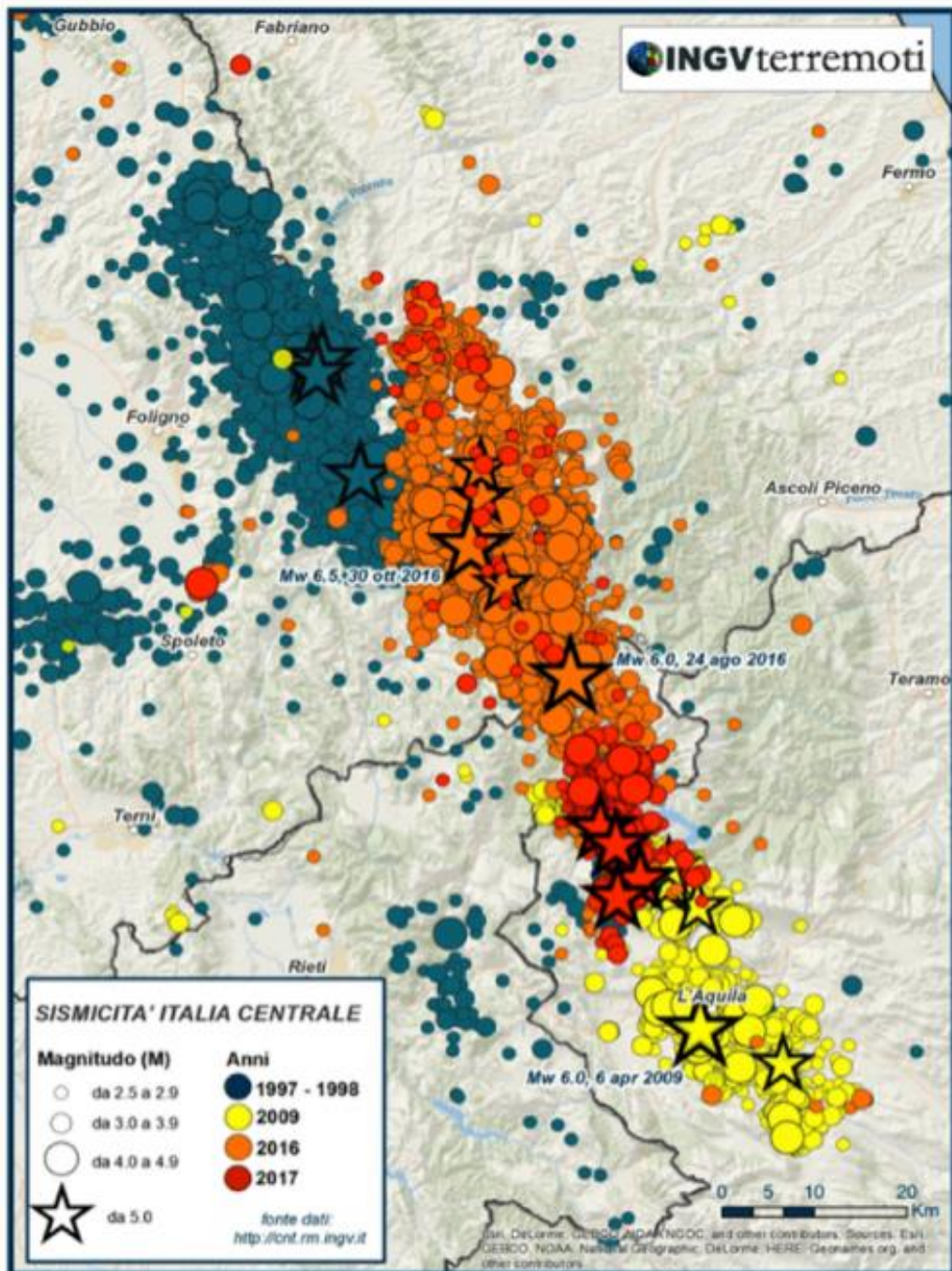


Fig. 5.1. Strongest seismic sequences happened in Italy in the last years. Earthquake epicenters are reported: the blue circles represent the 1997 sequence (Umbria-Marche, Colfiorito), the yellow ones the 2009 sequence (L'Aquila). The orange and the red circles are the 2016 and 2017 earthquakes respectively. (INGV, 2017)

The seismic sequence, at the beginning of February 2017, counts more than 50'000 localized shocks: 9 with  $Mw \geq 5.0$ , 59 with magnitude between 4.0 and 5.0, and about 1000 events with magnitude between 3.0 and 4.0.

The temporal trend of the sequence is shown in the plots (updated at the beginning of February 2017) of:

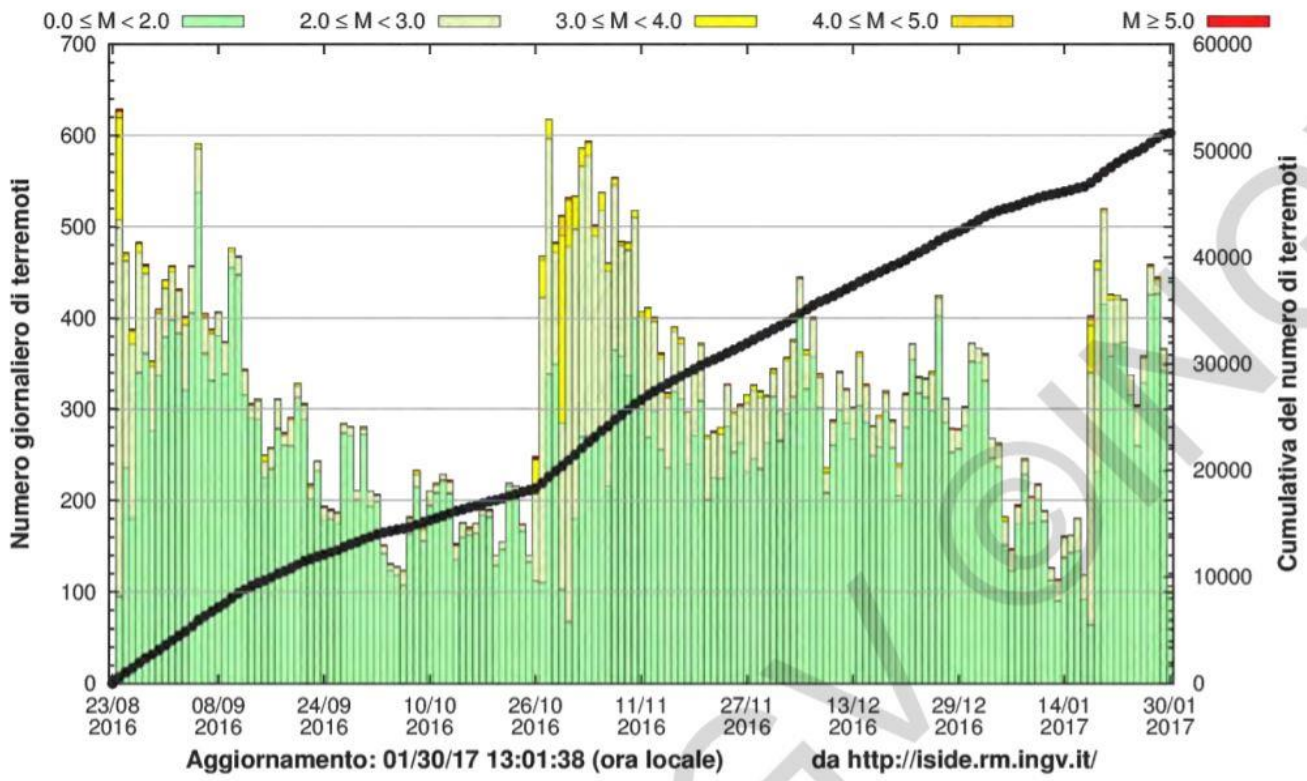


Fig. 5.2. The number of daily and cumulate earthquakes of the sequence. (INGV, 2017)

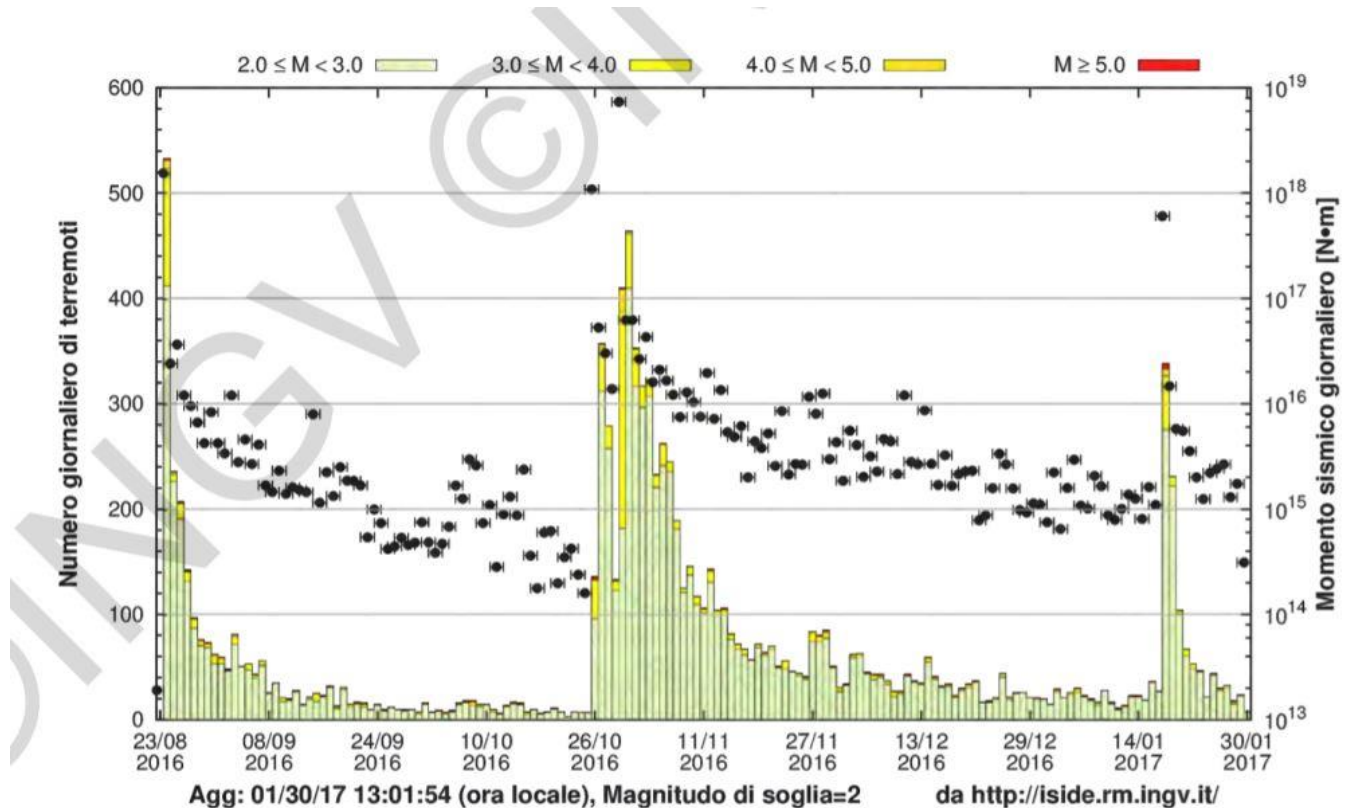


Fig 5.3. The number of daily events and the daily release of seismic moment. (INGV, 2017)

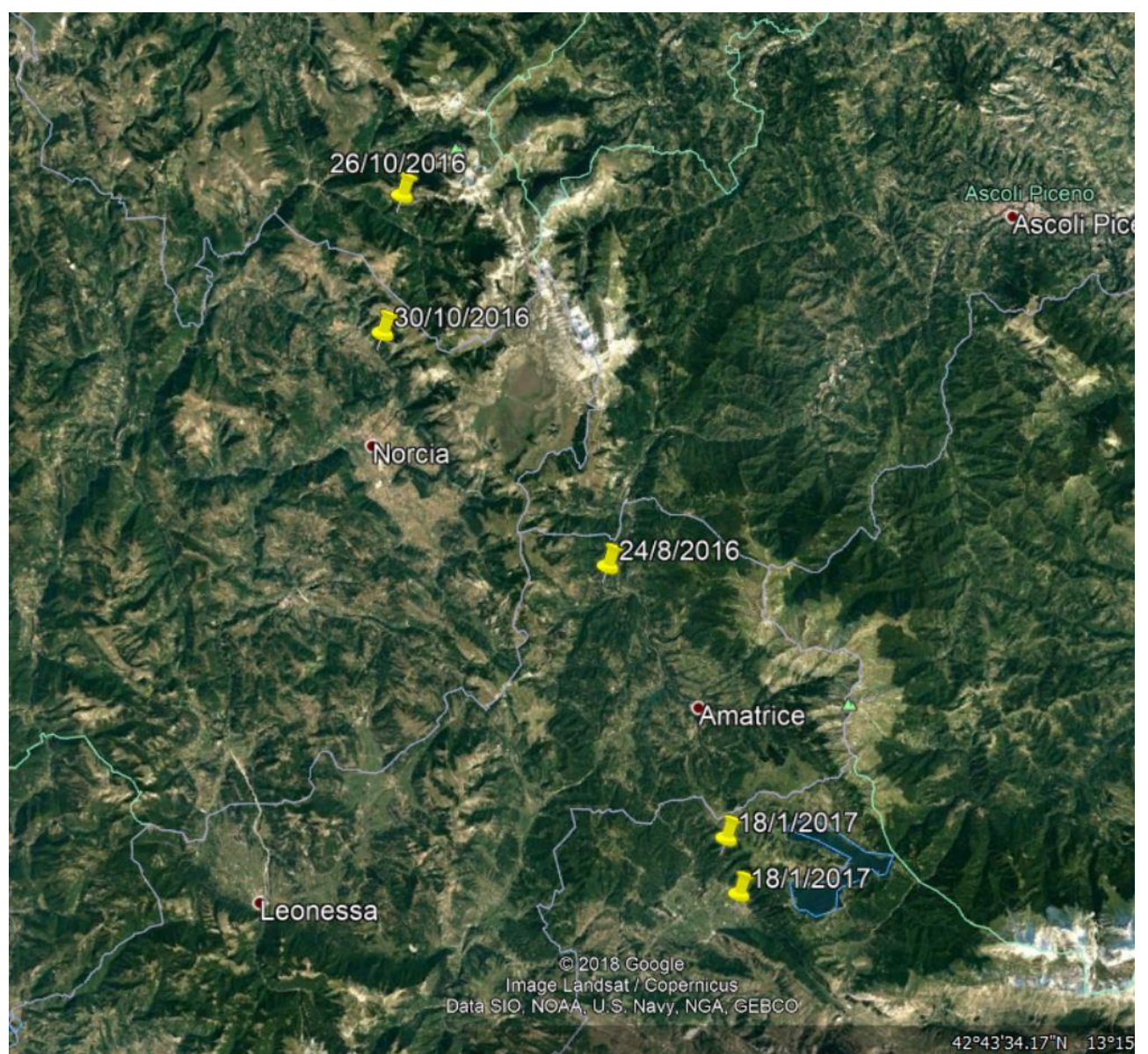


Fig 5.4. Epicenters of the 5 mainshocks of the 2016-2017 seismic sequence. ©Google Earth

The focal mechanisms of the main events are kinematically consistent with those of a NW-SE oriented and SW dipping normal fault: Monte Vettore – Monte Bove fault system (Fig. 5.5.). The southernmost termination of the 1997 sequence is nearly subparallel to the northernmost segment of the 2016 sequence; as well as the northernmost termination of the 2009 sequence is practically contiguous and well aligned to the southern tip of the 2016 fault system (Chiaraluce et al., 2017).

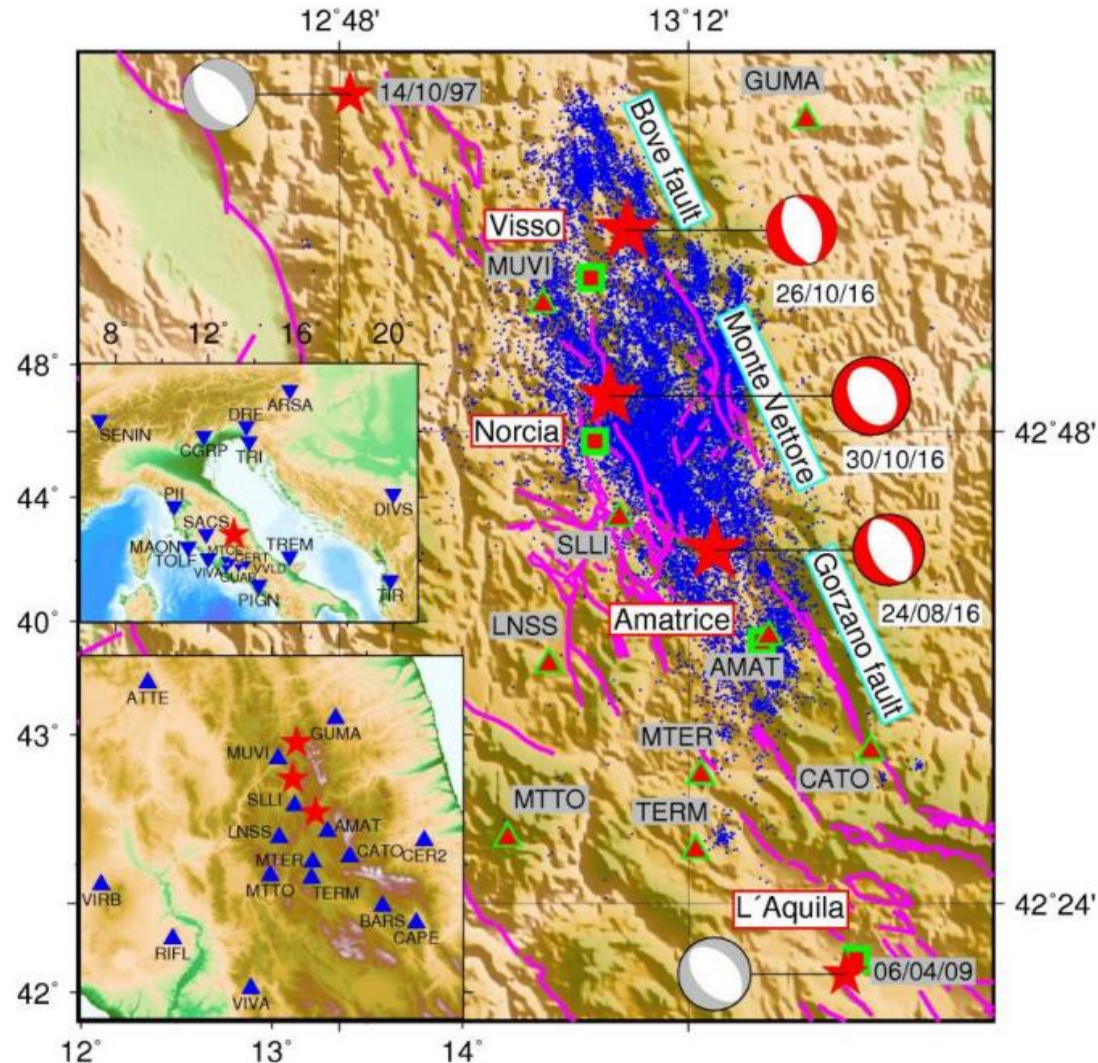


Fig 5.5. Red stars: epicentral location of the three mainshocks together with historical events. Beachballs, INGV focal mechanisms of the three mainshocks and historical events, respectively. Blue dots, aftershocks locations. Magenta lines, main faults extents in this area. Triangles and inversed triangles, high-rate Global Positioning System (GPS) stations and broadband seismometers. Shuhan et al. (2018)

The presence of inherited faults (Jurassic normal faults and neogenic thrusts) seems to modulate the evolution of the sequence, interfering with slip distribution and fault segment interaction. In addition, the whole fault system is characterized by the presence of the already quoted antithetic and synthetic shallow-normal faults located both in the hangingwall and footwall (Chiaraluce et al., 2017).

Concerning the primary coseismic effects (i.e. directly related to the earthquake rupture, as faulting and surface faulting), 28 km of surface faulting have been mapped between Arquata del Tronto and Cupi (Fig. 5.6.) (Civico et al., 2018).

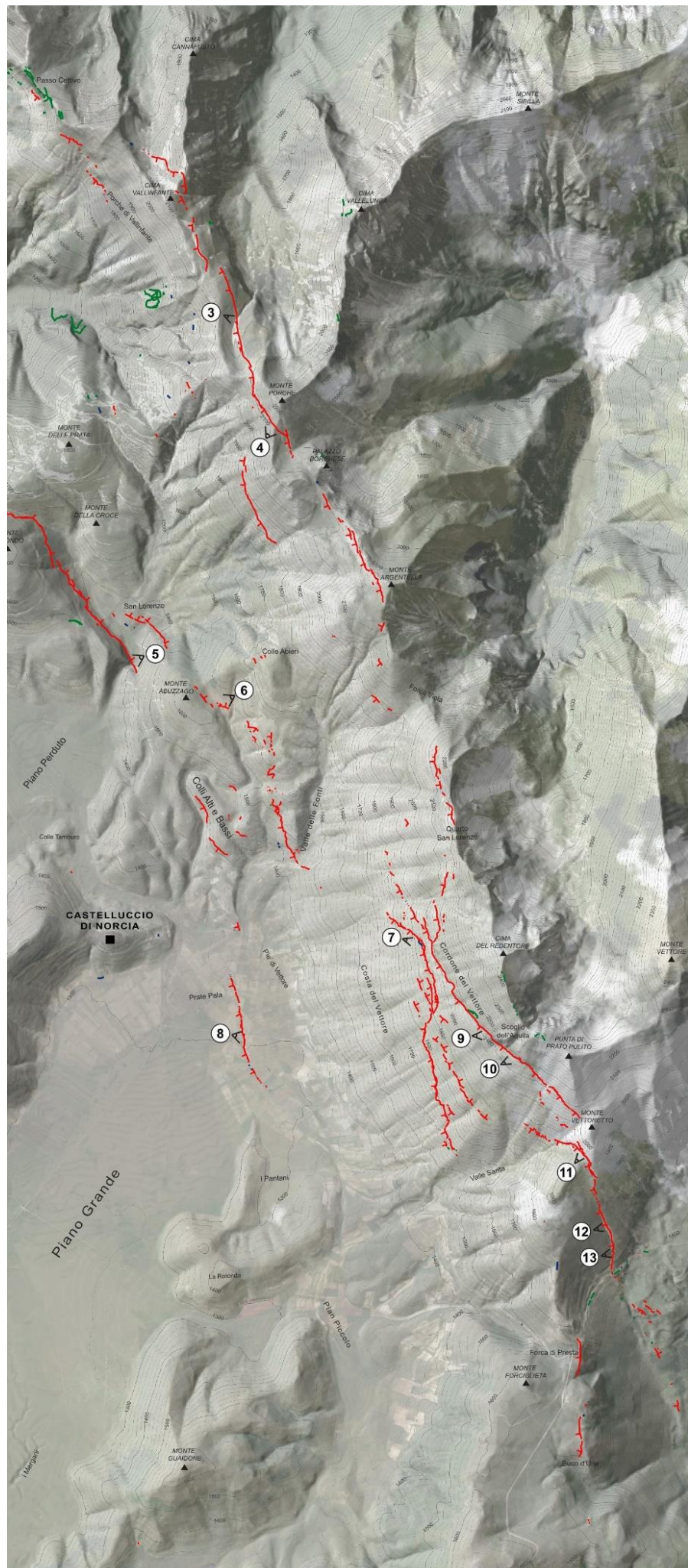


Fig. 5.6. A detail of the surface ruptures map following the October, 30<sup>th</sup> 2016 MW 6.5 Norcia earthquake. Civico et al. (2018)

Surveys performed in the area of the January, 18<sup>th</sup> shock have not shown relevant primary coseismic signals. Paleo-seismological studies (length of the surface faulting and geological insights) carried out in this area, along the active fault, allowed to conclude that the **Monte Vettore-Monte Bove fault system can generate earthquakes with a maximum magnitude of Mw 6.6.**

## 5.1. Historical earthquakes

The main shocks of the sequence (INGV, 2017), that happened among the Laga Mountains, Valnerina and Aquilano areas, have affected a region characterized by several very strong earthquakes in historical times, some of which happened in correspondence with complex sequences. However, none of them shows features fully comparable with the 2016-2017 sequence. Overall the seismic history of the area is quite well known, however the knowledge level changes in the different sectors. The spatial variability of the seismic response is the main reason of the seismic micro-zonation updating started after the earthquake.

The Amatrice area (August, 24<sup>th</sup> 2016 event) has been characterized by the presence of 4 earthquakes. The July 1627 shock (Acumuli, Mw 5.3); the October, 7<sup>th</sup> 1639 (Amatrice, Mw 6.2) – this late event destroyed the Amatrice center and the surrounding villages; the 1646 earthquake (Monti della Laga, Mw 5.9) and the 1672 event (Amatrice, Mw 5.3).

In Valnerina the historical earthquakes are those of: December, 1<sup>st</sup> 1328 (Valnerina, Mw 6.5); June, 27<sup>th</sup> 1719 (Valnerina, Mw 5.6); May, 12<sup>th</sup> 1730 (Valnerina, Mw 6) and August, 22<sup>nd</sup> 1859 (Valnerina, Mw 5.7). All localized close to the October, 30<sup>th</sup> mainshock epicenter.

The magnitudes registered in the area among Visso, Ussita and Castelsantangelo sul Nera, in October, 26<sup>th</sup> 2016, could represent the historical maximum for these municipalities.

In the southern sectors, where the January, 18<sup>th</sup> shocks occurred, the most important historical events happened during the XVII century: July, 7<sup>th</sup> 1619 earthquake (Aquilano, Mw 5.3), sensed in Rome and caused slight damages in L'Aquila; June, 8<sup>th</sup> 1672 event (Monti della Laga, Mw 5.3) also sensed in Rome and caused serious damages in Montereale and Campotosto. Another important earthquake happened on September, 5<sup>th</sup> 1950 (Io 8 MCS, Mw 5.7), that caused relevant damages among Amatrice, Montereale and the western sector of Teramano.

The 2016-2017 sequence is not comparable with the long and complex one of 1703 (January, 14<sup>th</sup>, Valnerina, Mw 6.9; February, 2<sup>nd</sup>, Aquilano, Mw 6.7) whose effects on the territory were heavier than those of the most recent one (INGV, 2017).

## 6. THE BASAL AQUIFER ANALYSIS

The Basal aquifer, holding the regional base flow, feeds several springs fundamental for the water supply of the southern Marche mountain, foothill and coastal areas. The knowledge about the earthquake effects on it is basically from a geological/hydrogeological point of view but also for economic and social reasons.

One of the main goals of the study is the understanding of the effects related to the Central Italy 2016-2017 seismic sequence on the Basal aquifer flow rates and piezometric level. This was performed by means of a comparison between pre-earthquake (2011) (Nanni & Petitta, 2010 & 2012) and post-earthquake data acquired from June to October 2018.

The analysis focuses on the Basal and Maiolica aquifers that, before the earthquake, fed the Aso river starting a little upstream the village of Foce (around 950 m a.s.l.) to the ENEL intake. Previous studies, (Nanni & Petitta, 2010 & 2012) also collected values further E, where Aso river is sustained by the Scaglia calcarea aquifer.

### 6.1. Work planning

The study, started in June 2018, has been planned as follows:

- river flow measurements, to evaluate Basal aquifer flow variation after the earthquake;
- reconstruction of the hydrostructure feeding the upper portion of the Aso river;
- data interpretation.



Fig 6.1.1. Geological setting of the uppermost sector of Aso river. Modified with ©ArcMap 10.2 after Nanni & Petitta (2010)

### 6.2. Methodology

Flow rate measurements started with a choice of a certain number of hydraulic cross-sections located on the base of pre-sequence studies and hydrogeological boundaries.

The first considered parameter is the river flow rate.

To collect the measurements, it was necessary to perform some hydraulic sections whose locations have been chosen on the base of the pre-sequence study and the hydrogeological boundaries.

In the map (Fig 6.2.1.), the red acronyms, such as As40, represents the old hydraulic cross-sections (indicated with red dashed lines) while the yellow stars indicate those employed during the 2018 surveys.

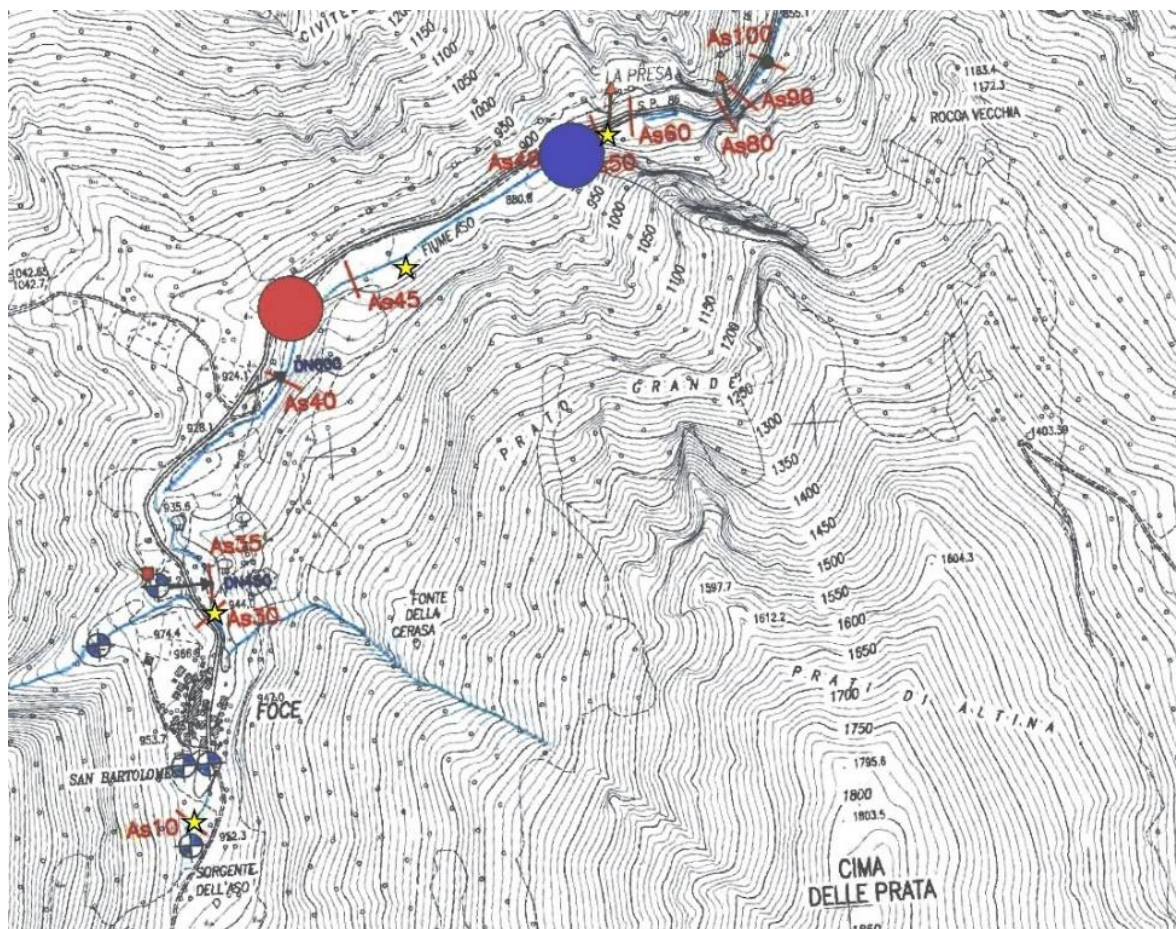


Fig. 6.2.1. Hydrological map of the uppermost portion of the Aso river showing the location of old and new measurement points (modified with ©ArcMap 10.2 after Nanni & Petitta, 2010). Orange arrows indicate the ENEL deviations; blue arrows are hydraulic restitutions by CIPI.

Flow rate differences have allowed to estimate earthquake-related variations in water volume.

### 6.2.1. Flow rate measurements

Flow rate passing through a river section of known geometry in the unit of time, has been calculated using a ©Ricky USGS AAA Current Meter. The device is made by a graduate rod and a rotating helix connected to a console. Its operating principle is simple: the water current makes the helix turn with a certain frequency, proportional to the current speed. The signal is transmitted to the console and reported on the display.



Fig. 6.2.1.1 ©AquaCMD, Current Meter Digitize



Fig. 6.2.1.2. During the surveys, August, 30<sup>th</sup> 2018

The geometry of the section is acquired staring a metric tape between the sides of the river with two fixing rods for the horizontal distance (Fig. 6.2.1.3.). The river channel depth is evaluated by means of the graduate rod.



Fig. 6.2.1.3. The measurement of the hydraulic section. June, 19<sup>th</sup> 2018

The velocity of flow is acquired at regular distance intervals and depths (i.e. every 50 cm laterally and 5, 10, 15... cm depth) making sure that stones or other things do not disturb the flow, generating turbulence. **This method assumes that the flow rate is uniform around the survey point for a certain area.**

At the end of the survey all the velocity data are entered in a software (Excel in our case, Fig. 6.2.1.4.) that returns the average flow rate passing through the section in the unit of time (l/s).

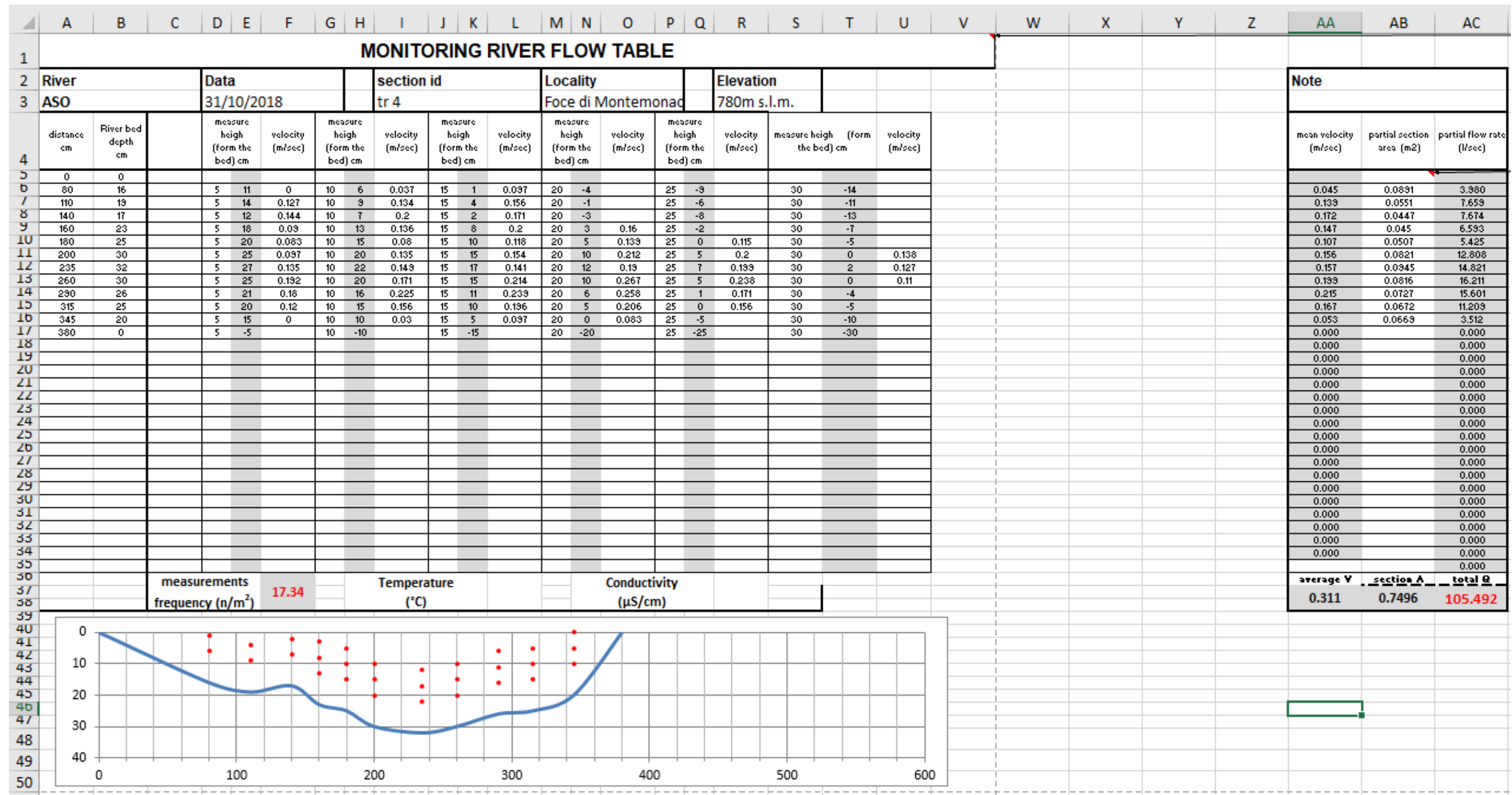


Fig. 6.2.1.4. The ©Microsoft Excel page used to convert current velocity measurements into the river flow value

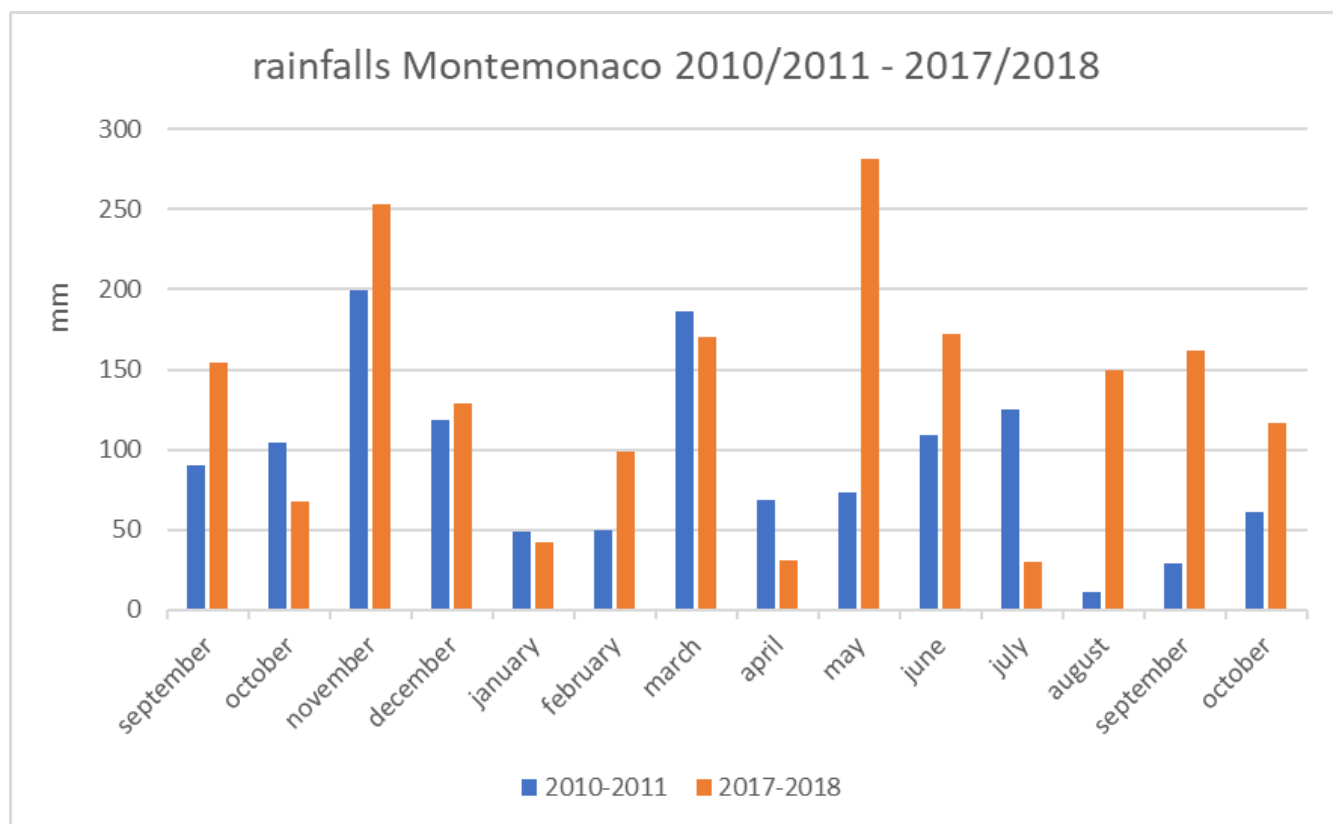
### 6.2.2. The hydrographs rebuilding

The next step was to rebuild a daily stream hydrograph (i.e. a graph showing the flow variation in time at a fixed point) starting from June to October 2010/2018 for each hydraulic section.

The hydrographs estimation starts from daily flow rate values for 2018 and average monthly data for 2011. In the first case the data are at the net of the runoff because they were collected with a lag of 2-3 days after the last precipitation event. Instead, the 2011 values consider all that happened during the month.

A linear regression procedure was used to calculate the entire period hydrograph starting from single daily values. **The method was reliable because the flow of this part of the river is fed mainly by the base flow, coming from the Basal aquifer, that does not strictly depend from rainfalls.** Nevertheless, average monthly of precipitation, have been collected for successive analyses; this also to take into account the effects of the scarcity of rainfalls during the summer 2011, a very dry season.

The considered pluviometric stations, whose data have been collected from the SIRMIP website (Sistema Informativo Regionale Meteo Idro-Pluviometrico – Protezione Civile Regione Marche), have been Montemonaco (RT-1586) for the N sector and Capodacqua (RT-1364) for the S part (Fig. 6.2.2.1.) because the hydrogeological and the hydrological basins extend both from N to S of Monte Vettore – Monte Cima della Prata ridge. More in detail, cumulative precipitation monthly data starting from the beginning of September 2010/2017 to the end of October 2011/2018 have been acquired. A longer period has been considered, to take into account the snow contribution that, in this area, may fall since the autumn beginning.



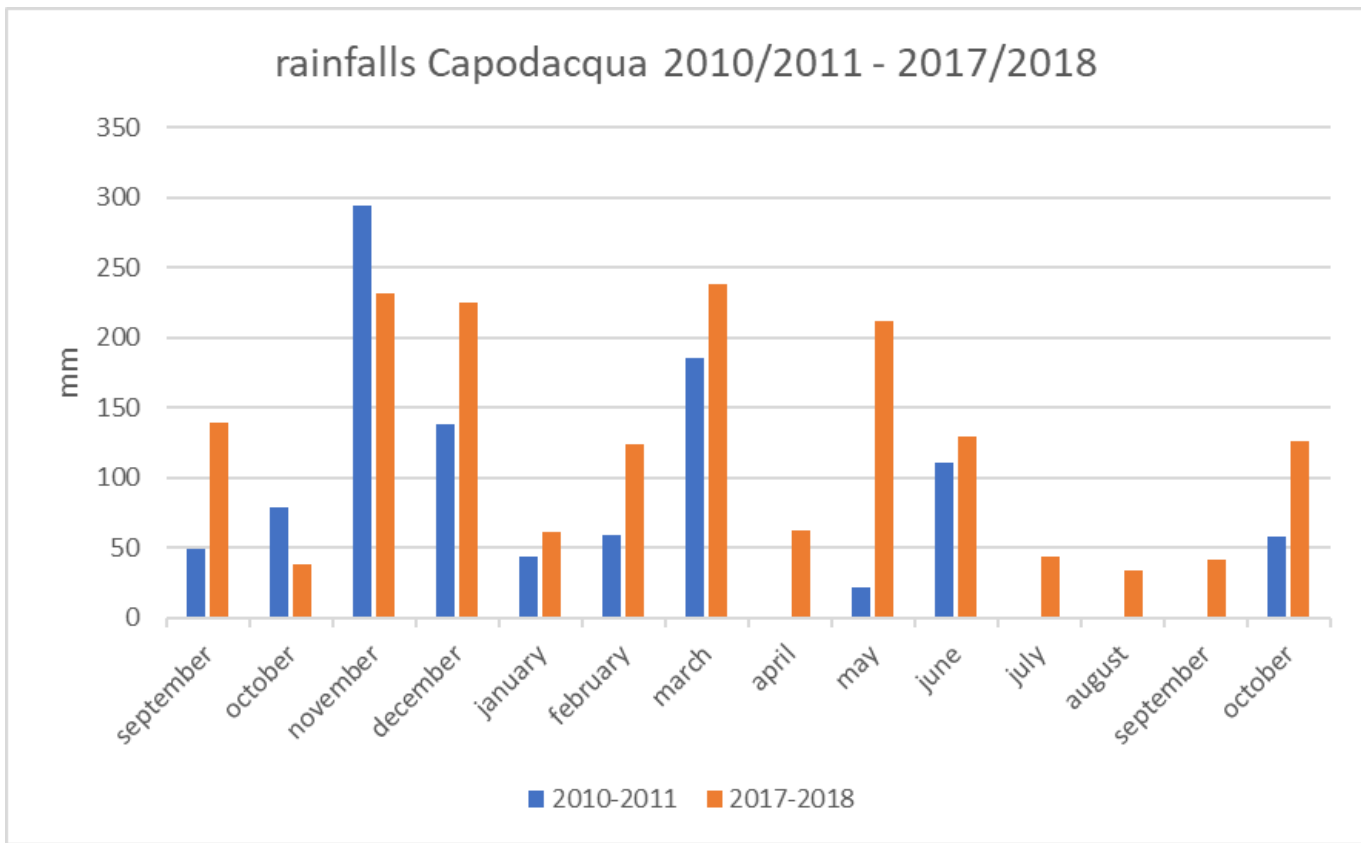


Fig. 6.2.2.1. - Precipitations registered in Montemonaco and Capodacqua for 2010/2011 and 2017/2018 periods. ©Microsoft Excel

A general overview of the precipitation data evidences that:

- at the Montemonaco station the total measured rainfall from September 2010 to October 2011 was 1273.8 mm while in the same 2017-2018 period was 1857 mm. This means that in the second period the rainfalls were 45.8% more abundant than in the first one.
- at the Capodacqua station the total measured rainfall in the 2010-2011 months was 1037 mm while in the 2017-2018 period was 1705.2 mm, with a cumulative percentage increase of 64.3%.

The results said that the pre-earthquake considered period has been generally drier than the post-earthquake one, so **the flow rate decrease could be considered not climatic-dependent**.

Because of Nanni & Petitta (2010 & 2012) values are average monthly data, it has been decided to assign each measure to the central day of the month. Then, the variation trend was defined between two flow rate values, making the difference and dividing it for the number of days elapsed. Subsequently, starting from one of the two data, considering constant the flow rate variation in time, all the days enclosed by the two extremes have been estimated. For example, for the section As10, the flow rate for June, 15<sup>th</sup> 2011 is 44 l/s and for July, 15<sup>th</sup> 2011 is 12 l/s. The difference is 32 l/s and 30 days elapsed, so the variation gradient is -1.07 (l/s)/day.

The same procedure was used for the 2018 values and it was more accurate because the number of elapsed days between the surveys was exactly known.

The ultimate goal was to calculate the volumes of water lost or gained, so we needed to know the amounts of water yielded by the aquifer in m<sup>3</sup>. Therefore, l/s data had to be initially converted into m<sup>3</sup>/day, then summed to obtain m<sup>3</sup>/month, and finally summed again to know the whole volume passing through the i<sup>th</sup> section from June, 1<sup>st</sup> 2011/2018 to October, 31<sup>th</sup> 2011/2018 (Fig. 6.2.2.2.).

1	As10	I/s	mc/s	mc/day			
14	13/06/2011	46.13	0.046	3985.92			
15	14/06/2011	45.07	0.045	3893.76			
16	15/06/2011	44.00	0.044	3801.6			
17	16/06/2011	42.93	0.043	3709.44			
18	17/06/2011	41.87	0.042	3617.28			
19	18/06/2011	40.80	0.041	3525.12			
20	19/06/2011	39.73	0.040	3432.96			
21	20/06/2011	38.67	0.039	3340.8			
22	21/06/2011	37.60	0.038	3248.64			
23	22/06/2011	36.53	0.037	3156.48			
24	23/06/2011	35.47	0.035	3064.32			
25	24/06/2011	34.40	0.034	2972.16			
26	25/06/2011	33.33	0.033	2880			
27	26/06/2011	32.27	0.032	2787.84			
28	27/06/2011	31.20	0.031	2695.68			flow rate difference
29	28/06/2011	30.13	0.030	2603.52			32 I/s
30	29/06/2011	29.07	0.029	2511.36	june total		variation gradient
31	30/06/2011	28.00	0.028	2419.2	112665.6 mc		1.06667 (I/s)/day
32	01/07/2011	26.93	0.027	2327.04			
33	02/07/2011	25.87	0.026	2234.88			
34	03/07/2011	24.80	0.025	2142.72			
35	04/07/2011	23.73	0.024	2050.56			
36	05/07/2011	22.67	0.023	1958.4			
37	06/07/2011	21.60	0.022	1866.24			
38	07/07/2011	20.53	0.021	1774.08			
39	08/07/2011	19.47	0.019	1681.92			
40	09/07/2011	18.40	0.018	1589.76			
41	10/07/2011	17.33	0.017	1497.6			
42	11/07/2011	16.27	0.016	1405.44			
43	12/07/2011	15.20	0.015	1313.28			
44	13/07/2011	14.13	0.014	1221.12			
45	14/07/2011	13.07	0.013	1128.96			
46	15/07/2011	12.00	0.012	1036.8			
47	16/07/2011	11.81	0.012	1020.08			

Fig. 6.2.2.2. Hydrographs rebuilding and total monthly yielded volumes. ©Microsoft Excel

### 6.3. The pre-earthquake state

As already cited, river flow values coming from the study of Nanni & Petitta (2010 & 2012) have been collected for the comparison. There are reported the 2011 values for same period and locations considered in the post-earthquake surveys (Tab 6.3.1.).

Section	Elevation m.a.s.l.	Description	June 2011 (I/s)	July 2011 (I/s)	Sept 2011 (I/s)	Oct 2011 (I/s)
As10	952	Highest spring	44	12	0	0
As30	945	Downstream Fonte Cerasa confluence	200	18	5	0
As45	895	CIIP hydrometer	595	515	454	222
As50	875	Upstream 1 <sup>st</sup> ENEL deviation	1026	865	507	496

Tab. 6.3.1. Average river flow values June 2011-October 2011.

### 6.3.1. Stream hydrographs and yielded volumes

To give a clearer view of the flow rate regimes of the Aso river during the considered time interval, 4 hydrographs showing the total monthly and whole season yielded volumes during the 2011 survey campaign are reported.

**Section As10 – Highest spring – 2011**

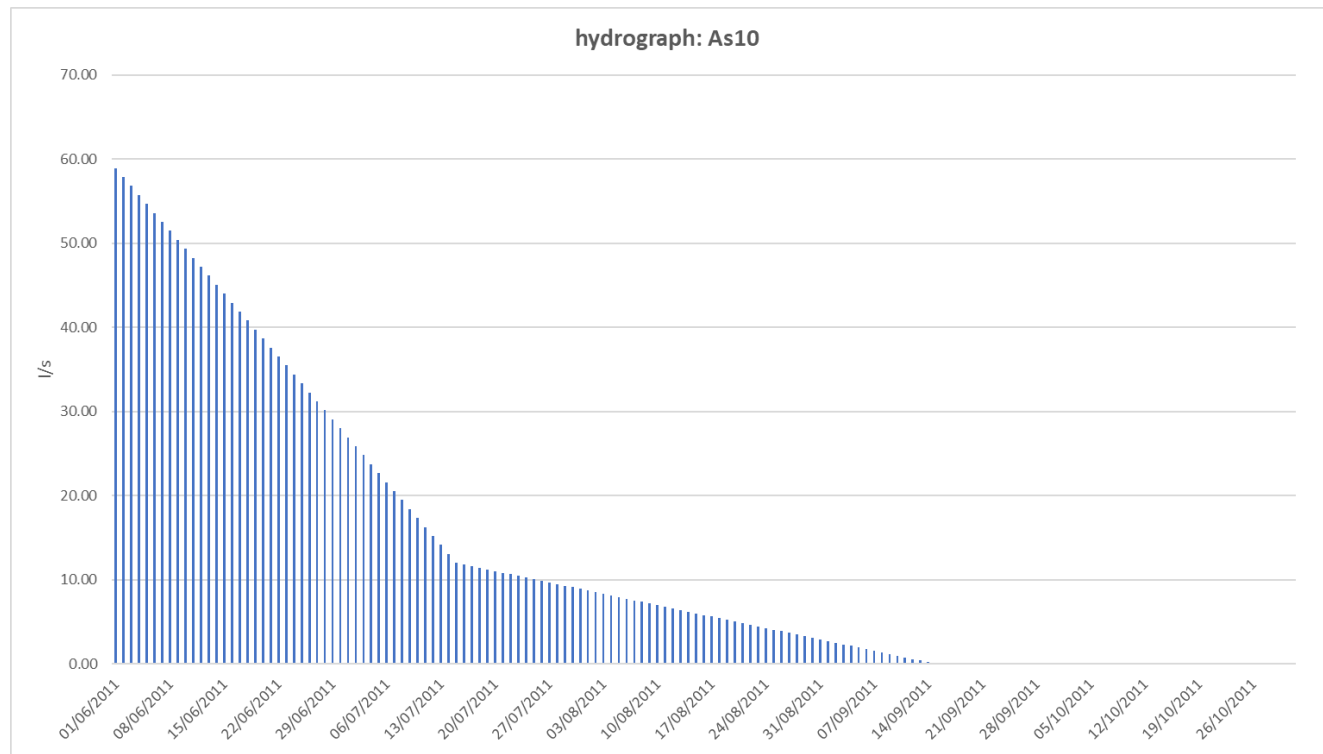


Fig. 6.3.1.1. As10 hydrograph for the 2011 period. ©Microsoft Excel

Section: <b>As10</b>	Elevation m a.s.l.	June 2011	July 2011	August 2011	September 2011	October 2011	Total
<b>Yielded volume (m<sup>3</sup>)</b>	952	112666	39543	15552	1756	0	169517

Tab. 6.3.1.1. As10 yielded volumes in the 2011 period

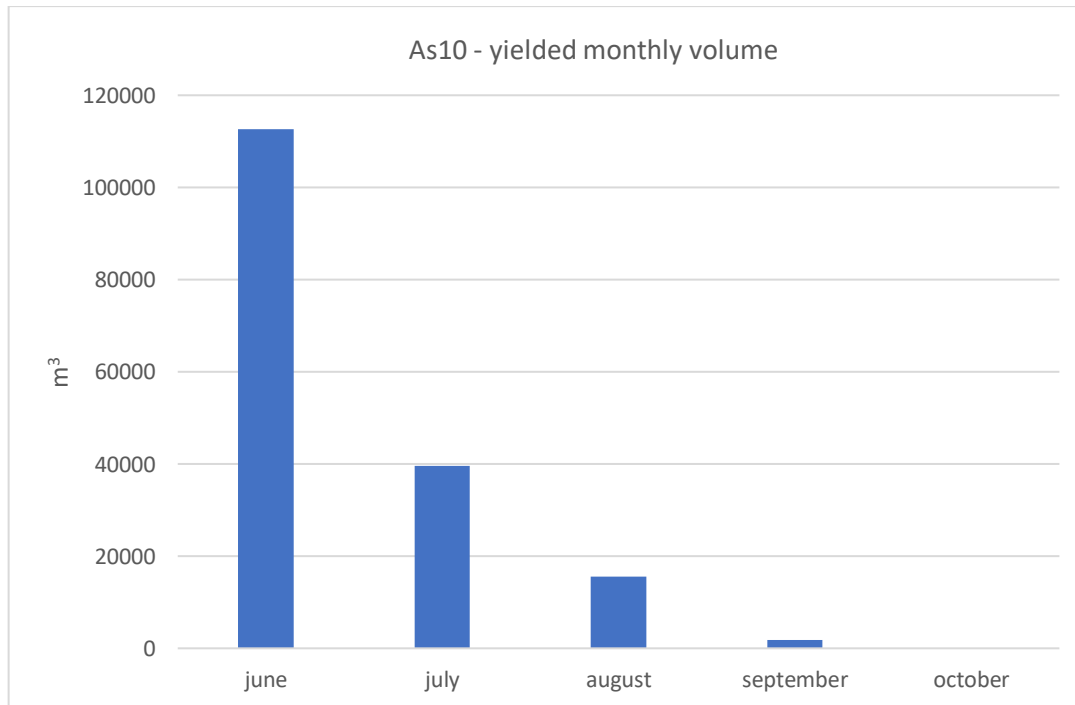


Fig. 6.3.1.2. As10 yielded volumes in the 2011 period. ©Microsoft Excel

### Section As30 – Downstream Fonte Ceresa confluence – 2011

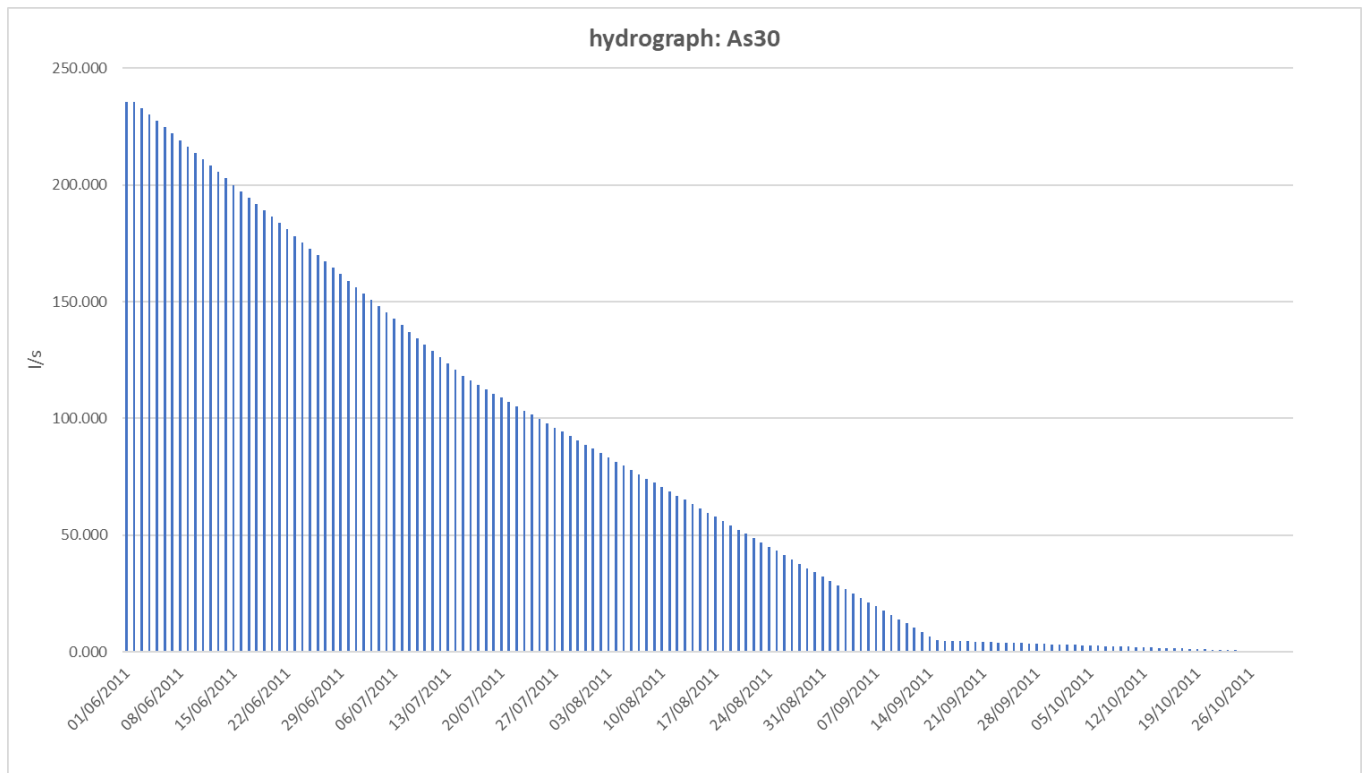


Fig. 6.3.1.3. As30 hydrograph for the 2011 period. ©Microsoft Excel

<b>Section: As30</b>	Elevation m a.s.l.	June 2011	July 2011	August 2011	September 2011	October 2011	<b>Total</b>
<b>Yielded volume (m<sup>3</sup>)</b>	945	514621	319432	159840	28367	4367	1026628

Tab. 6.3.1.2. As30 yielded volumes in the 2011 period

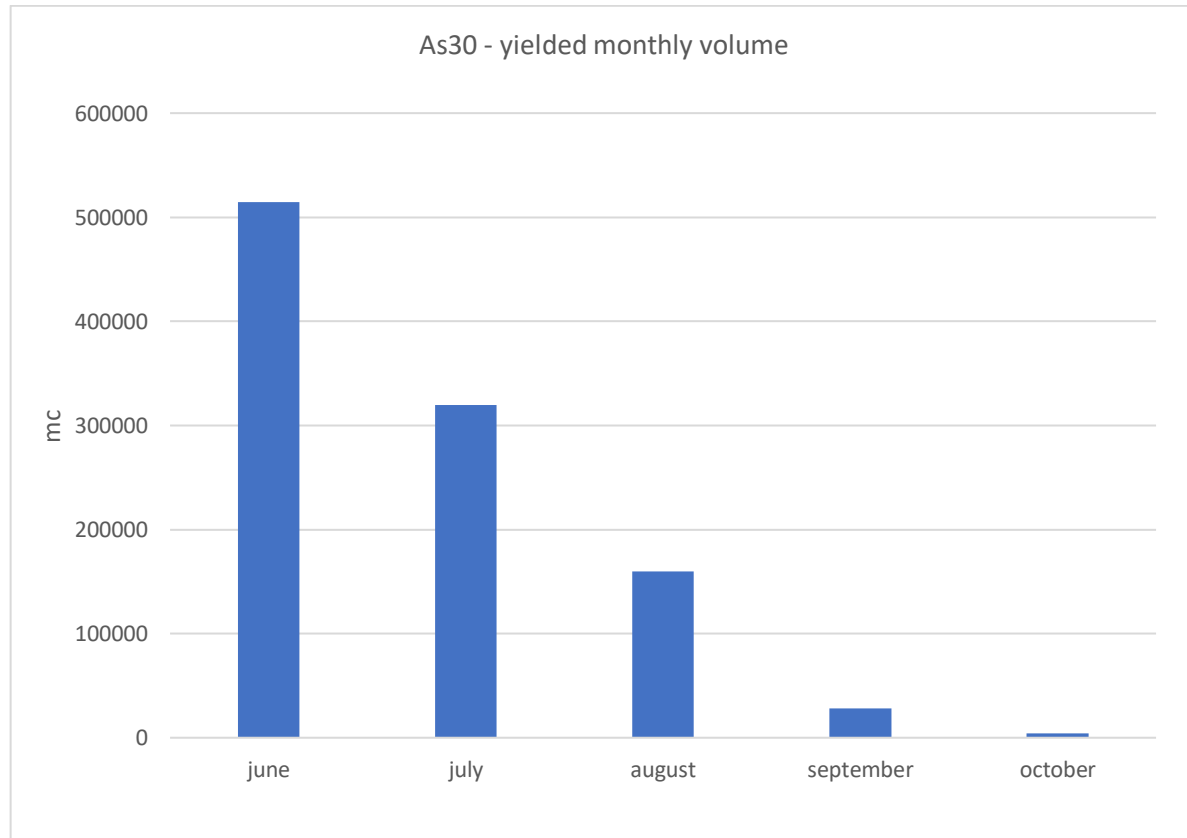


Fig. 6.3.1.4. As30 yielded volumes in the 2011 period. ©Microsoft Excel

### Section As45 – CIIP hydrometer – 2011

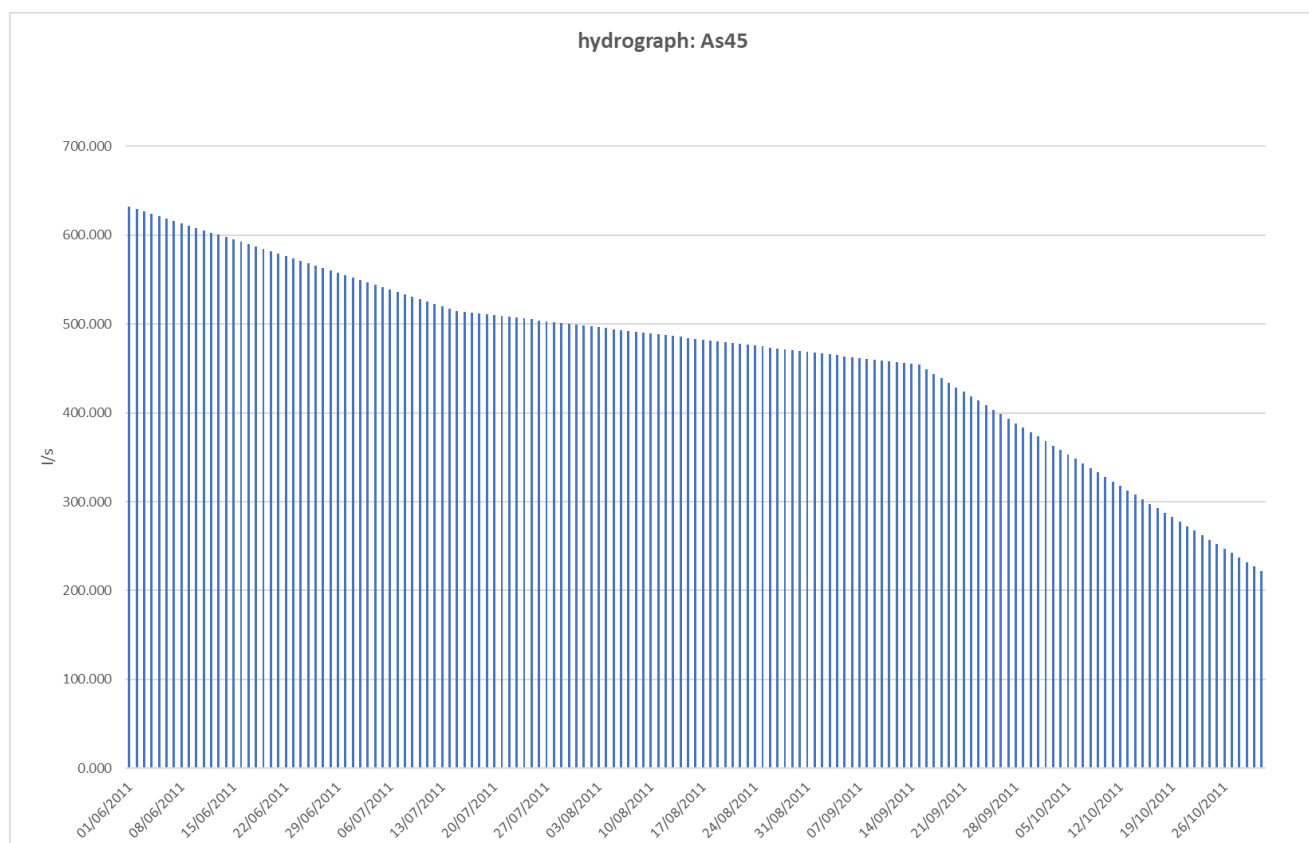


Fig. 6.3.1.5. As45 hydrograph for the 2011 period. ©Microsoft Excel

<b>Section: As45</b>	Elevation m a.s.l.	June 2011	July 2011	August 2011	September 2011	October 2011	<b>Total</b>
<b>Yielded volume (m<sup>3</sup>)</b>	895	1538784	1392007	1295050	1133403	797232	6156475

Tab. 6.3.1.3. As45 yielded volumes in the 2011 period

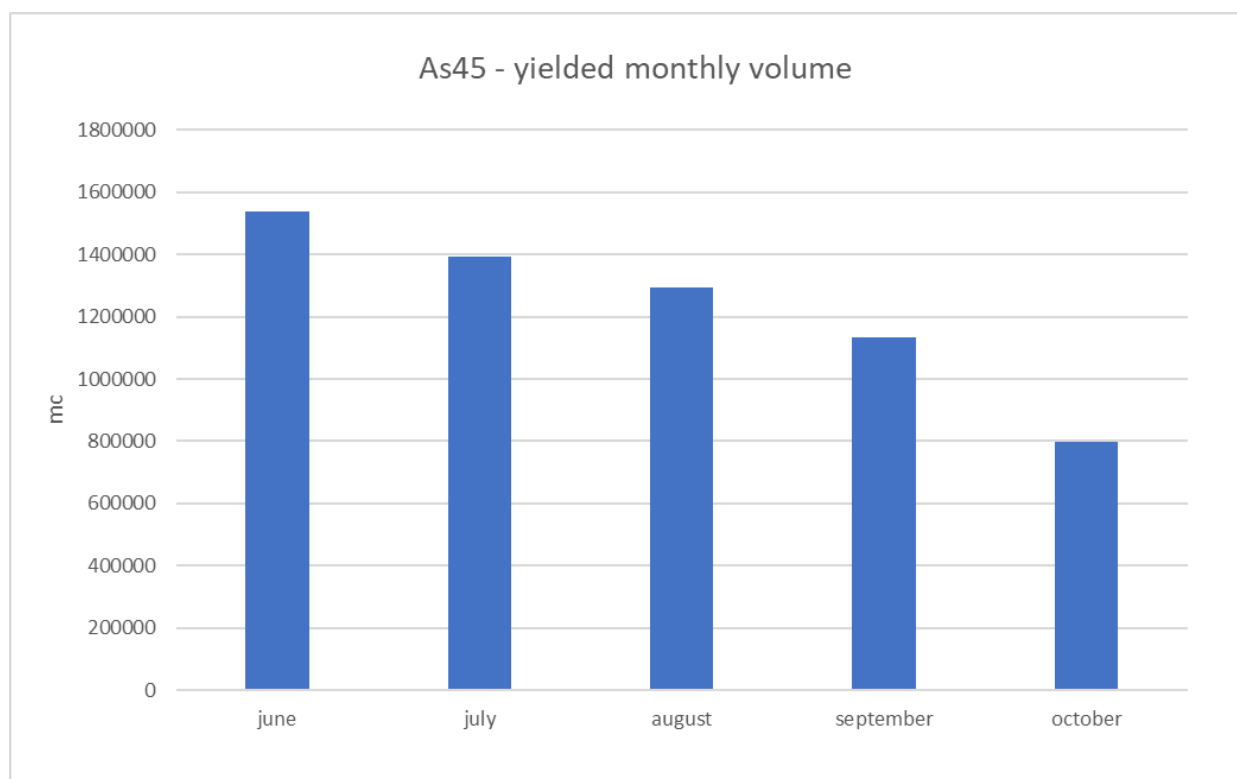


Fig. 6.3.1.6. As45 yielded volumes in the 2011 period. ©Microsoft Excel

### Section As50 – Upstream 1<sup>st</sup> ENEL deviation – 2011

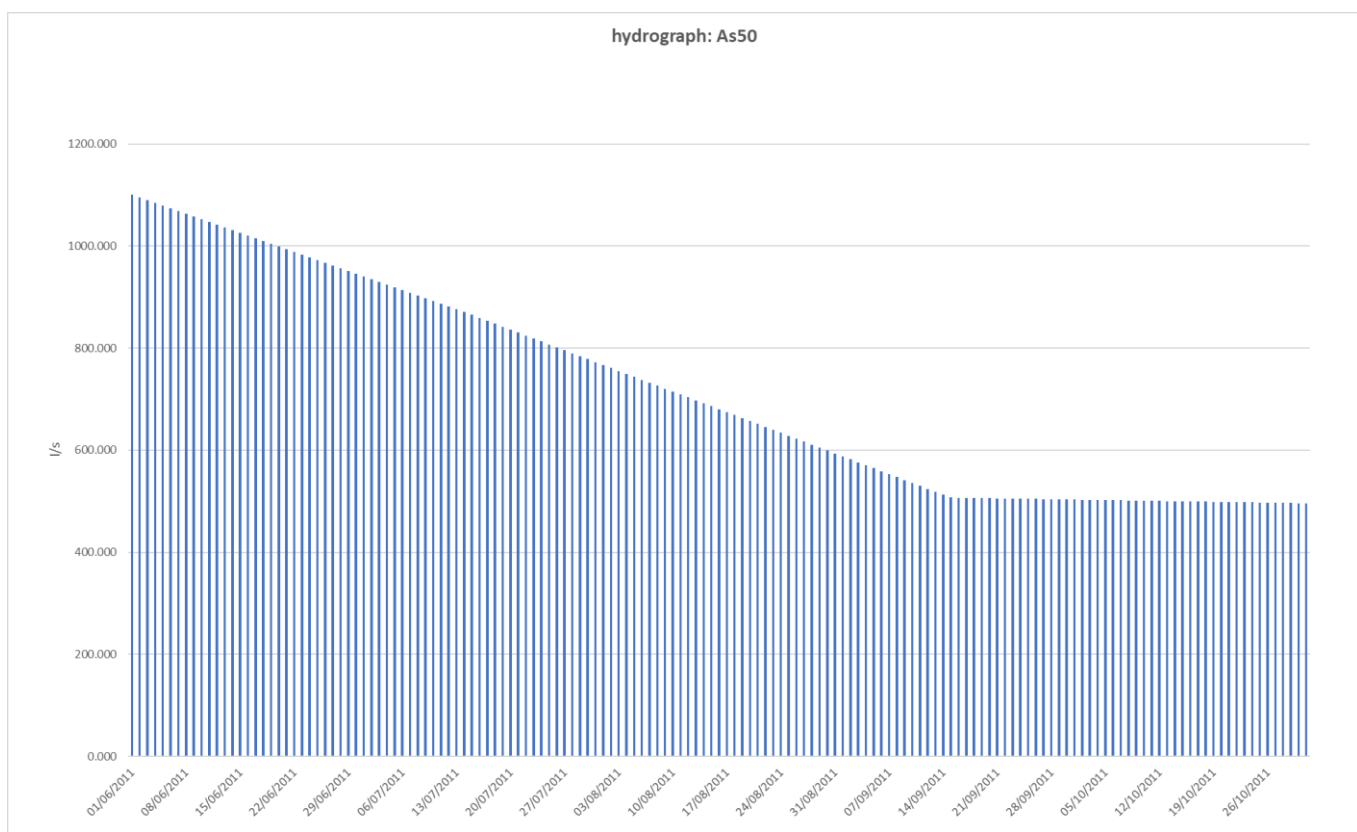


Fig. 6.3.1.7. As50 hydrograph for the 2011 period. ©Microsoft Excel

<b>Section: As50</b>	Elevation m a.s.l.	June 2011	July 2011	August 2011	September 2011	October 2011	<b>Total</b>
<b>Yielded volume (m<sup>3</sup>)</b>	875	2652437	2297653	1821917	1364048	1338094	9474149

Tab. 6.3.1.4. As50 yielded volumes in the 2011 period

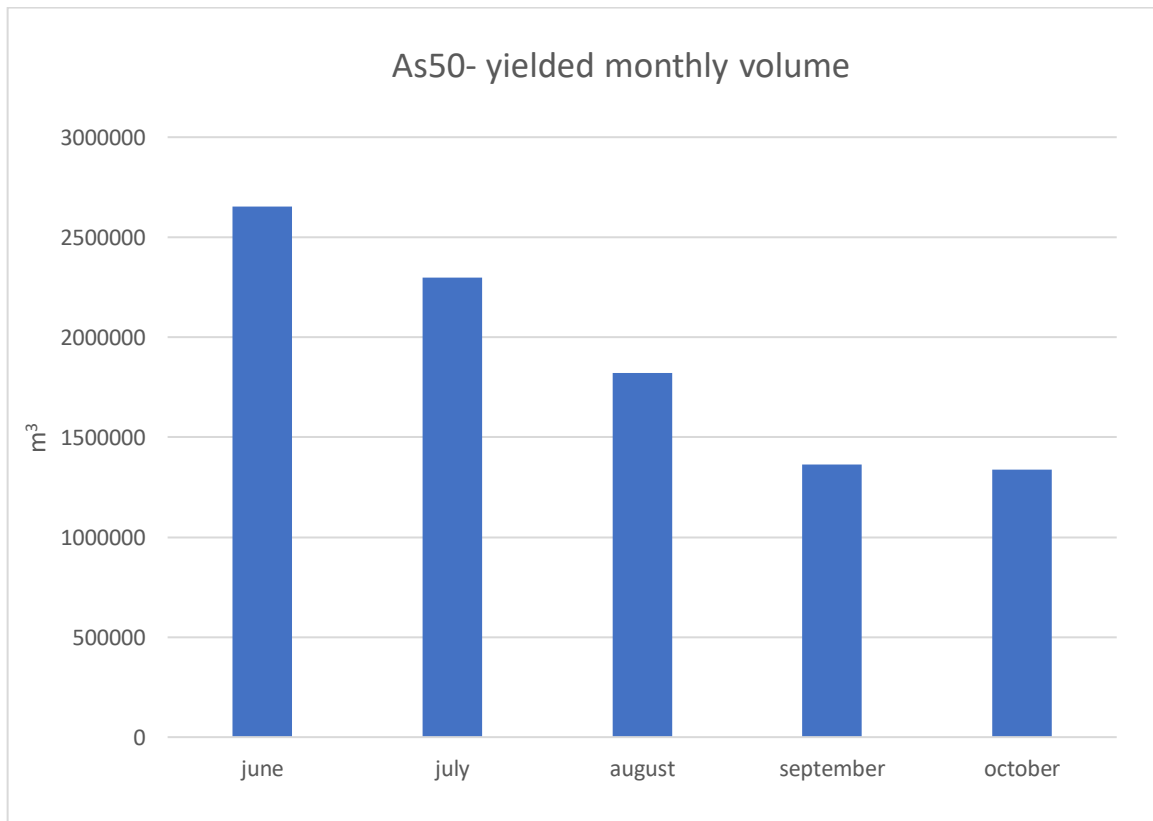


Fig. 6.3.1.7. As50 yielded volumes in the 2011 period. ©Microsoft Excel

Each hydraulic section borders a river segment directly fed by the aquifer through a linear spring (Fig. 6.3.1.8.). Therefore, the measured flow rate at the  $i^{\text{th}}$  section could be the sum of the water coming from the uppermost spring As10 and of the one that comes out between the As10 section and the  $i^{\text{th}}$  section. This latter component has been called ***sector increment*** between the  $i^{\text{th}}$  section and the one immediately upstream. Henceforth, the aquifer contributions will be expressed by means of the sector increments.

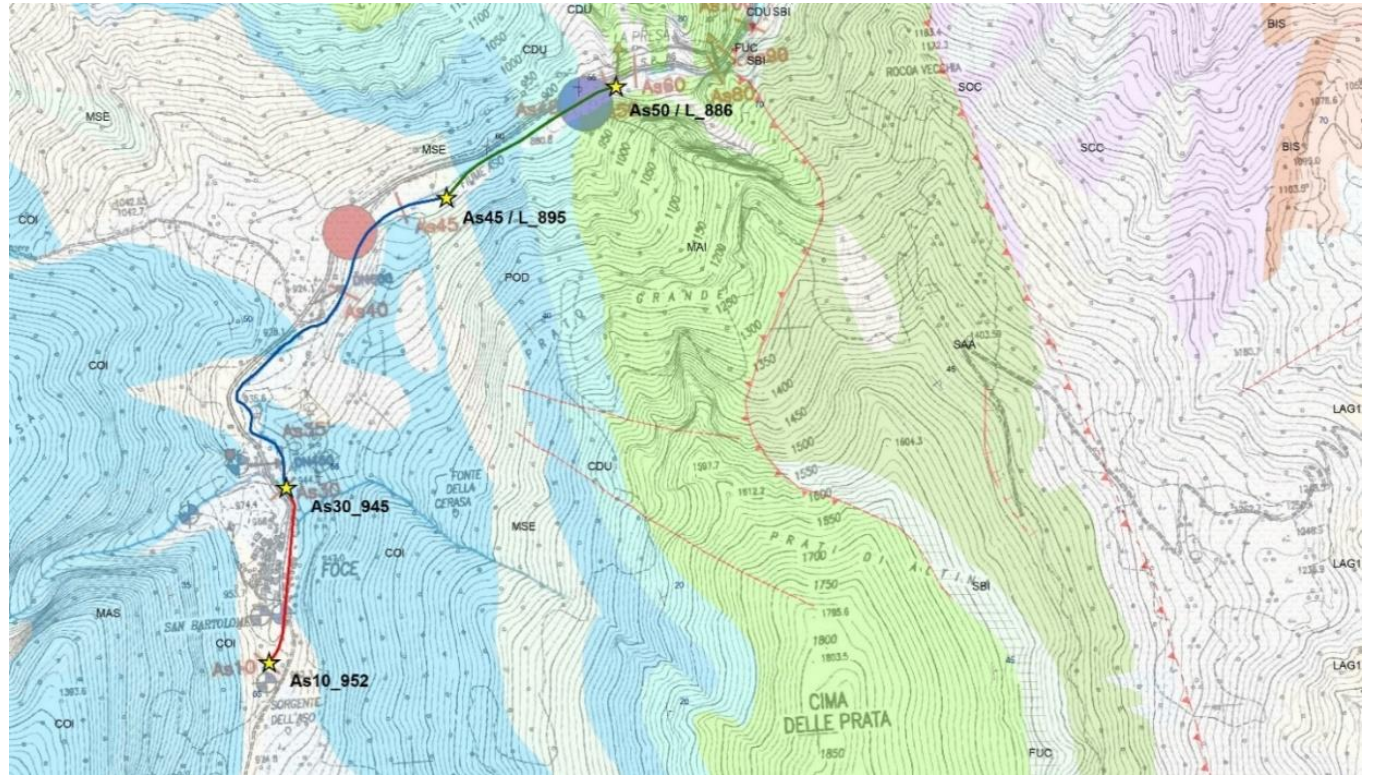


Fig. 6.3.1.8. Aso river analyzed sectors. Basemap: modified with ©ArcMap 10.2 after Nanni & Petitta (2010)

In the table below (Tab. 6.3.1.5.) there are the monthly and whole period data of segment increments.

SECTOR	June 2011 ( $\text{m}^3$ )	July 2011( $\text{m}^3$ )	August 2011 ( $\text{m}^3$ )	September 2011 ( $\text{m}^3$ )	October 2011 ( $\text{m}^3$ )	WHOLE PERIOD LINEAR SPRINGS CONTRIBUTION
As10-As30	401956	279889	144288	26612	4367	857111
As30-As45	1024163	1072575	1135210	1105035	792865	5129847
As45-As50	1113653	905646	526867	230645	540862	3317674
					<b>TOTAL</b>	<b>9304632</b>

Tab. 6.3.1.5. Linear springs contribution from June to October 2011

## 6.4. The post-earthquake state

In the table below (Tab. 6.4.1.) are reported daily river flow data from June to October 2018, collected with the methodology previously described.

Section	Elevation m.a.s.l.	Description	June 2018 (l/s)	Aug 2018 (l/s)	Sept 2018 (l/s)	Oct 2018 (l/s)
As10	952	Highest spring	0	0	0	0
As30	945	Downstream Fonte Cerasa confluence	0	0	0	0
As45	895	CIIP hydrometer	56	0	0	0
As50	875	Upstream 1 <sup>st</sup> ENEL deviation	262	32	15	34

Tab. 6.4.1. Daily river flow values June 2018-October 2018

### 6.4.1. Stream hydrographs and yielded volumes

Here below are reported hydrographs, total monthly and whole season yielded volumes of the single hydraulic sections after the 2016-2017 seismic sequence.

#### Section As10 – Highest spring – 2018

During the entire 2018 survey campaign no water has been observed here, so the flow rate is 0 l/s and the yielded volume is 0 m<sup>3</sup> from June, 1<sup>st</sup> 2018 to October, 31<sup>st</sup> 2018.

#### Section As30 – Downstream Fonte Cerasa confluence – 2018

No water observed for the same period: flow rate is 0 l/s and yielded volume is 0 m<sup>3</sup>.

#### Section As45 / L\_895 – CIIP hydrometer – 2018

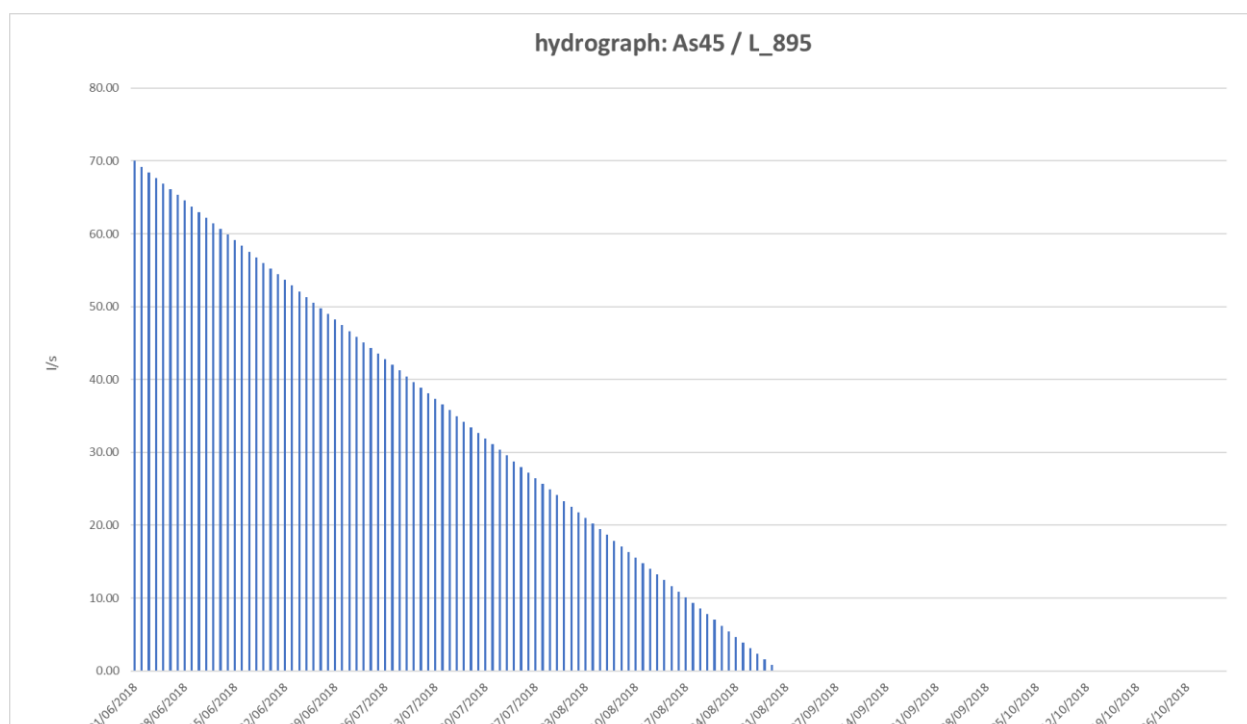


Fig. 6.4.1.1. As45 hydrograph for the 2018 period. ©Microsoft Excel

<b>Section: As45 / L_895</b>	Elevation m a.s.l.	June 2018	July 2018	August 2018	September 2018	October 2018	<b>Total</b>
<b>Yielded volume (m<sup>3</sup>)</b>	895	152208	93744	29232	0	0	275184

Tab. 6.4.1.1. As45 yielded volumes in the 2018 period

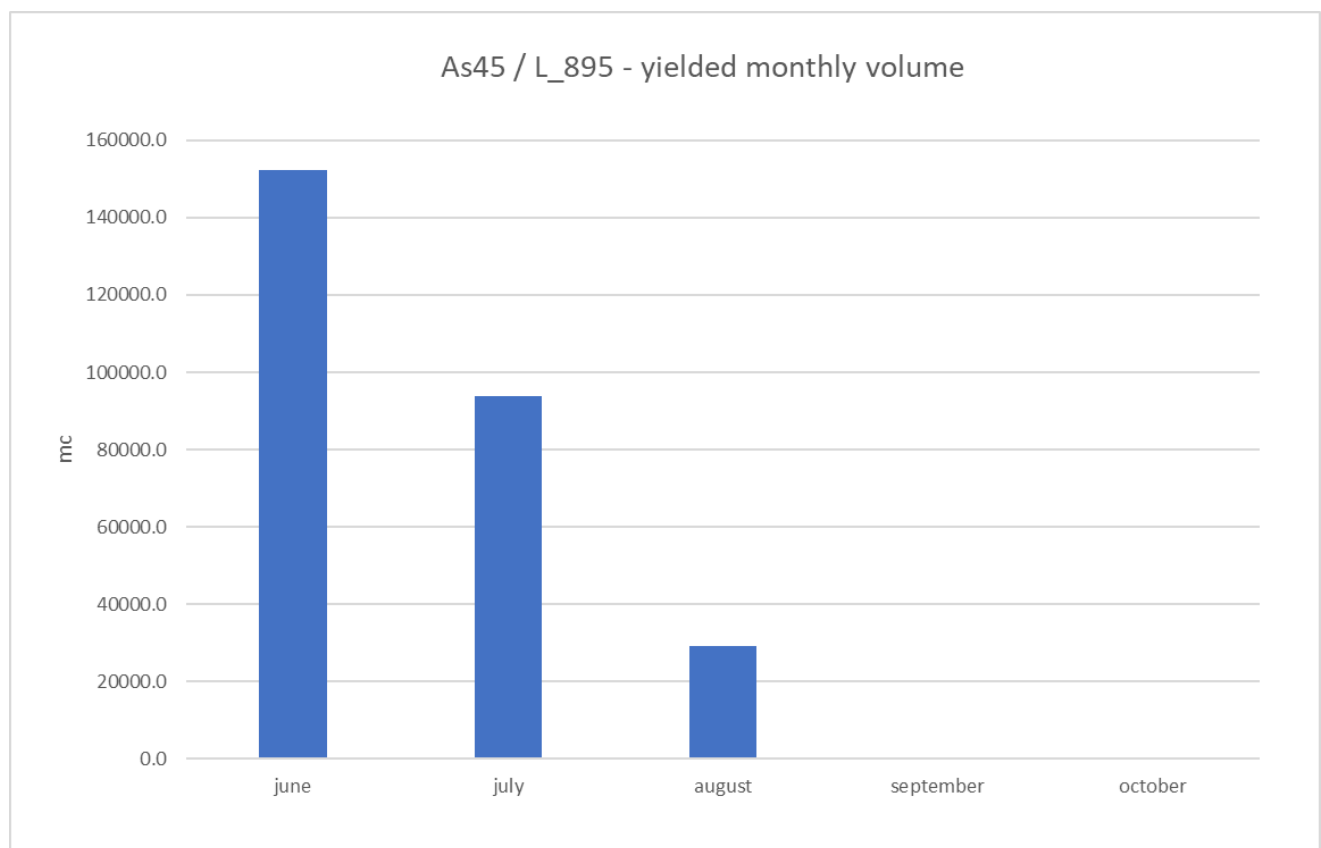


Fig. 6.4.1.2. As45 yielded volumes in the 2018 period. ©Microsoft Excel

#### Section As50 / L\_886 – Upstream 1<sup>st</sup> ENEL deviation – 2018

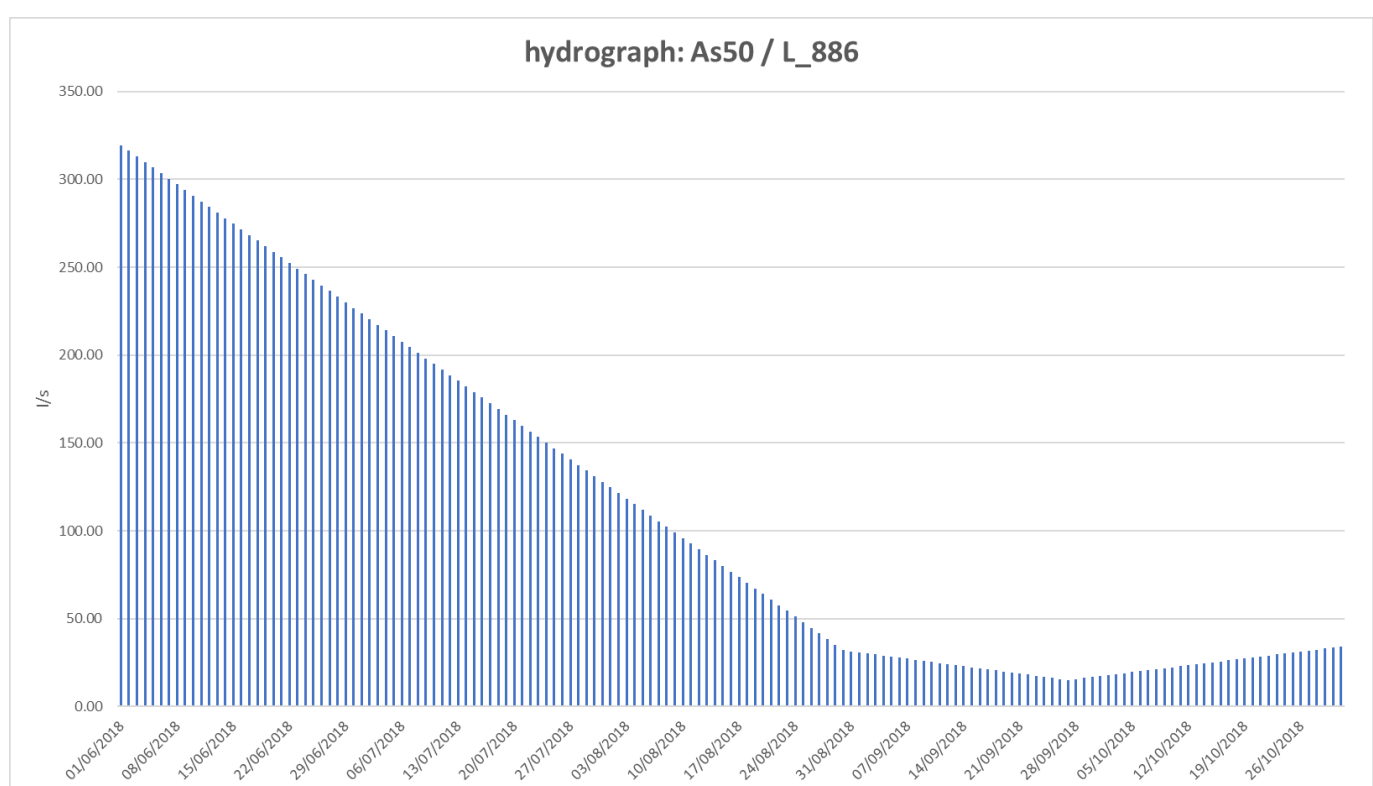


Fig. 6.4.1.3. As50 hydrograph for the 2018 period. ©Microsoft Excel

Section: As50 / L_886	Elevation m a.s.l.	June 2018	July 2018	August 2018	September 2018	October 2018	Total
Yielded volume (m <sup>3</sup> )	886	708084	470729	205716	57582	68614	1510726

Tab. 6.4.1.2. As50 yielded volumes in the 2018 period

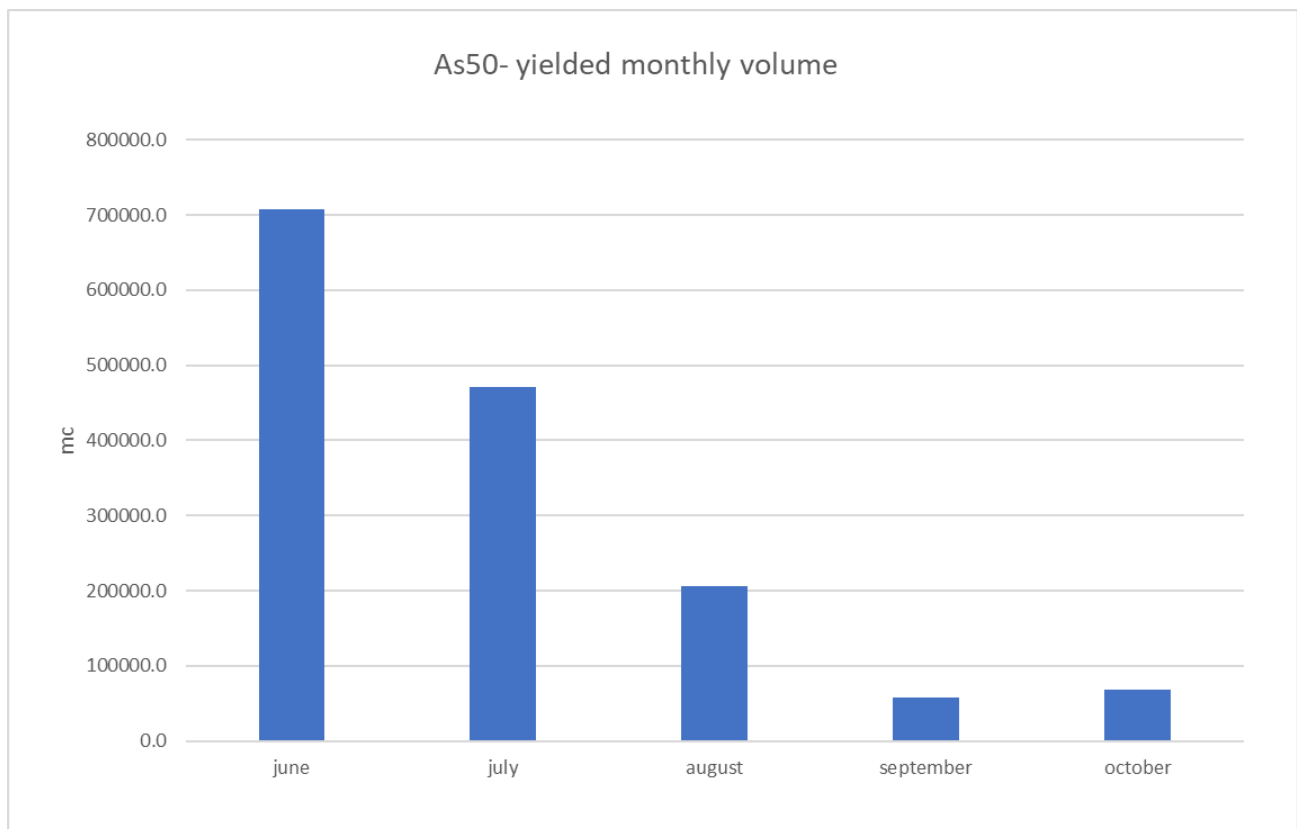


Fig. 6.4.1.4. As50 yielded volumes in the 2018 period. ©Microsoft Excel

Monthly and whole period data of segment increments.

SECTOR	June 2018 (m <sup>3</sup> )	July 2018 (m <sup>3</sup> )	August 2018 (m <sup>3</sup> )	September 2018 (m <sup>3</sup> )	October 2018 (m <sup>3</sup> )	WHOLE PERIOD LINEAR SPRING CONTRIBUTION
As10-As30	0	0	0	0	0	0
As30-As45/L_895	152208	93744	29232	0	0	275184
As45/L_895-As50/L_886	555876	376985	176484	57582	68614	1235542
					<b>TOTAL</b>	<b>1510726</b>

Tab. 6.4.1.3. Linear springs contribution from June to October 2018

## 6.5. The pre/post-earthquake comparison

In the underlying diagram (Fig. 6.5.1.), the total volumes provided by the aquifers in the different sectors from July 2011/2018 to October 2011/2018 are reported.

It is evident that, from Tab. 6.4.1.3. and Fig. 6.5.1.:

1. In 2011 the greater aquifer contribution came from the As30 – As45/L\_895 sector. The most upstream sector, showed the lower value.
2. **A sharp decrease in the yielded volume is immediately noticeable, with the As10-As30 sector completely dried during the 2018 post-earthquake surveys.**
3. After the earthquake the greater contribution came from the most downstream sector.

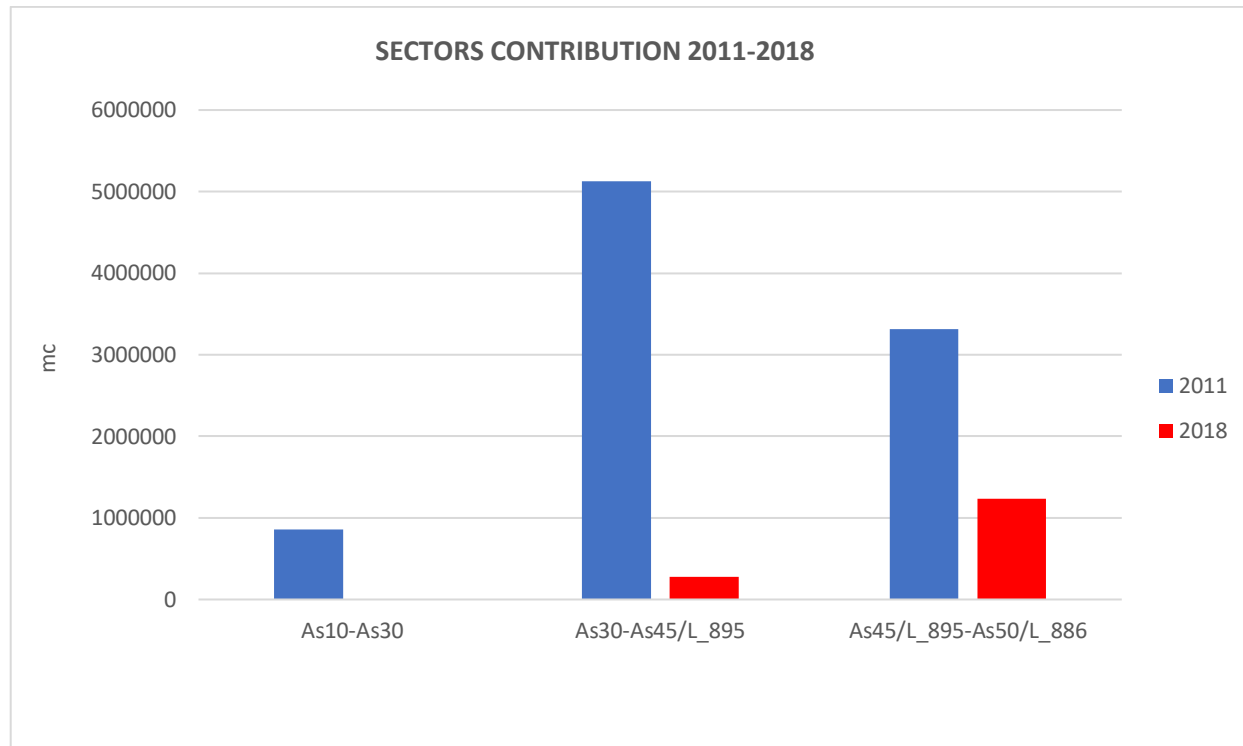


Fig. 6.5.1. Linear springs contribution in 2011 and 2018 periods. ©Microsoft Excel

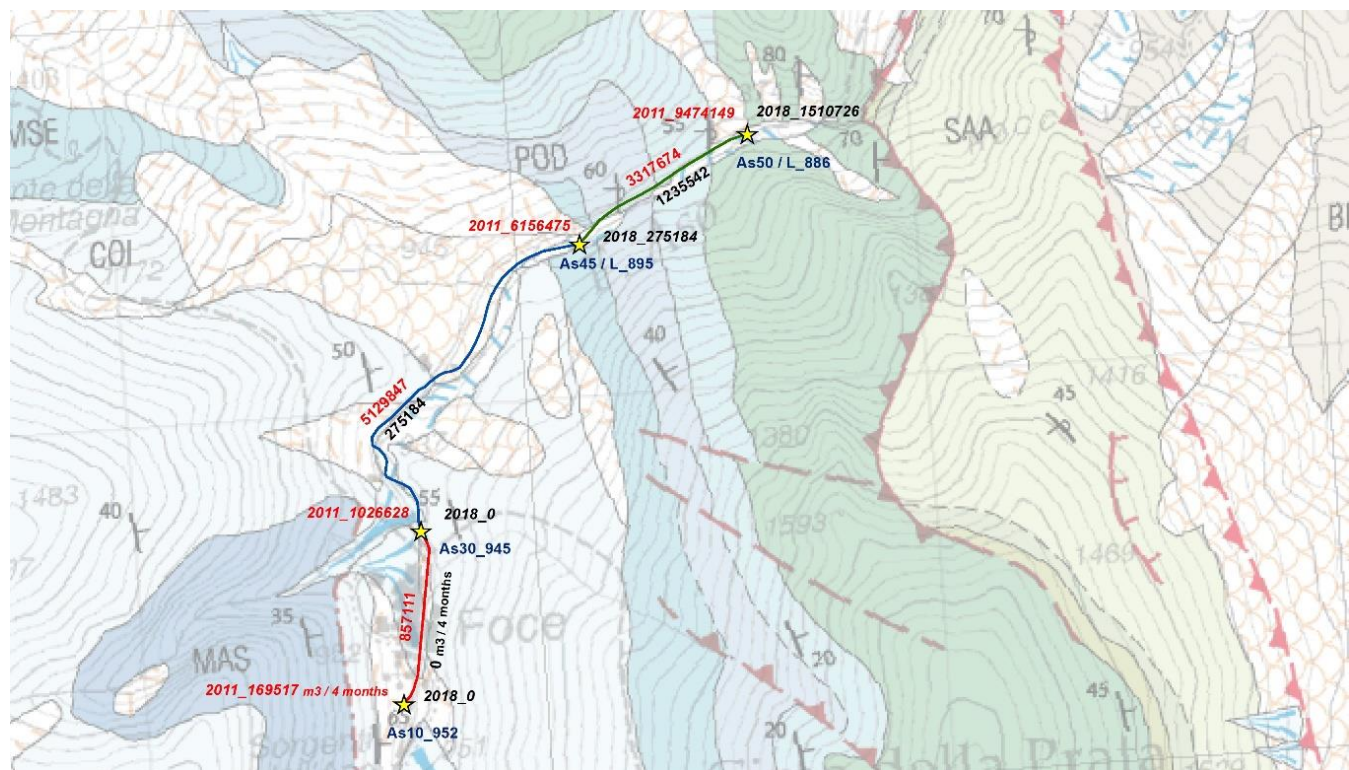


Fig. 6.5.2. The 2011/2018 linear spring segments loss. Basemap: modified with ©ArcMap 10.2 after Pierantoni et al. (2013)

Considering the results, it was therefore necessary to estimate the volumes of water lost between June and October for each segment (Tab. 6.5.1.), to better understand the effects of the 2016-2017 seismic sequence on the hydrogeological setting of the area.

LINEAR SPRING MONTH LOSS (m <sup>3</sup> )	June	July	August	September	October	LINEAR SPRING TOTAL LOSS	% Loss
As10-As30	-401956	-279889	-144288	-26612	-4367	-857111	<b>-100</b>
As30-As45/L_895	-871955	-978831	-1105978	-1105035	-792865	-4854663	<b>-95</b>
As45/L_895- As50/L_886	-557777	-528661	-350383	-173063	-472248	-2082132	<b>-63</b>
					<b>TOTAL</b>	<b>-7793906</b>	<b>-84</b>

Tab. 6.5.1. Linear spring monthly and total losses

The higher total absolute loss has been calculated for the As30 – As45/L\_895 sector with a magnitude slightly lower than 5 million m<sup>3</sup> (Tab. 6.5.1. and Fig. 6.5.3.) The estimated cumulative lost water volume over 5 months touches the 8 million m<sup>3</sup> (Tab. 6.5.1.).

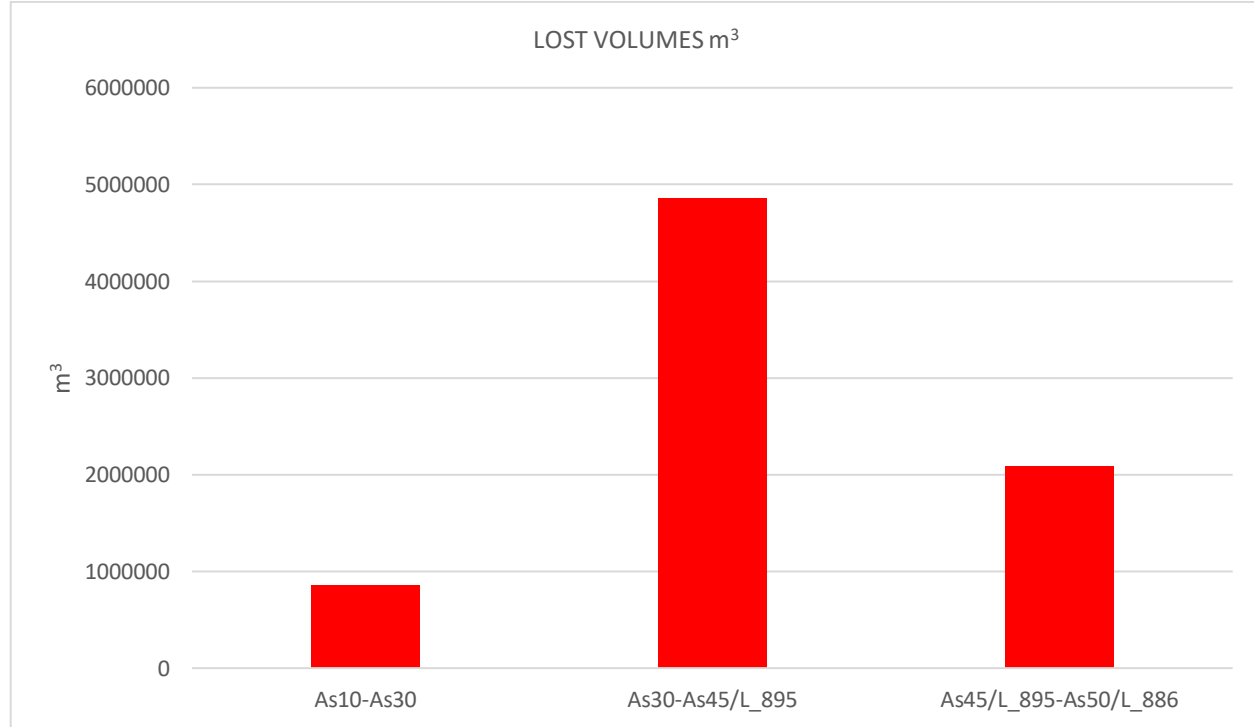


Fig. 6.5.3. Linear spring total losses. ©Microsoft Excel

The underlying graph displays the volume percentage lost (Fig. 6.5.4.):

1. the complete drying of the As10 – As30 sector (-100%);
2. a 95% decrease in the As30 – As45/L\_895 part;
3. a 63% decrease between the As45/L\_895 and As50/L\_886 sections.

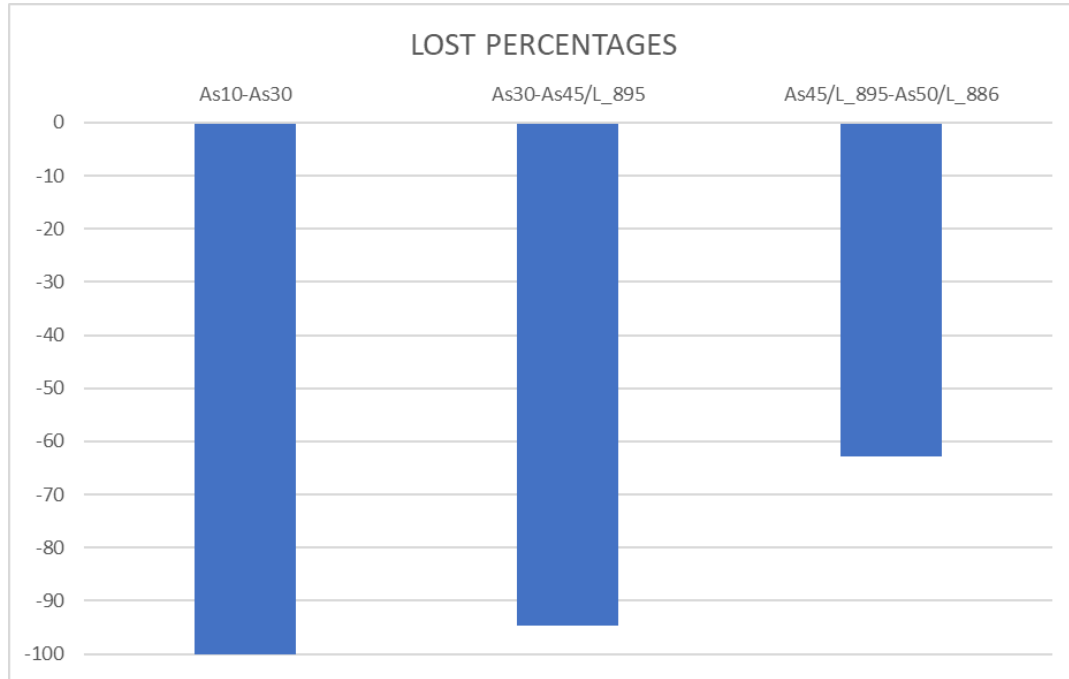


Fig. 6.5.4. Linear spring percentage losses. ©Microsoft Excel

The percentage total loss over the considered time interval is about the 84%.

The correlation between these data and the hydrogeological setting of the area suggests a different behavior for each hydrogeological complex. **The river flow between the sections As10 and As45/L\_895 seems to have more suffered the earthquake effects respect to the further downstream segment (As45/L\_895 – As50\_886).**

## 6.6. The river first-emergence evolution

To have an even more defined view of the earthquake-related hydrogeological effects on this part of M.S. National Park, a monitoring of the river first-emergence was performed, collecting GPS coordinates (by GARMIN-GPSMAP® 64s) throughout the survey period, with a time lag of 2-3 days after the last rainfall (except for the October survey) to consider only the baseflow contribution.

In the following table (Tab. 6.6.1.) first emergences (monthly step), elevation and planimetric changes during the summer-autumn season are listed.

DATE	19/6/2018	16/7/2018	30/8/2018	27/9/2018	31/10/2018	AVERAGE
ELEVATION (m a.s.l.)	904	901	895	892	893	897
DELTA ELEVATION (m)		-3	-6	-3	+1	-
PLANIMETRIC DISTANCE (m)		-28	-65	-104	+12	-

Table 6.6.1. River first emergence evolution: positive = towards upstream / negative = towards downstream

The following map (Fig. 6.6.1.) shows the seasonal downstream migration of the river first emergence, (except between September and October), when it slightly rises upstream probably because of the rainfalls in the previous days of the October sampling.

This fact evidences that:

- a) the river first emergence point, net of the surface runoff, steadily moves downstream in the considered time period;
- b) the river first emergence point slightly rises up in correspondence of rainfalls events. Later, when the runoff vanishes, it returns to the initial level.

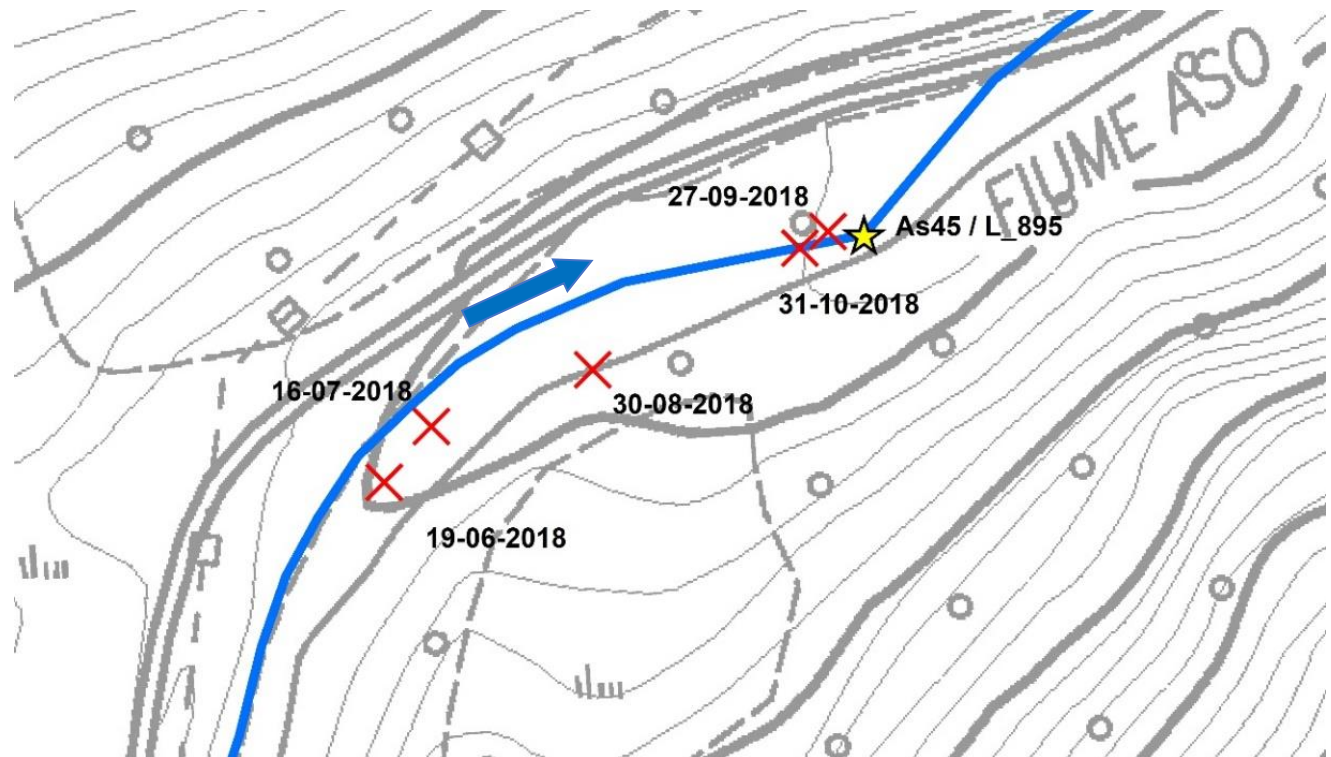


Fig. 6.6.1. Migration of Aso river first emergence during the 2018 survey period. The blue arrow indicates the river flow direction. Basemap: modified with ©ArcMap 10.2 from CTR Regione Marche Foglio 325120

However, to exclude possible short-term influence of rainfalls on the first emergence location, net of the runoff, daily pluviometric data from June to October 2018 are reported (Fig. 6.6.2. and Fig. 6.6.3.) for a comparison.

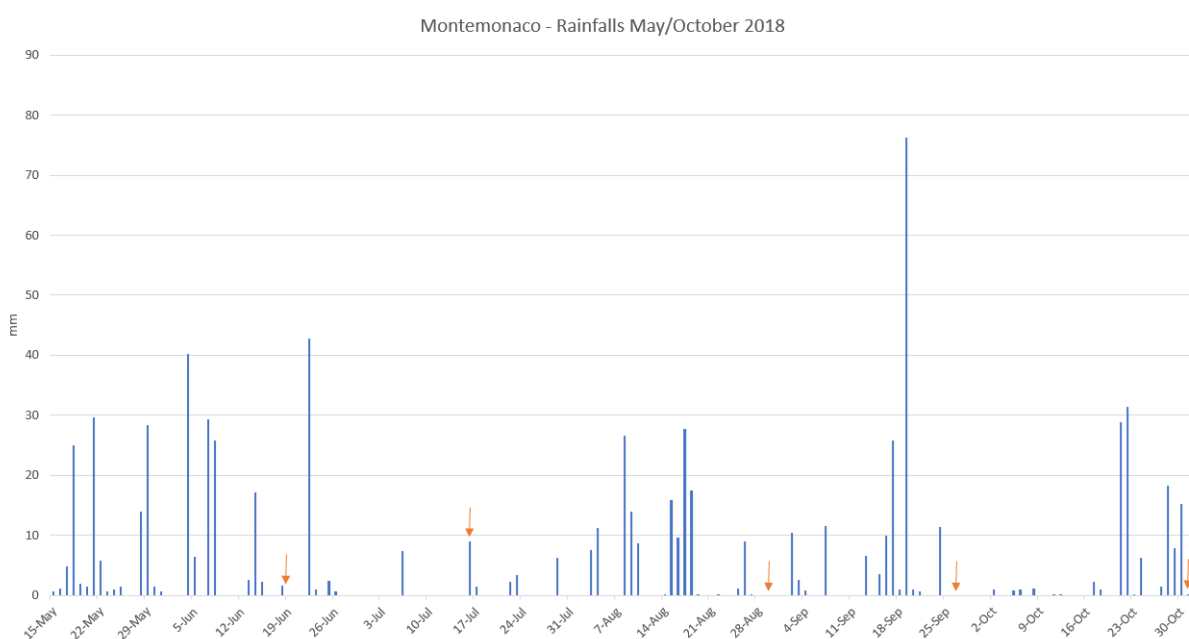
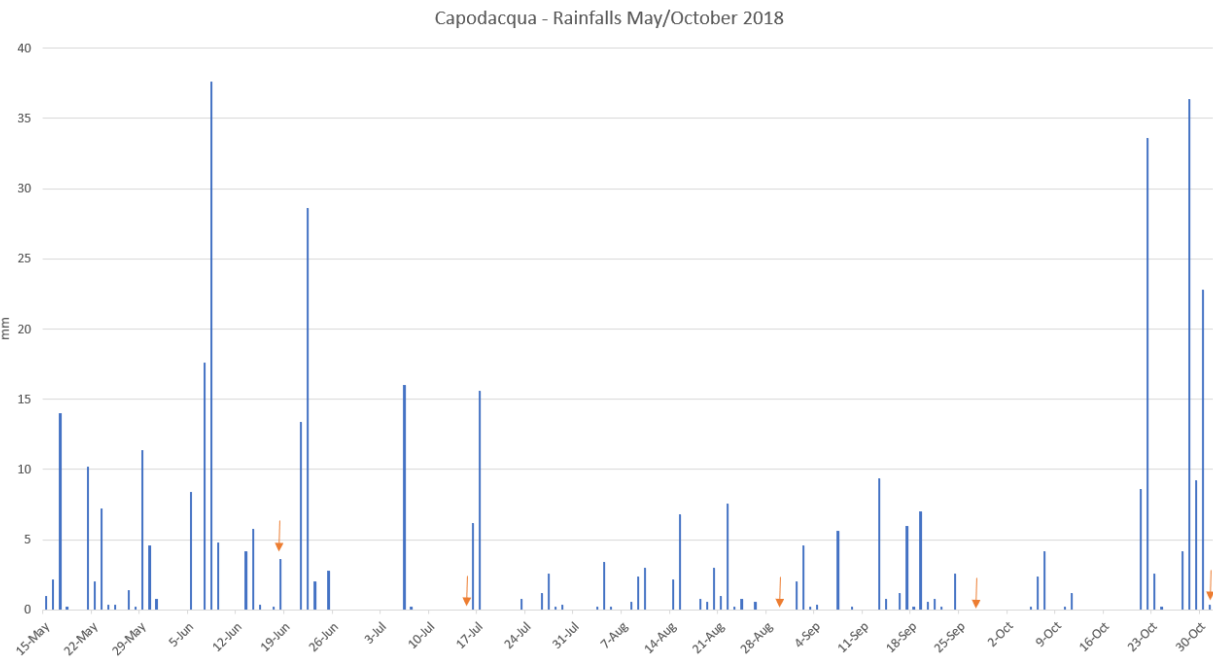


Fig. 6.6.2. Rainfalls recorded in Montemonaco from May to October 2018. ©Microsoft Excel



6.6.3. Rainfalls recorded in Capodacqua from May to October 2018. ©Microsoft Excel

## 6.7. Considerations

The most relevant and noticeable event caused by the 2016-2017 seismic sequence, directly connected to the flow rate loss previously analyzed, is the **important downstream migration of the river first emergence**. During the 2011 survey campaign it was located approximately in correspondence of the As10 section (945 m a.s.l.), immediately upstream of Foce (Fig. 6.6.4.). In 2018 the river first-emergence was situated 1 km before the village, on average at about 900 m a.s.l (Fig. 6.6.5.). **Conceivably, everything is probably tied to a ~ 50 m lowering of the aquifer piezometric level.**



Fig.6.6.4. The Aso river bed close to the As10 section. This is the situation in April, 25<sup>th</sup> 2019, i.e. the same found during all the 2018 surveys.

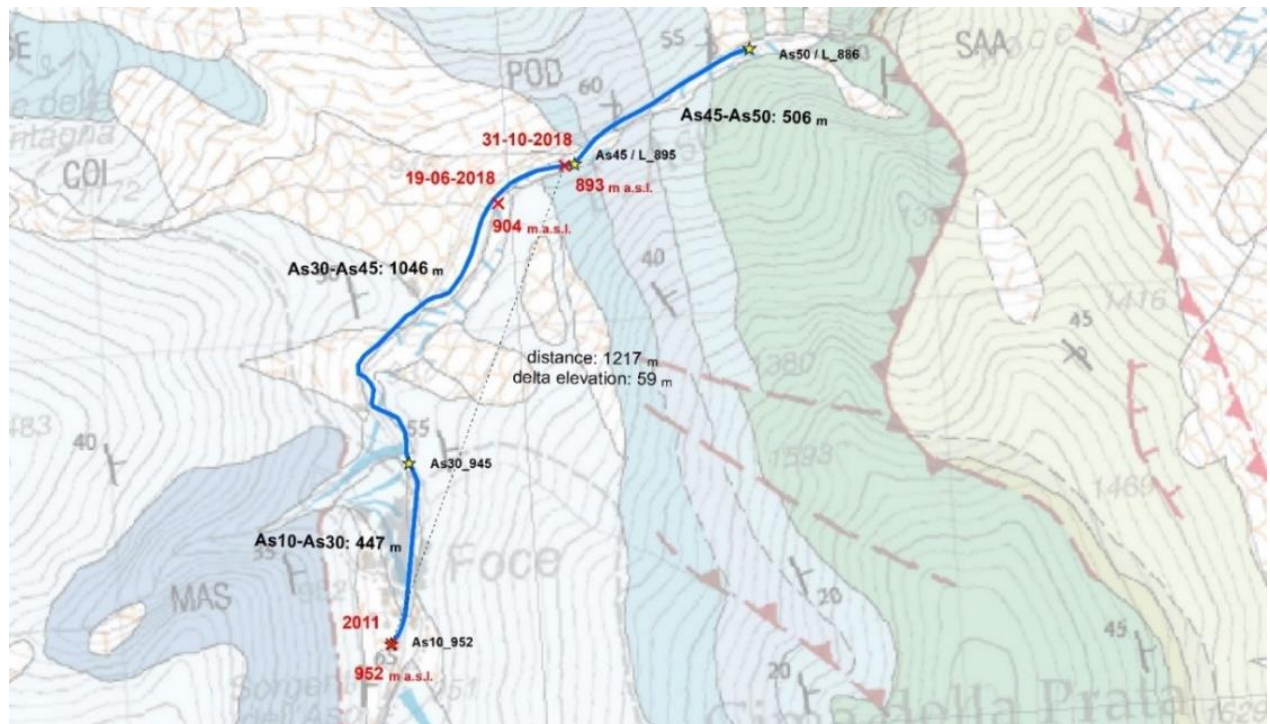


Fig.6.6.5. The huge downstream migration of the first emergence between 2011 and 2018. Basemap: modified with ©ArcMap 10.2 after Pierantoni et al. (2013)

The previous sector contribution chart (Fig. 6.5.1.) highlights that in 2018 the higher contribution to the Aso river flow rate came from the As45-As50 sector. A clearer view on this part of the aquifer setting can be obtained looking at the NNW-SSE geological section (Fig. 6.6.5.). In the geological cross section, we can recognize the Basal aquifer, overlying the *Formazione della Laga* by means of the Sibillini thrust plane, which extends for about 9 km from the on-thrust projection of the Jurassic normal fault, crossing the S slopes of Monte Vettore, to the Aso river linear emergence and further north.

Our goal is the recharge area estimation of the As45-As50 sector and, based on the geological study of Pierantoni et al. (2013), we have hypothesized its initial areal extension of about 10 km<sup>2</sup>.

By means of the hydrogeological balance (Fig. 6.6.8.), according to which the precipitations (entrances) in the area should almost coincide with the aquifer yielded water volume (outcomes), it was possible to correct the recharge area extent.

The entrances estimation was made with the cumulative annual precipitations, considering the following equation (valid in the Monti Sibillini area) relating the site excepted precipitation with its elevation:

$$P(x) = 0.636 * x + 691.1$$

where:  $x$  is a certain elevation and  $P(x)$  is the annual cumulative precipitation expected for that elevation.

The recharge area average elevation is 1720 m a.s.l., so the obtained precipitation value equals 1785 mm both for 2011 and 2018. This may seem too much approximate, but considering that the Basal aquifer has a renewal time often higher than one or more hydrologic years, the method is enough reliable.

The calculation of the evapotranspiration, made with Turc and Thornthwaite methods, needs also the knowledge of the average monthly temperature (Montemonaco climatic station RT-1588) for the whole 2011 and 2018. Finally, we obtain the recharge value for the hydrologic year.

TURC								
$A_{\text{basin}} (\text{m}^2)$								
8528066								
<b>2011</b>								
$Q_0 (\text{l/s})$	$Q_t (\text{l/s})$	$T (\text{d})$	$\alpha$	$P (\text{mm})$	$ETR (\text{mm})$	$P_{\text{eff}} (\text{mm})$	$I_{\text{eff}} (\text{mm})$	$V_{\text{tot}} (\text{m}^3/\text{y})$
566	53	123	0.01925469	1785.02	378.958	1406.06	1265.45603	10523491.9
$W_0 (\text{m}^3)$	$W_t (\text{m}^3)$	$\Delta W (\text{m}^3)$	$T_{\text{rin}} (\%)$	$t_{\text{rin}} (\text{yr})$	$DT_t (\text{d})$	$R (\text{m}^3/\text{y})$	$I_{\text{eff}} (\text{mm})$	
2539765.92	237875.20	2301890.72	0.90634	1.10334	51.9342	10791892.6	1233.9834	
$Q_0 (\text{l/s})$ = starting recession flow								
$Q_t (\text{l/s})$ = ending recession flow								
$T (\text{g})$ = recession time								
$\alpha$ = recession coefficient								
$W_0 (\text{m}^3)$ = dynamic storage								
$W_t (\text{m}^3)$ = ending recession storage								
$\Delta W (\text{m}^3)$ = recession yielded volume								
$T_{\text{rin}} (\%)$ = renewal rate								
$t_{\text{rin}} (\text{a})$ = renewal time								
$DT_t (\text{d})$ = delay time								
$P (\text{mm})$ = precipitations								
$ETR (\text{mm})$ = real evapotranspiration								
$P_{\text{eff}} (\text{mm})$ = effective precipitations								
$I_{\text{eff}} (\text{mm})$ = effective infiltration								
$R (\text{m}^3)$ = recharge during the hydrologic year								

Fig. 6.6.8. Hydrogeological balance computation table. ©Microsoft Excel

The water outcomes have been estimated through the whole-year extension of the As45-As50 sector hydrograph, already calculated for the sampling period. To get an idea of the annual trend of the Aso river flow rate we have used the hydrometer values of San Giorgio all'Isola (RT-3246) for 2018, but not for 2011 because it was installed only recently. The values obtained from the study of Nanni & Petitta (2010 & 2012) help us for the 2011 trend estimate. Once obtained the hydrograph, the calculation of the annual yielded volume was simple.

Finally, from the comparison between entrances and outcomes, it results that the obtained recharge values are congruent with the annual yielded volumes. Therefore, a recharge area wide approximately  $8.5 \text{ km}^2$  is almost correct (Fig. 6.6.6.). However, the interpolation used for the rainfalls may underestimate the data; as a consequence, the achieved area may be slightly larger than that obtained.

## Cross section Monte Vettore - Aso river

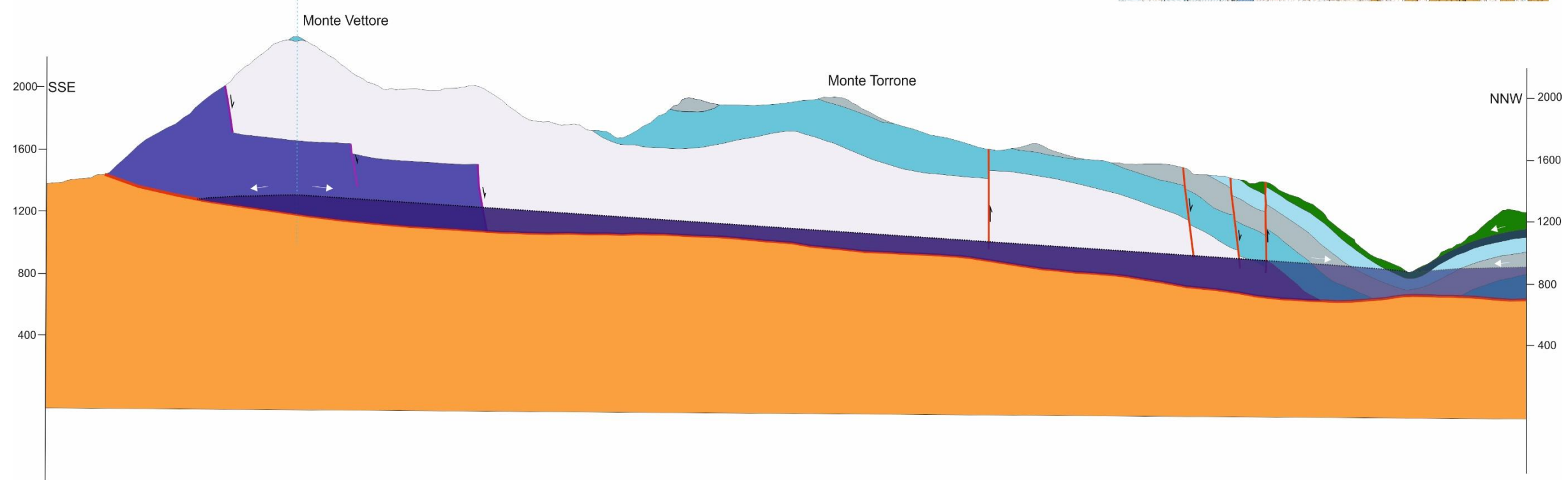
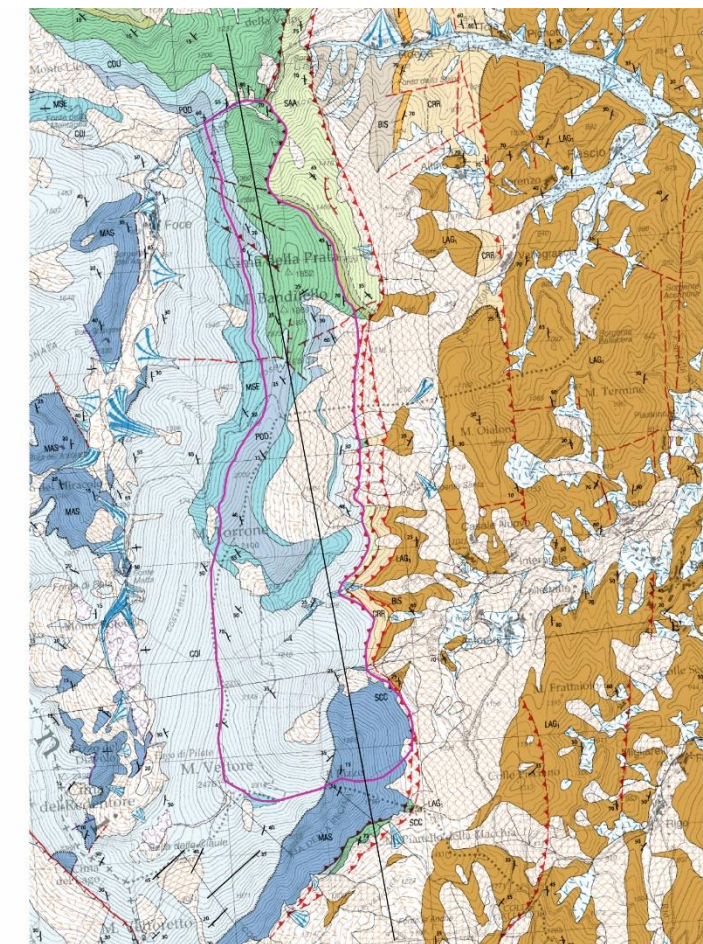


Fig. 6.6.5. Cross section of Monte Vettore – Aso river hydrogeological system. The light blue vertical dashed line highlights the underground watershed. ©CorelDraw 2018. On top-right the reference map from Pierantoni et al. (2013).

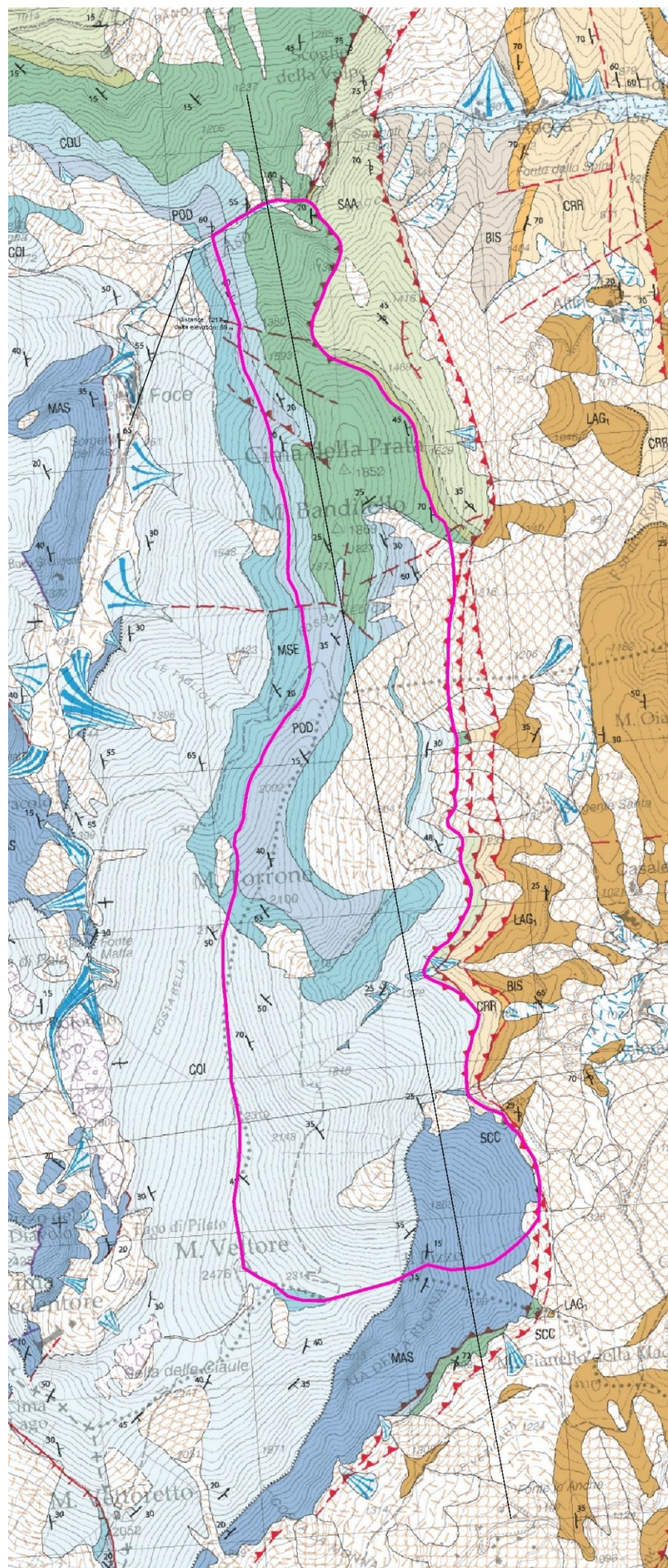


Fig. 6.6.6. Recharge area for the As45-As50 sector in violet. Border: in the N part it coincides with the Aso river; in the E one it is represented by the thrust line; southwards the watershed winds along the Monte Vettore-II Pizzo ridge while westwards with the Monte Vettore - Cima della Prata ridge. The black line indicates the section of Fig. 6.6.5. Basemap: modified with ©ArcMap 10.2 after Pierantoni et al. (2013)

## BASAL AQUIFER PIEZOMETRIC LINES FOR THE N SECTOR

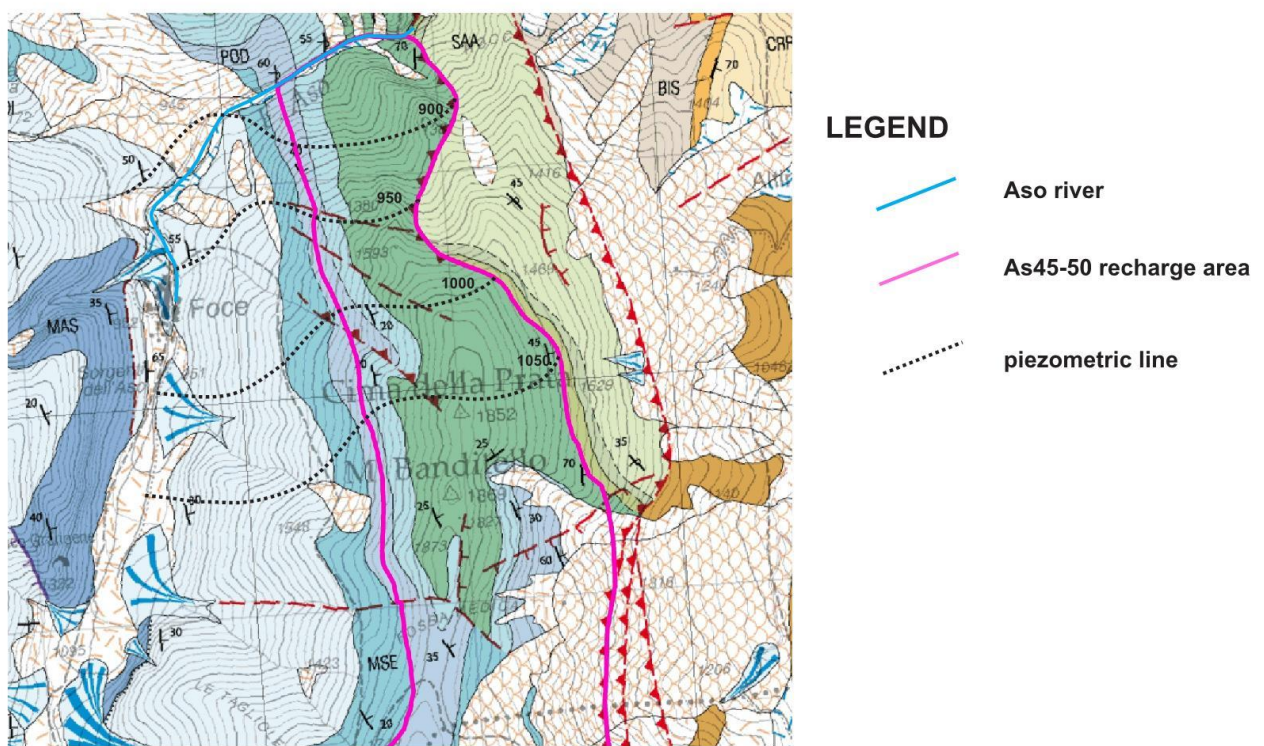


Fig. 6.6.7. Detail of the N part of the area. Basemap: modified with ©ArcMap 10.2 and ©CorelDRAW 2018 from Pierantoni et al. (2013).

**The hypothesized hydrogeological model.** The light-blue dashed line in the section (Fig. 6.6.5.) represents the underground watershed proposed by the model, which coincides with the Monte Vettore – Il Pizzo E-W trending ridge, where the piezometric level reaches its maximum elevation, of about 1300 m a.s.l.. The water table runs out against the thrust plane southwards, while northwards the Basal aquifer is hosted by *Calcare massiccio* and *Corniola*, emerging after 7 km, in the Aso gorge. The linear spring ranges around 900 m a.s.l., with an elevation difference of about 400 m, implying a 57.1 % gradient of the water table. **We can conclude that this uppermost part of the Aso river is mainly sustained by a S to N flow hosted in the Basal aquifer. However, the Maiolica aquifer, hosted in the S slopes of Monte Sibilla, could partly contribute to the river flow.** The part of the Basal aquifer not directly crossed by the section is transparent because of the calcareous-silicic-marly aquiclude complex (*Marne del Monte Serrone*, *Calcari a Posidonia* and *Calcari diasprigni*, whose beds dips ENE), that separates it from the Maiolica aquifer despite the presence of several normal and reverse faults.

## 7. THE SPRINGS

As already mentioned in the hydrogeological setting chapter, S.M. are characterized by three main aquifers, hosted in the Basal, Maiolica and Scaglia calcarea complexes. In the previous section we tried to explain how the 2016-2017 earthquake has altered the Basal aquifer setting. The second part of the work focuses on the possible seismic-related modifications on high altitude springs, which are perched over one or more levels (depending on the structural-stratigraphic setting). An important difference, (other than the discharge), between the baseflow-fed springs and the “high springs” (HS) is the trend of discharges. In the former, the discharge seasonal signal is very weak or even absent, while the latter will show, almost certainly, a higher flow rate seasonal change mainly based on the extension of the recharge area and the length of groundwater circuits.

A common feature of the punctual springs is their geological setting. As can be seen from the underlying geological map (Fig. 7.1.), mostly are located on the E side of anticlinal or, in case of river/glacier-incised valleys, in the central part of the folds.

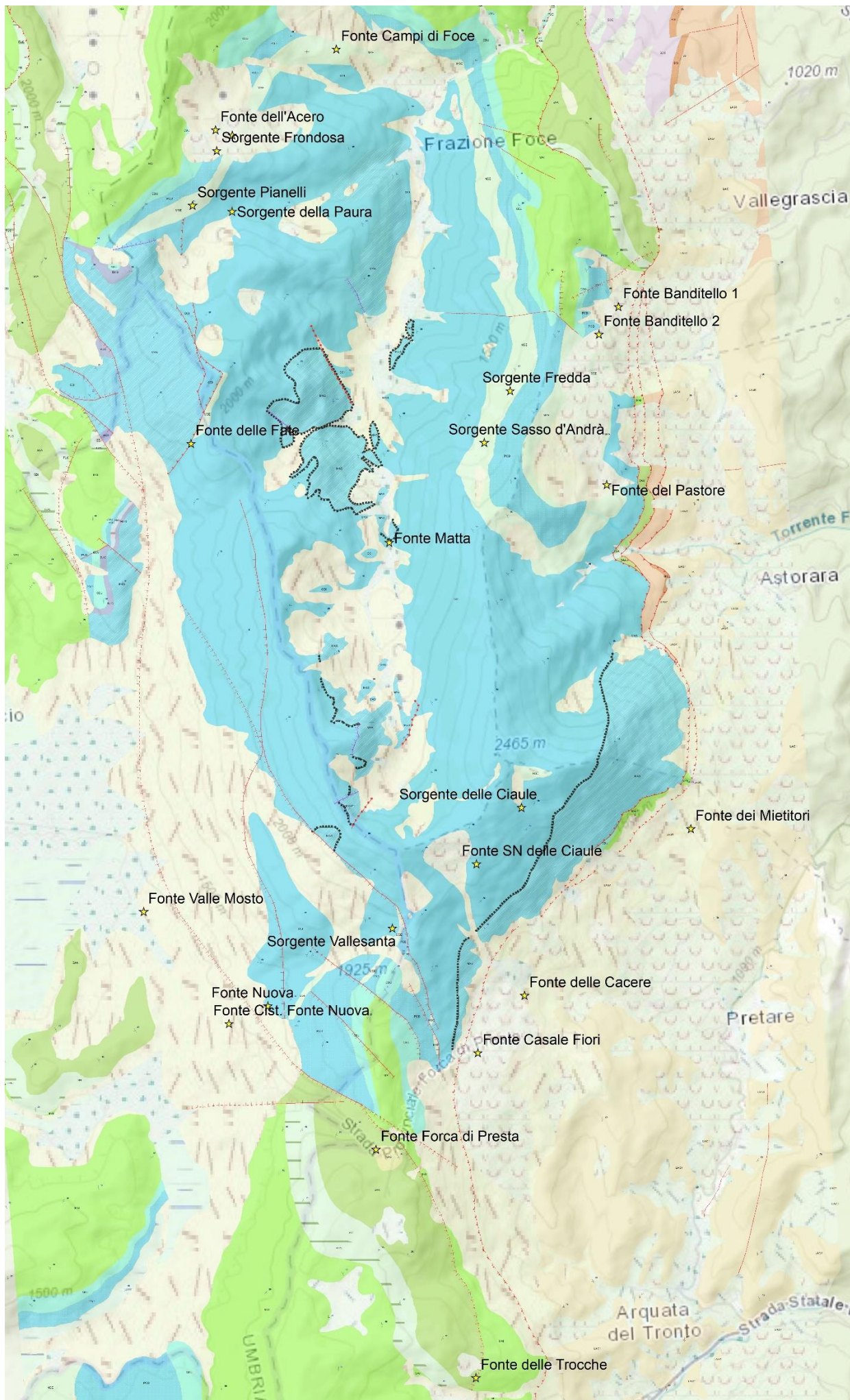


Fig. 7.4. Geological map of the S.M. studied area. Yellow stars: indicate all the springs sampled during the summer-autumn monitoring campaign of 2018, that will continue probably in the next months. Basemap: World Topographic Map modified with ©ArcMap 10.2

Almost all these emergences can be classified as springs with “threshold of permeability” (following the classification of Civita, 2005), and are associated to the presence of thrusts. In this case the feeding is mainly linked to the Maiolica and Basal aquifers, bordered at the base by thrust planes. Three main springs are located on the S-E slopes of Monte Vettore between 1300 and 1400 m a.s.l. (Fonte Casale Fiori, Fonte delle Cacere and Fonte dei Mietitori). In addition, two other emergences have been studied: Fonte delle Ciaule and Fonte SN delle Ciaule, which are fed by slope detrital deposits or by the water circulating in the upper interlayers of the underlying complexes. These springs are characterized by precarious temporary regimes and much poorer flow rates respect to those with a deeper water circulation and a wider supply basin.

However, different areas could have experimented distinct seismic effects on the base of their hydrogeological settings. Therefore, one of the starting points is a detailed geological survey and mapping of the area surrounding each spring. Following this principle, it was possible to subdivide the five springs, all belonging to the SE slope of Monte Vettore, in two groups (Fig. 7.5.):

- those located in the lower area (above the village of Pretare), overlooking the Tronto valley and lying on the Laga sandstones: Fonte Casale Fiori, Fonte delle Cacere and Fonte dei Mietitori;
- the high-altitude springs, sited a little further down the Monte Vettore top, emerging both from the widespread Corniola outcrops: Fonte delle Ciaule and Fonte SN delle Ciaule.

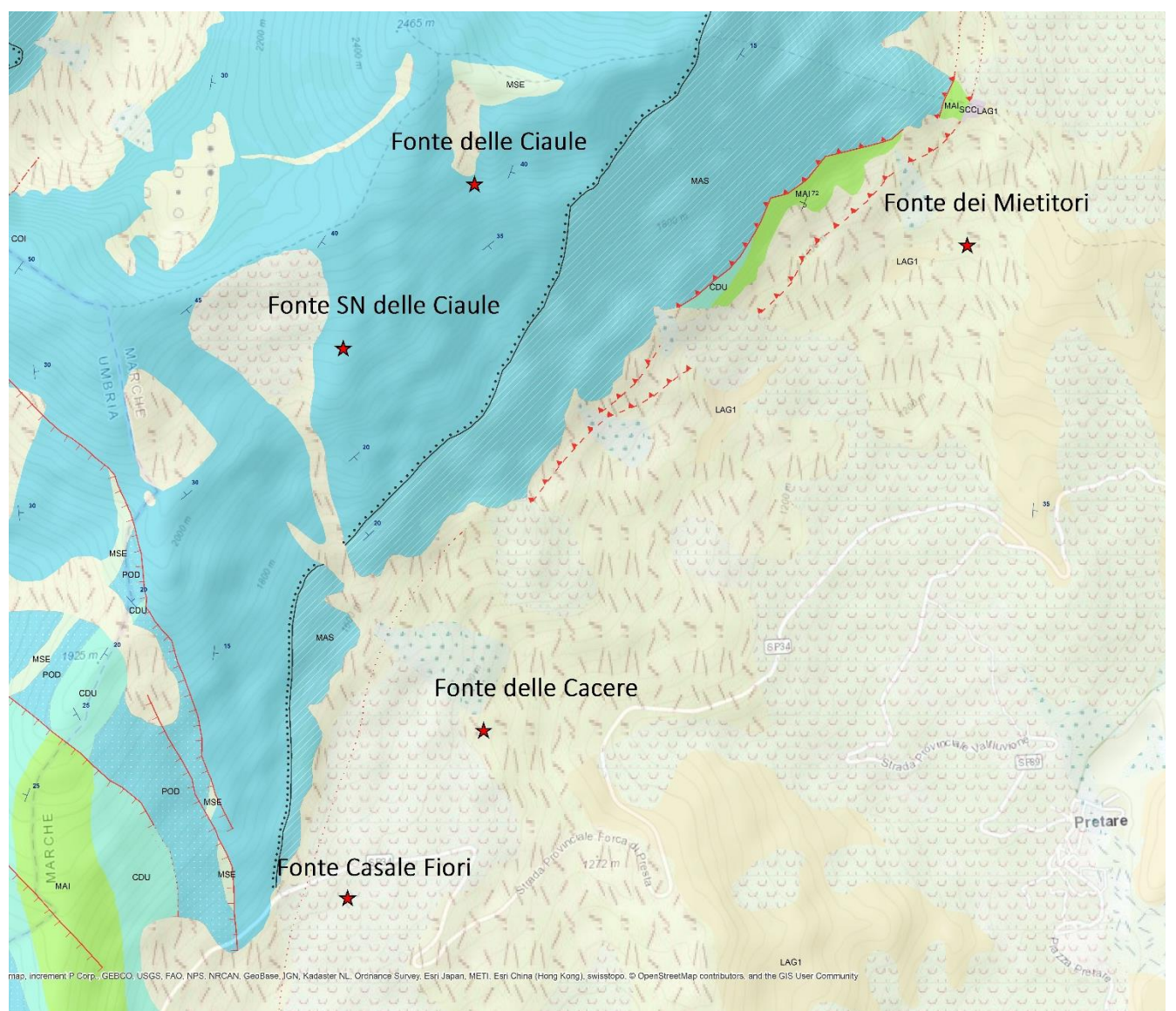


Fig. 7.5. Geological map of the springs area. Basemap: World Topographic Map modified with ©ArcMap 10.2

The underlying geological section (Fig. 7.6.) clearly displays the geological setting where the carbonatic units (*Calcare massiccio* and *Corniola*) lie above the younger turbidites (*Formazione della Laga*), separated by the thrust plane.

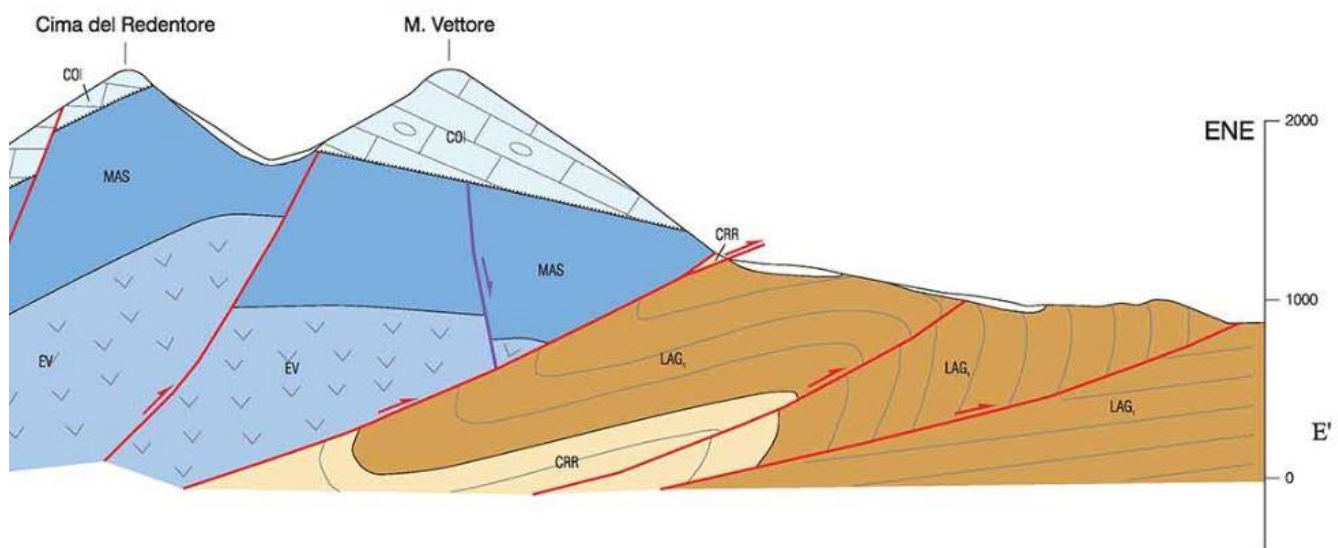


Fig. 7.6. E-W geological cross section crossing the Monte Redentore – Monte Vettore massif. Pierantoni et al. (2013)

### 7.1. Work planning

The method employed is the same used for the Basal aquifer: the pre/post-earthquake data comparison.

Different surveys were performed by the Regional Section of C.A.I. (Club Alpino Italiano) during the years 2010-2011, with the aim of collecting data about:

- flow rate;
- water and air temperature;
- acidity (pH);
- conductivity;
- salinity (hardness and alkalinity).

The new surveys, aimed to detecting any changes in the previously measured parameters, started in the summer 2018.



Fig. 7.1.1. The sampling equipment used during the 2018 surveys: on the left the conductivity/pH-meter (PCE-PHD 1, PCE Instruments©), on the right the graduate bucket

Two phases of springs sampling have been performed: the first, in July 2018, representative of the nearly higher discharge, and the second between September and October 2018 for the seasonal minimum. Due to the 2018-2019 snowy winter, a third sampling has been carried out in February 2019 only for the lower group, because the higher one was inaccessible.

Water samples have been then analyzed with the aim of the researchers of the Chemistry Dept. of the University of Camerino. Following a list of the parameters investigated with significance and method of analysis.

**Total hardness** (sum of calcium and magnesium hardness, in mg/L as CaCO<sub>3</sub>, expressed in French degrees °F): it increases as much as the water travels through the rock volume.

**The method.** The sample is adjusted to a pH of 10 or 12 by means of a buffer solution. In any case the sample is then titrated to its equivalence point using a standard EDTA solution (like complex agent). The indicator is an organic molecule dye (NET or Calconcarbonic) able to form chelant complexes with cations of different colors respect to free molecules. Mg<sup>2+</sup> ions can form a complex with NET only at pH 10, unlike Ca<sup>2+</sup> that can form a stable complex with Carboncarbonic also at pH 12, giving a red color to the solution. The total hardness of the sample is calculated using the precise volume of EDTA solution added when the indicator changes color, as well as the EDTA concentration, in mol/L.

The samples total alkalinity is a measure of water acid-neutralizing capacity to a designated pH. In other words, it is the sum of all titratable bases, including carbonates, bicarbonates, hydroxides, borates, phosphates, silicates and other bases if they are present. The alkalinity has been determined by means of an HCl (hydrochloric acid) titration with the device in Fig. 7.1.2.



Fig. 7.1.2. Mettler© DL21 Titrator

Also, through the ion chromatography, it was possible to determine anions and cations content.

**Ions concentrations**, expressed both in mg/L and meq/L. A milliequivalent is the thousandth fraction, derived from the ratio between the ion concentration (expressed in g/L or mg/L) and its equivalent weight. Respect to the molar mass, it considers the ion valence; so that 1 meq always holds the same number of ions independently by their valence. Milliequivalents allow to compare directly the sum of cations and anions in a series of measurements within a certain solution. In addition, if all the ions of the different dissolved species have been considered, the sum of cations and anions have to coincide (ionic balance).

The steps concerned data interpretation and the pre/post-earthquake comparison, integrated with climatic and geological detailed information, to understand if the 2016-2017 seismic sequence has somehow modified the groundwater circulation in this part of the M.S. National Park.

The presence of several data-hiatus (of different nature) should be pointed out, both in 2010-2011 and 2018-2019 data. An example are the pH values of the pre-sequence surveys collected with the *litmus test* (Fig. 7.1.3.), whose outcome has a low precision compared with the 2018 values measured with an electronic pH-meter (Fig. 7.1.4.). Other cases are the different sampling seasons (that could make the comparison more difficult) or the few ions (only 3), available in the pre-earthquake data, in contrast with the detailed chemical parameters gained for this study. Despite these limitations we tried to get as much knowledge as possible from the available data and, in presence of gaps, founded assumptions have been made.



Fig. 7.1.3. The litmus test



Fig. 7.1.4. The conductivity-meter in pH-mode used during the 2018 surveys (conductivity/pH-meter PCE-PHD 1, ©PCE Instruments)

#### 7.1.1. The interpretation criterion and a general Total Dissolved Solids (T.D.S.) analysis

In order to understand the springs seismic-related effects and the hydrogeological features of the supply basin, pre/post-earthquake measurements have been compared and also, we tried to correlate the available data with the geological features reported in the description.

For instance, if the 2010 conductivity is much lower than that of the 2018, it could mean that the water salinity was increased. A hypothetical triggering factor may be a shaking-induced solubilization of the ions related to the increasing pressure and to the friction inside the porous space. Other assumptions linked to the salt-content, but

regarding both the underground water residence-time and the crossed rocks composition, could be the following:

- a higher hardness could be an index of a longer and deeper underground circulation (with equal crossed rock types);
- instead, considering two underground routes of the same length but with different crossed rocks, the water having the higher hardness will be the one which has crossed the more soluble rock type.

Total dissolved solids (TDS) concentration is the sum of the cations and anions, providing a qualitative measure of the extent of dissolved ions, but does not tell us the nature or ion relationships. It can be measured by means of a direct evaporation method or indirectly from the electrical conductivity. As the conductivity, TDS increases with the water residence time inside the aquifer. Often freshwater TDS is between 0 and 1000 mg/l. Here below are reported the second sampling post-earthquake values (Fig. 7.1.5.) to get a general idea about the overall salinity.

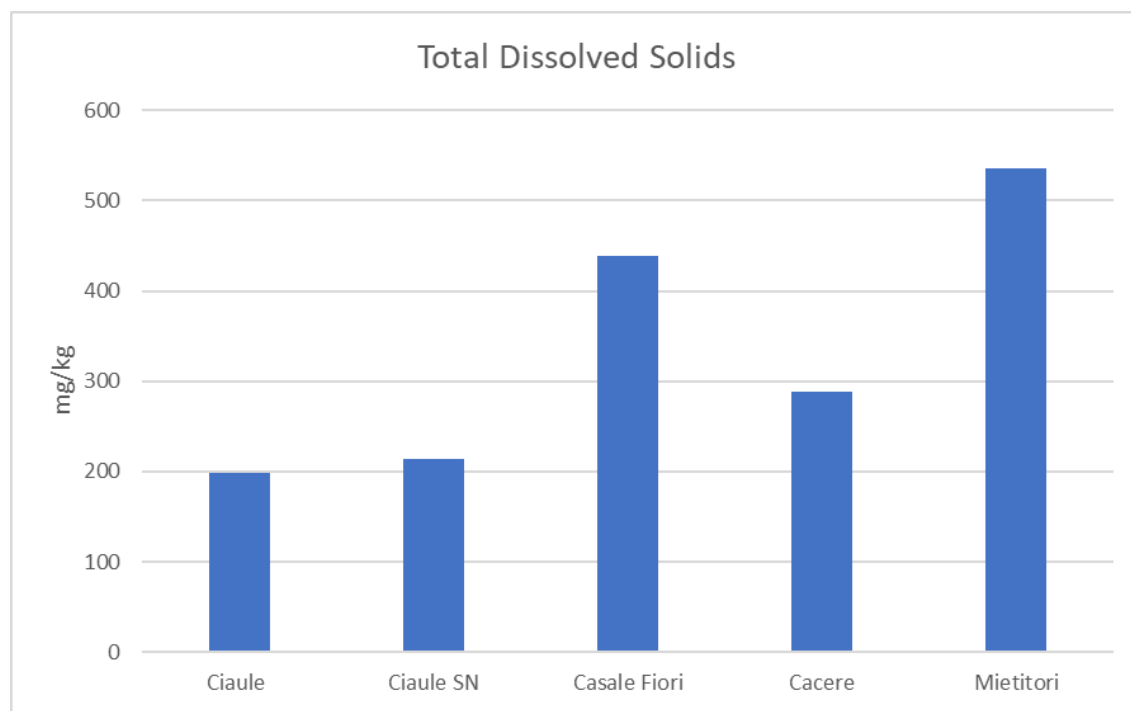


Fig. 7.1.5. Springs TDS data for the September/October period. ©Microsoft Excel

In the next chapters the springs are described also with a detailed geological setting. Later, pre/post-earthquake data are reported and finally discussed.

## 7.2. Fonte delle Ciaule

### 7.2.1. Detailed features and geological setting

Elevation: 2145 m a.s.l. – Hydrographic basin: Tronto

Coordinates: 33T 359214 4742207 UTM / 13°16'40,071" E 42°49'10,13" N

Description: the spring consists of a small drainage tunnel (Fig. 7.2.1.2. and Fig. 7.2.1.3.) that leaves the water flow into the underlying valley. There is also, on the orographic right, a locked intake with a permanent flow (Fig. 7.2.1.1.), (registered both during the 2010-2011 and 2018 surveys) (Aringoli et al., 2017) that during the 2010-2011 surveys, through a pipe, carried the water to the underlying Fonte SN delle Ciaule.



Fig. 7.2.1.1. Fonte delle Ciaule (August, 1<sup>st</sup> 2018); on the left the locked intake. In the pictures below the collection tunnel outside and inside



Fig. 7.2.1.2. and Fig. 7.2.1.3. Spring details (October, 10<sup>th</sup> 2018)

Location: it is found close to the head of a canal that from the top of Monte Vettore (Fig. 7.2.1.4.) falls steeply towards SSE. The spring can be reached following the track from Forca di Presta to Rifugio Zilioli. At Monte Vettoretto turning towards NE, leaving the main track, the Fonte SN delle Ciaule will be reached. Continuing on the same path, sometimes slightly exposed on a steep slope, up to getting around the right shoulder of the canal beyond which there is the spring.

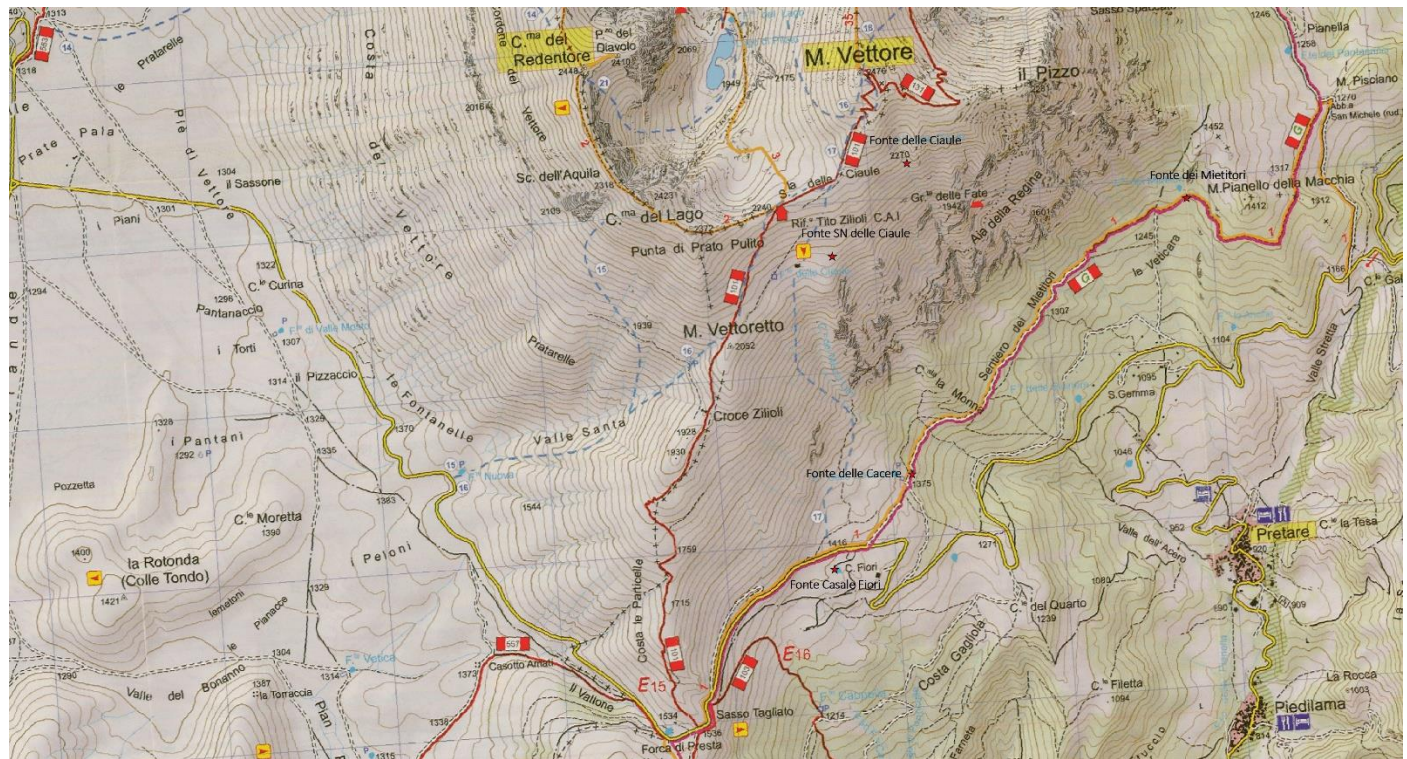


Fig. 7.2.1.4. Map of the southern side of Monte Vettore. CAI – Monti Sibillini – Carta dei Sentieri 1:25'000

**Geological features.** The spring (group b) emerges from the *Corniola* (COI) formation dipping 35°–40° SE (Fig. 7.2.1.5.). Due to the elevation, the hydrogeological basin is very limited and the alimentation is probably linked to the most surficial *Corniola* strata and to the slope deposit located in the canal immediately above the spring. The fact is confirmed, as will be seen later, by the pronounced seasonal flow regime.

## Cross section Fonte SN delle Ciaule

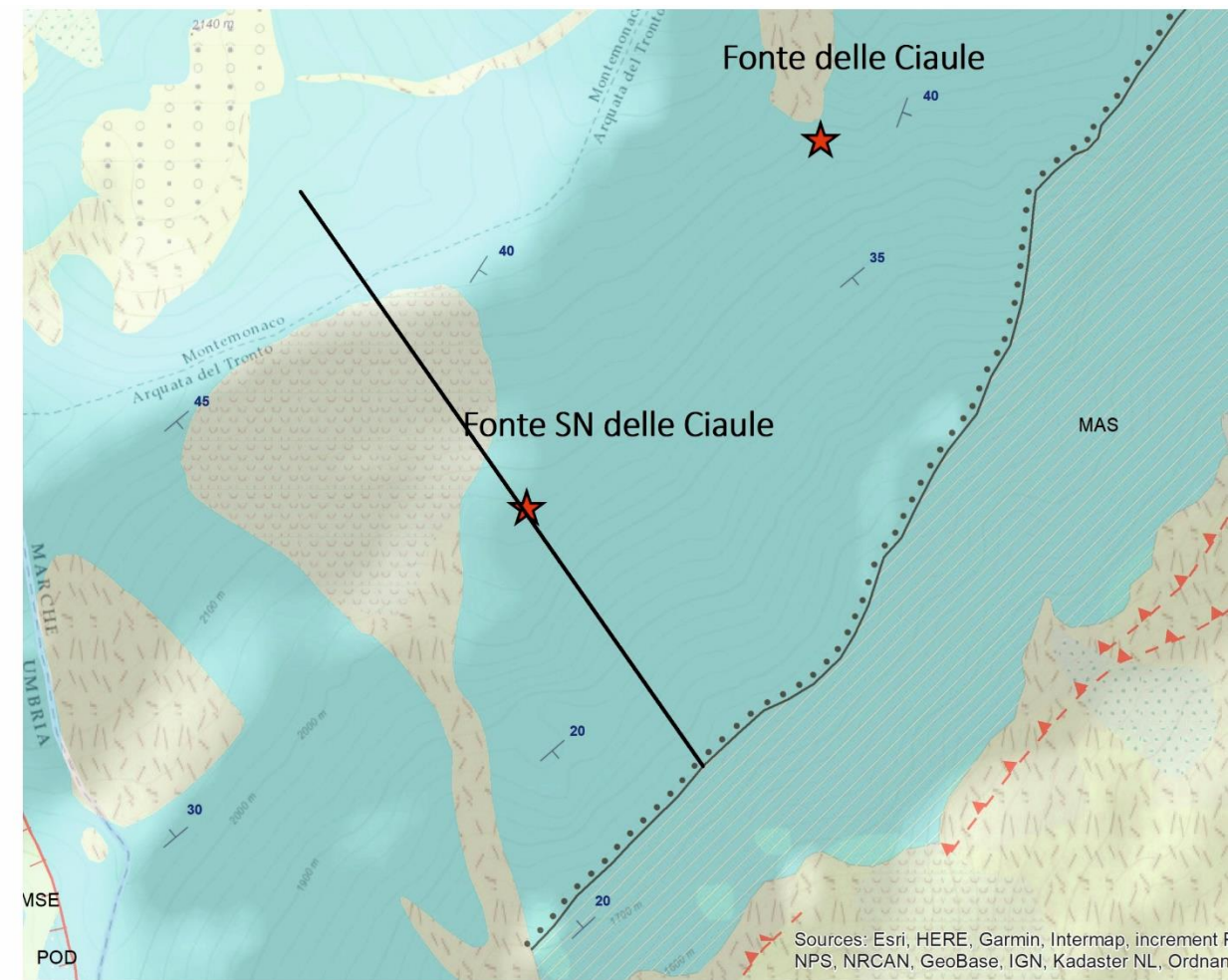
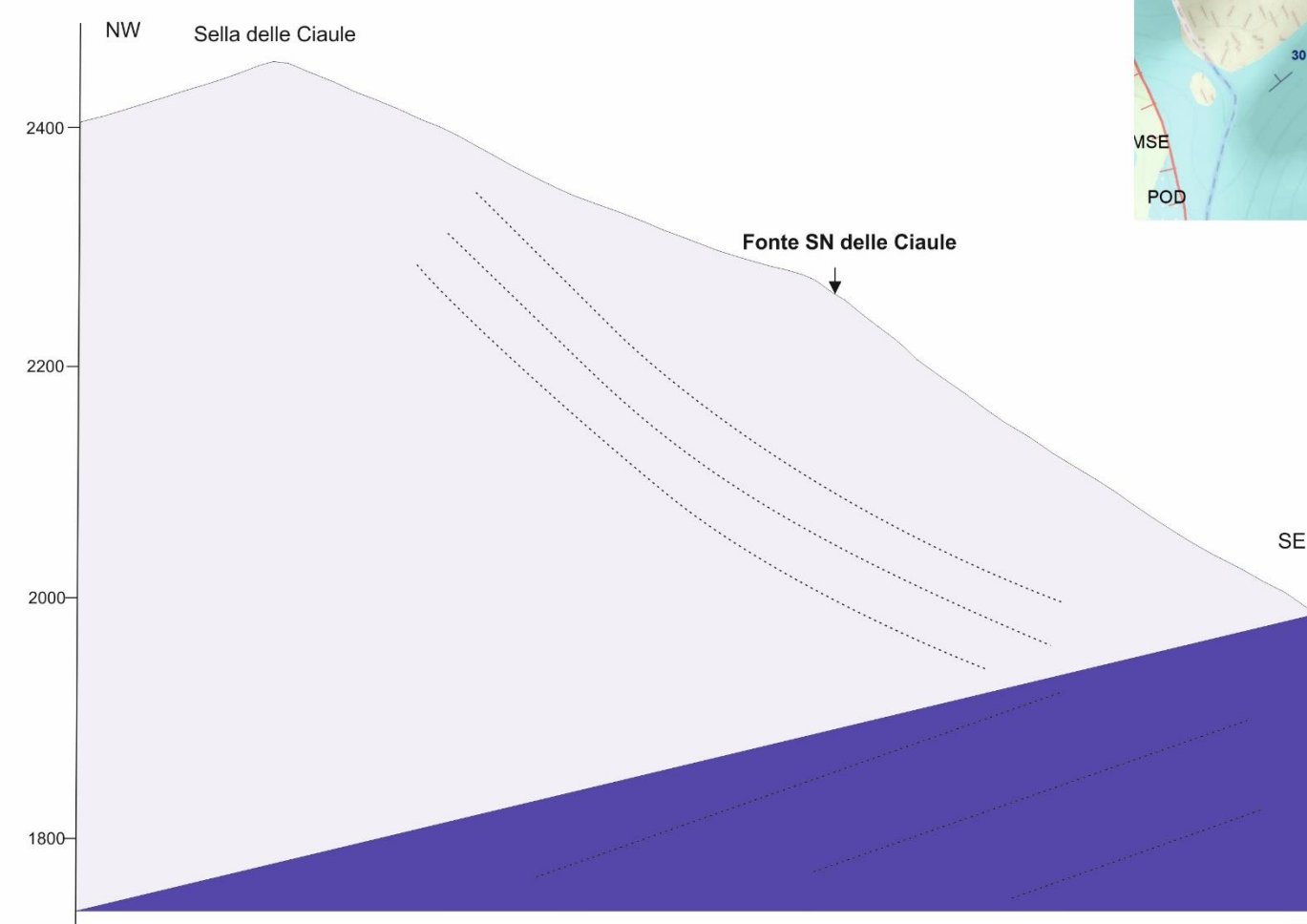


Fig. 7.2.1.5. Fonte delle Ciaule geologic cross section. ©CorelDraw 2018

### 7.2.2. Physical and chemical data

Below, pre/post-earthquake physical and chemical data are reported.

#### PRE-EARTHQUAKE STATE

Physical data

Data	Air Temperature	Water Temperature	Flow rate (l/min)
30/6/2010	16.5	2.2	~3
23/6/2011	16.4	2.3	~3
15/11/2011	5.6	2.8	~1

Tab. 7.2.2.1. Pre-earthquake physical data

Chemical analysis

Data	pH	Conductivity ( $\mu\text{S}/\text{cm}$ )	Ca mg/l	Ca meq/l	Mg mg/l	Mg meq/l	HCO <sub>3</sub> mg/l	HCO <sub>3</sub> meq/l	Hardness (Ca+Mg) °F
30/6/2010	6.5	185.0	37.5	1.87	3.3	0.27	124.6	2.04	10.72
23/6/2011	7.5	168.0	31.6	1.58	1.6	0.13	122.0	2.00	8.55
15/11/2011	7	166.0	37.2	1.86	3.4	0.28	102.1	1.67	10.69

Tab. 7.2.2.2. Pre-earthquake chemical data

#### POST-EARTHQUAKE STATE

Physical data

Data	Air Temperature	Water Temperature	Flow rate (l/min)	Annotations
1/8/2018				impossible to sample
10/10/2018	10	8.1		~1

Tab. 7.2.2.3. Post-earthquake physical data

Chemical analysis

As previously mentioned in the paragraph 7.1., the 2018 chemical analysis are much more detailed than those of the pre-earthquake period. In the table below (Tab.7.2.2.4.), only data for common parameters are reported. The complete data are shown further on (Fig. 7.2.2.1.).

Data	pH	Conductivity ( $\mu\text{S}/\text{cm}$ )	Ca mg/l	Ca meq/l	Mg mg/l	Mg meq/l	HCO <sub>3</sub> mg/l	HCO <sub>3</sub> Mg/l	Hardness (Ca+Mg) °F
10/10/2018	8.69	210	42.59	2.13	4.42	0.36	129.29	2.12	12.46

Tab. 7.2.2.4. Post-earthquake chemical data

Here below the chemical analysis table (Fig. 7.2.2.1.) made by the Water Analysis Laboratory - UNICAM Chemical Division.

Spring	Fonte delle Ciaule			Data:	10/10/18	
pH at the emergence			8.69	Hydrogen ion activity at the spring		2.04E-09
spring temp			8.1			
lab temp		°C	22.1			
R.F. (180°C)	133	D.T.(G.F.)	13		Balance: cat	2.577287
K20 ( $\mu\text{S}/\text{cm}$ )	210	Alcal.Tot.	21.19	0.635	ani	2.583241
					-0.23% =Δ=	-0.005954
Cationic Substances	mg/l		m.mol/l	m.equiv/l	m.eq/m.eq.tot	
Lithium	0.00073		0.000104742	0.000104742	0.000020	
Sodium	1.35356		0.058876033	0.058876033	0.011409	
Potassium	0.90557		0.023161543	0.023161543	0.004488	
Calcium	42.59102		1.062650116	2.125300233	0.411838	
Magnesium	4.42373		0.182009052	0.364018103	0.070539	
Strontium	0.24968		0.002849606	0.005699213	0.001104	
Aluminum	0.00000		0	0	0.000000	
Contaminants or cationic unwanted:						
Barium	0.00852		6.20403E-05	0.000124081	0.000024	
Selenium	0.00000		0	0	0.000000	
Chromium	0.00003		5.39817E-07	3.2389E-06	0.000001	
Nickel	0.00000		0	0	0.000000	
Anionic:			1.32971367	2.57728719		
Fluoride	0.06980		0.003674071	0.003674071	0.000712	
Chloride	1.22390		0.034521761	0.034521761	0.006690	
Bromine	0.00000		0	0	0.000000	
Bicarbonate	129.29290		2.119003473	2.119003473	0.410618	
Carbonate	2.84744		0.047451024	0.094902048	0.018390	
Sulfate	15.26976		0.158967269	0.317934538	0.061609	
Contaminants or anionic unwanted:						
Nitrite	0.00000		0	0	0.000000	
Nitrate	0.81880		0.0132056	0.0132056	0.002559	
Neutral:			2.3768232	2.58324149		
Contaminants or neutral unwanted:						
Boron	0.00336					
FIXED RESIDUE		mg/L	133.344483			
				TOTAL HARDNESS	°F	13
				TOTAL CALCULATED ALCALINITY		21.19

Fig. 7.2.2.1. Chemical analysis table elaborated by UNICAM – Water Analysis Laboratory

### 7.2.3. Data analysis

The first analyzed parameter is the **flow rate** in different times.

Regrettably, the ground morphology close to the spring did not ever allow to take accurate measurements (Fig. 7.2.3.1.). The 2010 and 2011 data, in fact were only estimations of the flow, and during the post-earthquake surveys it was not possible to collect data because the equipment was not able to measure such a small flow. In addition, the moss on the bottom of the opening would have made the amplitude not true.



Fig. 7.2.3.1. Fonte delle Ciaule detail (August, 1<sup>st</sup> 2018). In October the situation was the same.

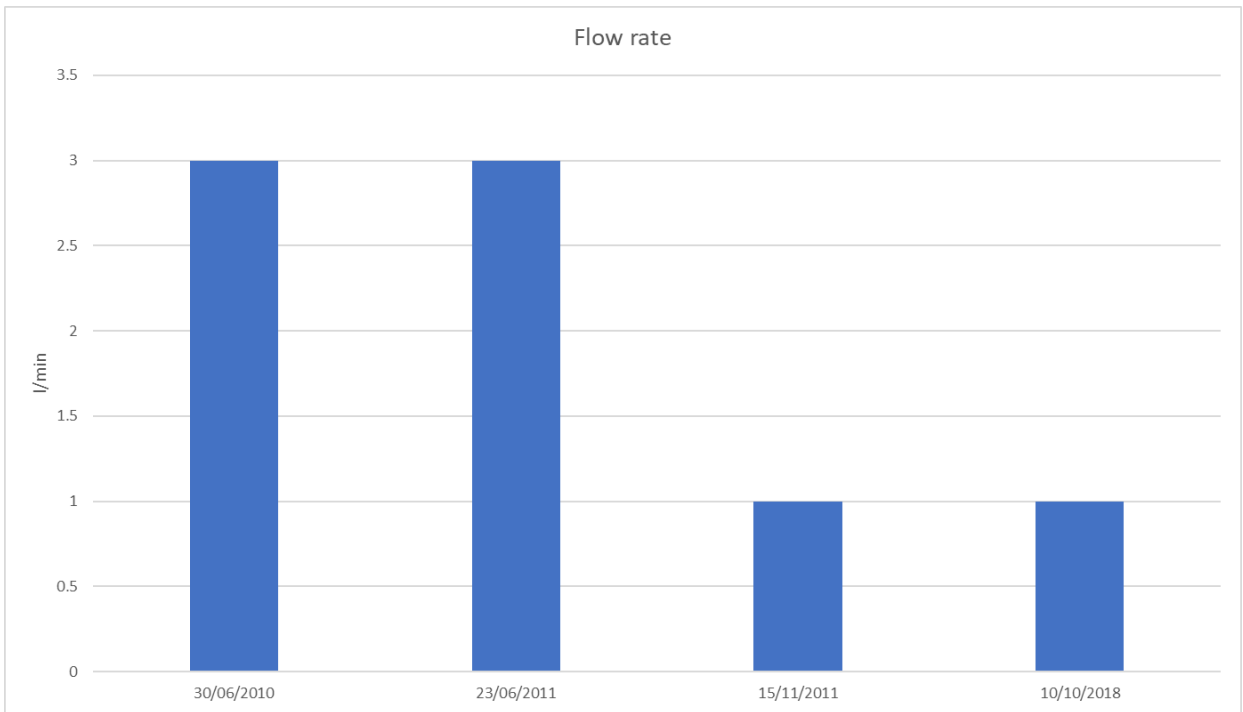


Fig.7.2.3.2. Flow rate data. ©Microsoft Excel

From the graph (Fig. 7.2.3.2.) it can be said that:

- in 2011 there was a decrease, from June to November, as one would normally expect;
- the approximated values of November 2011 and October 2018 are similar.

To take more founded considerations, cumulative rainfalls have been considered for a period trying to include the snow factor, whose contribution to the recharge depends on the melting rate. The climatic station is Capodacqua (RT-1366). Because of the low accuracy it is not possible to achieve a short-term flow response analysis.

Autumn pre/post-earthquake data can be understood better with the support of the rainfall amounts. In the period September 2010 - November 2011 the cumulative data is 1045 mm, while since September 2017 to October 2018, 1585.8 mm fell.

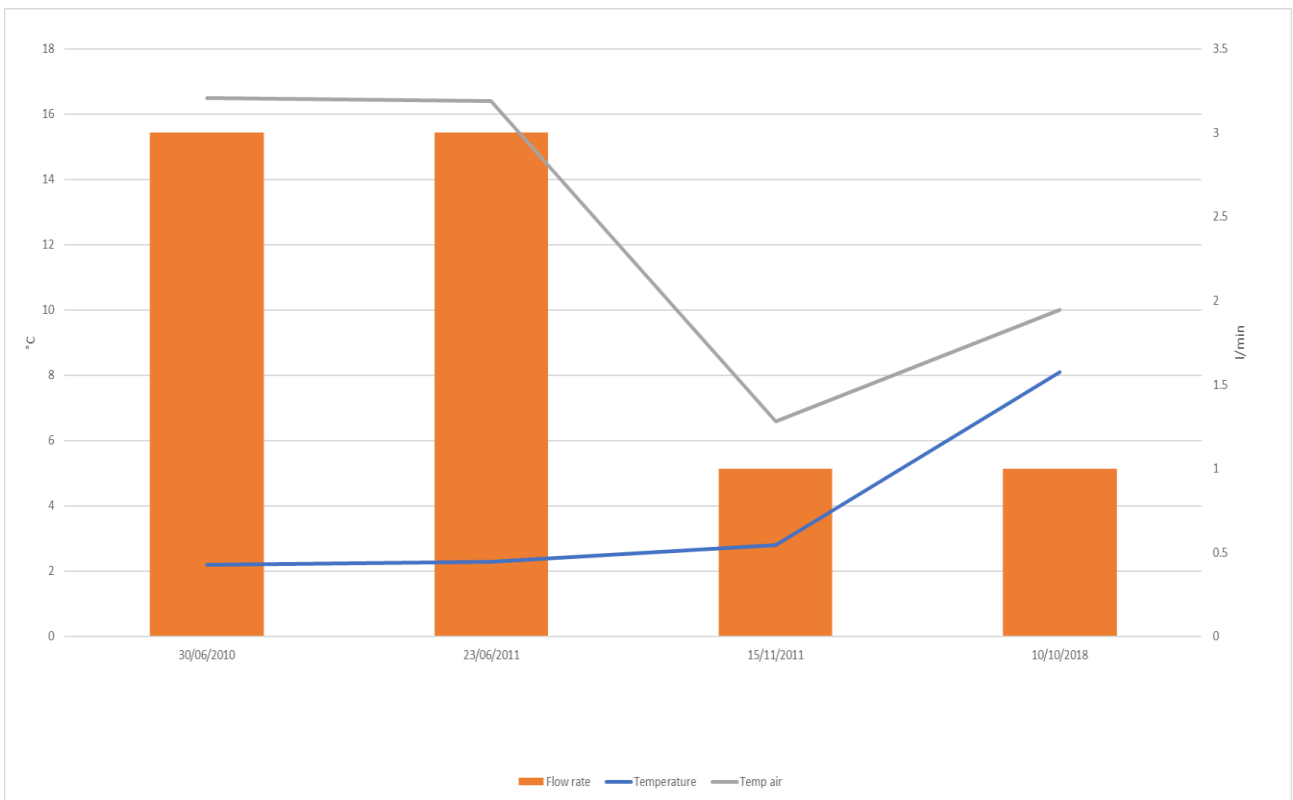


Fig. 7.2.3.3. Flow rate, water and air temperatures data. ©Microsoft Excel

The above graph (Fig. 7.2.3.3.) shows that the **water temperature** was almost constant before the earthquake and it did not seem to be influenced by the external temperature. The October 2018 survey has registered an unexpected increase in water temperature respect to November 2011, however it was not possible to know if this is related to the earthquake. In addition, during the previous days of the measurements no precipitations occurred.

Therefore, it seems that the Fonte delle Ciaule flow in the dry season should be fed by the snowmelt that slowly penetrates the *Corniola* beds, because it shows a seasonal decrease from June to November.

The electric **conductivity** (the ability of a material to conduct electric current) is a water fundamental property and is strictly dependent on the salinity, since that electrons are transported by the ions. Therefore, it is reasonable to expect that conductivity and salt content are directly dependent, as can be seen from the graphs (Fig. 7.2.3.4.).

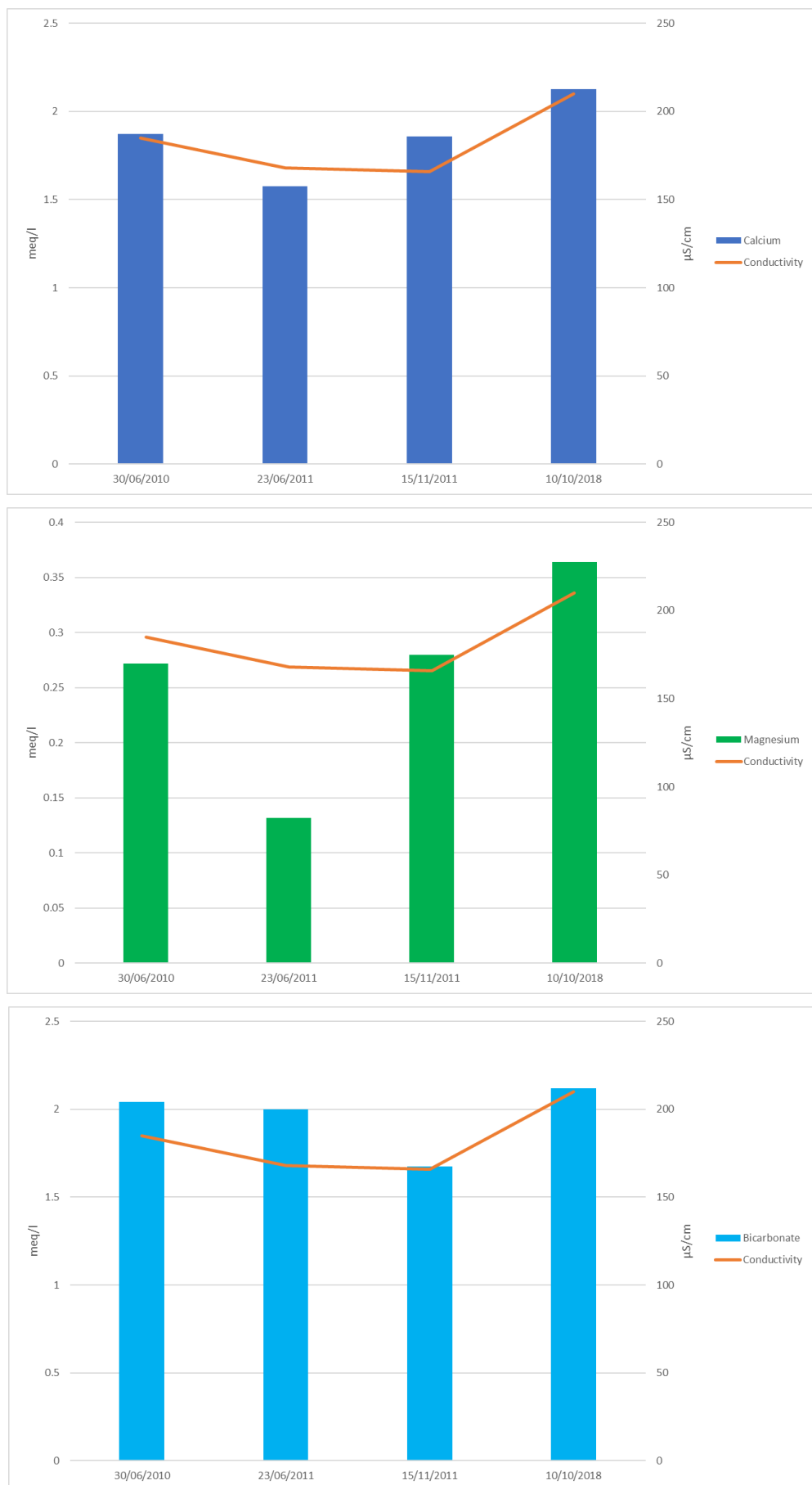


Fig. 7.2.3.4. Conductivity vs Calcium, Magnesium and Bicarbonate contents. ©Microsoft Excel

Fonte delle Ciaule conductivity values are low because of the short path travelled inside the rock, consequently the water has not the time to enrich in salts. This is common for high-altitude emergences.

Comparing June 2010-2011 there is a conductivity decrease (-17  $\mu\text{S}/\text{cm}$ ), presumably linked to the more regular-infiltrating June 2011 precipitations, respect to the 2010 ones. The value of October 2018, if compared with the November 2011 one (+ 44  $\mu\text{S}/\text{cm}$ ), appears maybe a little too much elevated, considering that the 2017-2018 season was rainier than the corresponding 2010-2011 period (on a climatic basis the former data should be lower than the latter because of the dilution). This could depend on the shaking that led to a higher solubility of the ions inside the rock. However, due to the missing data we cannot demonstrate this.

Therefore, the **chemical composition** and the relative proportions of the different elements depend both on the crossed lithologies. The Piper diagram (Fig. 7.2.3.5.) helps to understand the sources of the dissolved constituents in water. Ciaule water belongs to the bicarbonate-calcium and/or magnesium facies, in agreement with the carbonatic rocks composition.

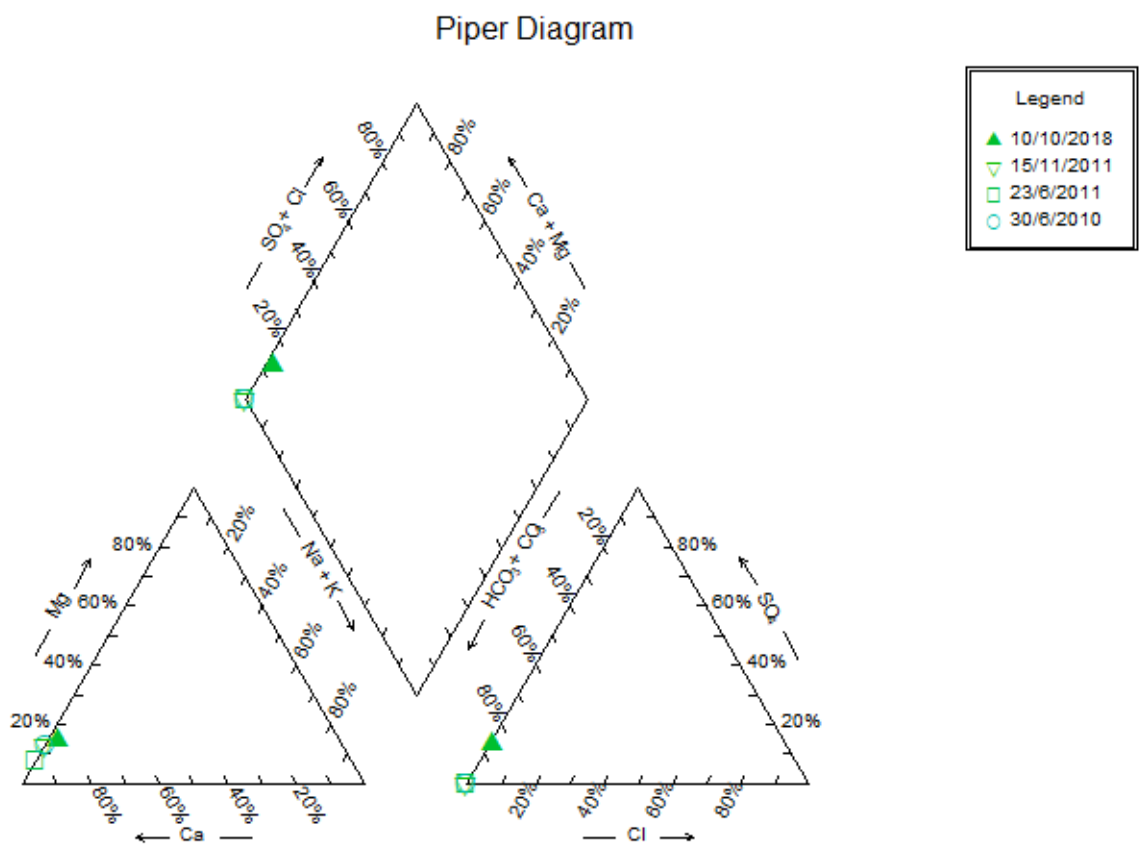


Fig. 7.2.3.5. The Piper diagram; ©RockWare - AqQA

Before, it has been specified that the chemical comparison is possible only among 3 common ions (Calcium, Magnesium and Bicarbonate).

To get a clearer view of the data, they have been reported on a ternary and column charts (Fig. 7.2.3.6.). The concentrations are expressed in meq/l %. The first correlation is the pre/post-earthquake.

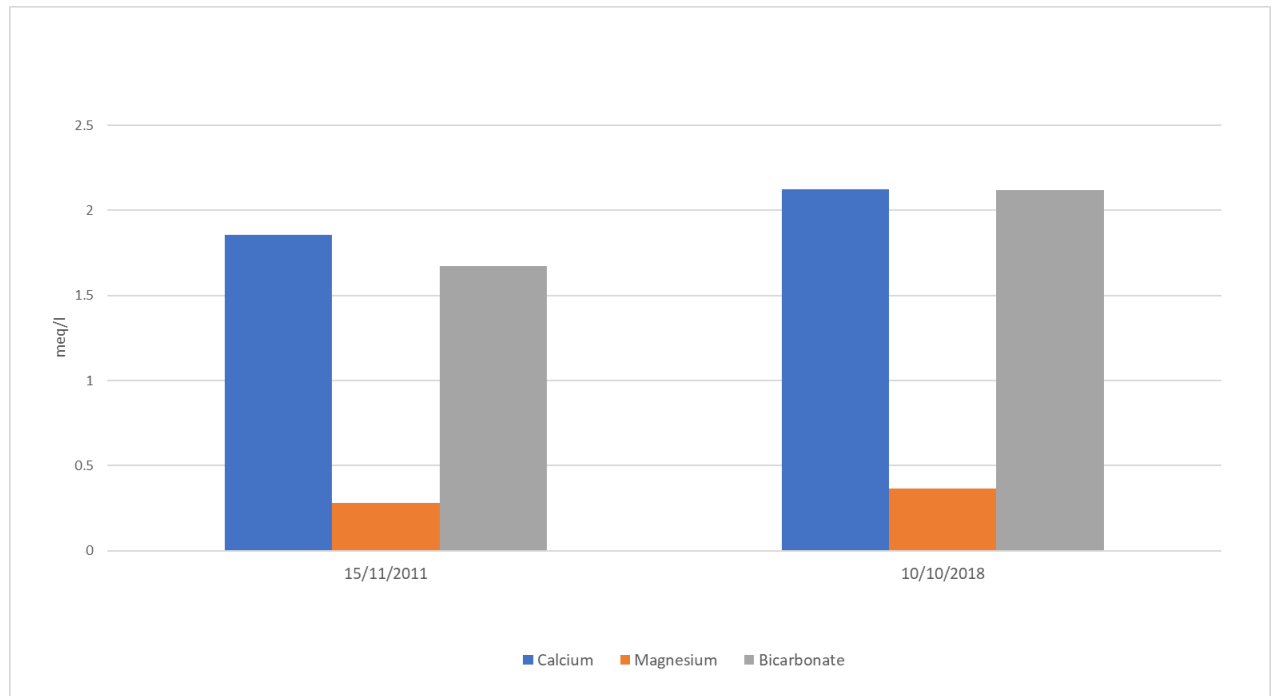


Fig. 7.2.3.6. Ca, Mg and  $\text{HCO}_3^-$  levels. ©Microsoft Excel

There is a slight increase in Ca (+0.27 meq/l) and Mg (+0.08 meq/l), and a more relevant one in Bicarbonate (+0.45 meq/l). The conductivity displays the same trend. Remembering that 2018 winter was more rainy than the 2011 one, this could be a sign of an earthquake-induced ions solubilization. Dilution phenomena can be excluded, because in the months prior to the sampling there were no persisting rainfalls. **Anyhow, we are taking about of very exiguous variations that may be related to other factors.**

The underlying chart (Fig. 7.2.3.7.) shows a Calcium (-0.3 meq/l) and Mg (-1.7 meq/l) decrease between June 2010 and 2011. Bicarbonate is stable. The conductivity is reduced of 17  $\mu$ S/cm.

Fonte delle Ciaule

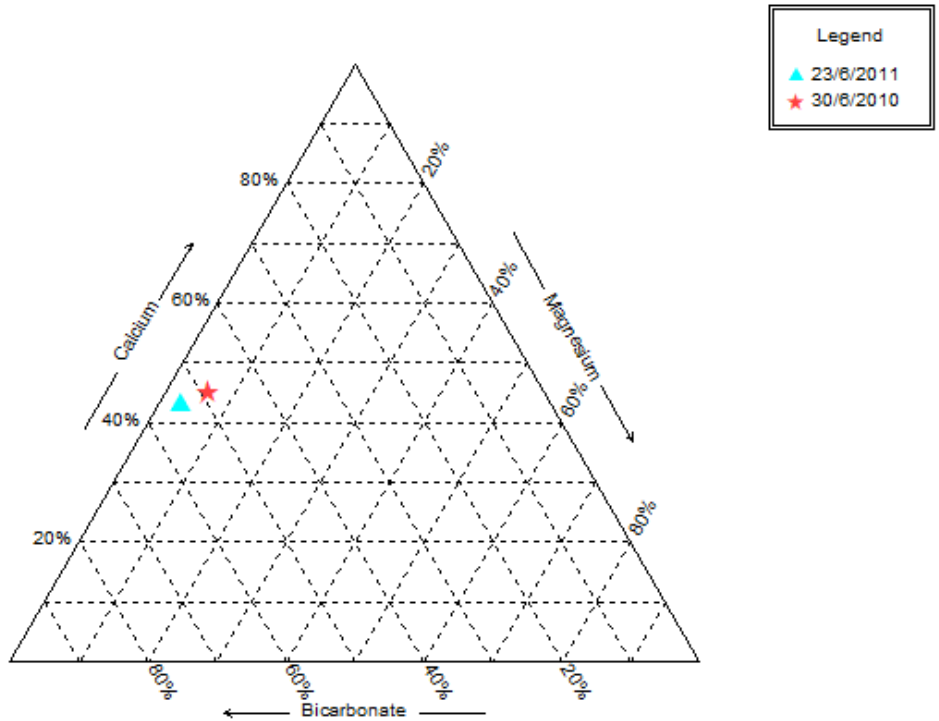


Fig. 7.2.3.7. Ca vs Mg vs  $\text{HCO}_3^-$  ternary diagram. ©RockWare – AqWa

The difference is probably caused by the more 2011 regular rainfalls in the month before the sampling. The June 2010 was characterized by heavier events, which probably did not infiltrate, with respect to the 2011 ones. Precipitations could have diluted the water sampled 8 days after they ended.

The last observation is from June to November 2011 (Fig. 7.2.3.8.), where Calcium (+ 0.18 meq/l) and Magnesium (+0.14 meq/l) increased, with the typical seasonal trend. The conductivity is constant. This is probably due to a Bicarbonate compensation-effect, as its value decreases of 33 meq/l.

## Fonte delle Ciaule

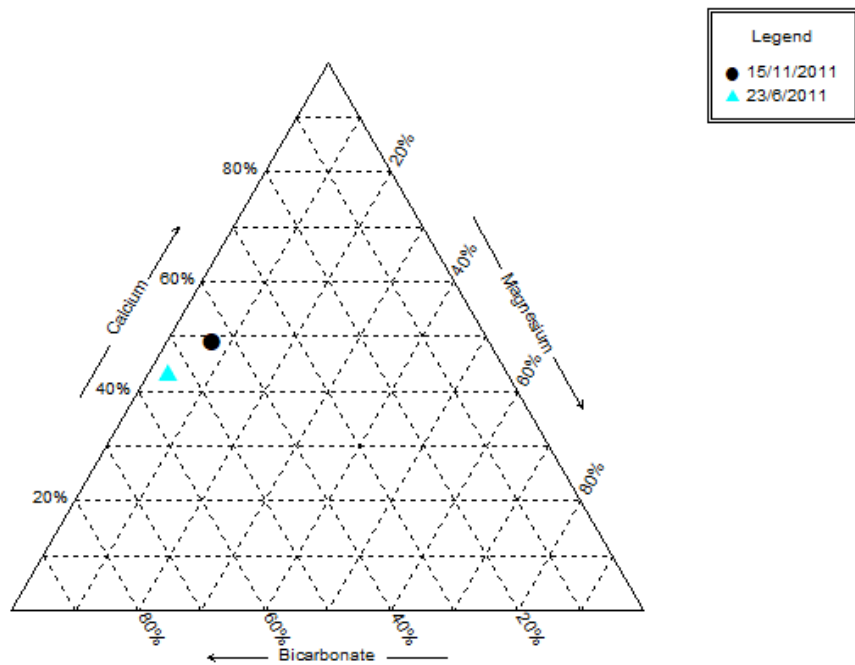


Fig. 7.2.3.8. Ca vs Mg vs  $\text{HCO}_3^-$  ternary diagram. ©RockWare - AqQa

### 7.3. Fonte SN delle Ciaule

#### 7.3.1. Detailed features and geological setting

Elevation: 2034 m a.s.l. – Hydrographic basin: Tronto

Coordinates: 33T 358736 4741696 UTM /  $13^{\circ}16'19,51''$  E  $42^{\circ}48'53,269''$  N

Description: the fountain (Fig. 7.3.1.1. and Fig. 7.3.1.2.) was directly supplied by a pipeline coming from Fonte delle Ciaule in 2010-2011, as reported by Aringoli et al. (2017). During the 2018 surveys there were noticed some discrepancies with the pre-earthquake information. In August 2018, inside the Ciaule locked intake you could clearly hear the water running while at the Fonte SN delle Ciaule there was no water flowing, probably because the connecting-pipeline was broken (maybe by the shocks). Also, in October 2018 the aqueduct was broken but this time there was water flowing in both springs. This is enough to conclude that, after the earthquake, Fonte SN delle Ciaule is not sustained by Fonte delle Ciaule and that it has its own feeding basin.



Fig. 7.3.1.1. and Fig. 7.3.1.2. Fonte SN delle Ciaule (August, 1<sup>st</sup> 2018 and October, 10<sup>th</sup> 2018)

Location: it is sited NE of Monte Vettoretto (Fig. 7.3.1.3.), at the northernmost edge of Pratopulito following the same path of the previous spring. The fountain will appear only at the end since it has to be reached from below and it is often hidden by the vegetation.

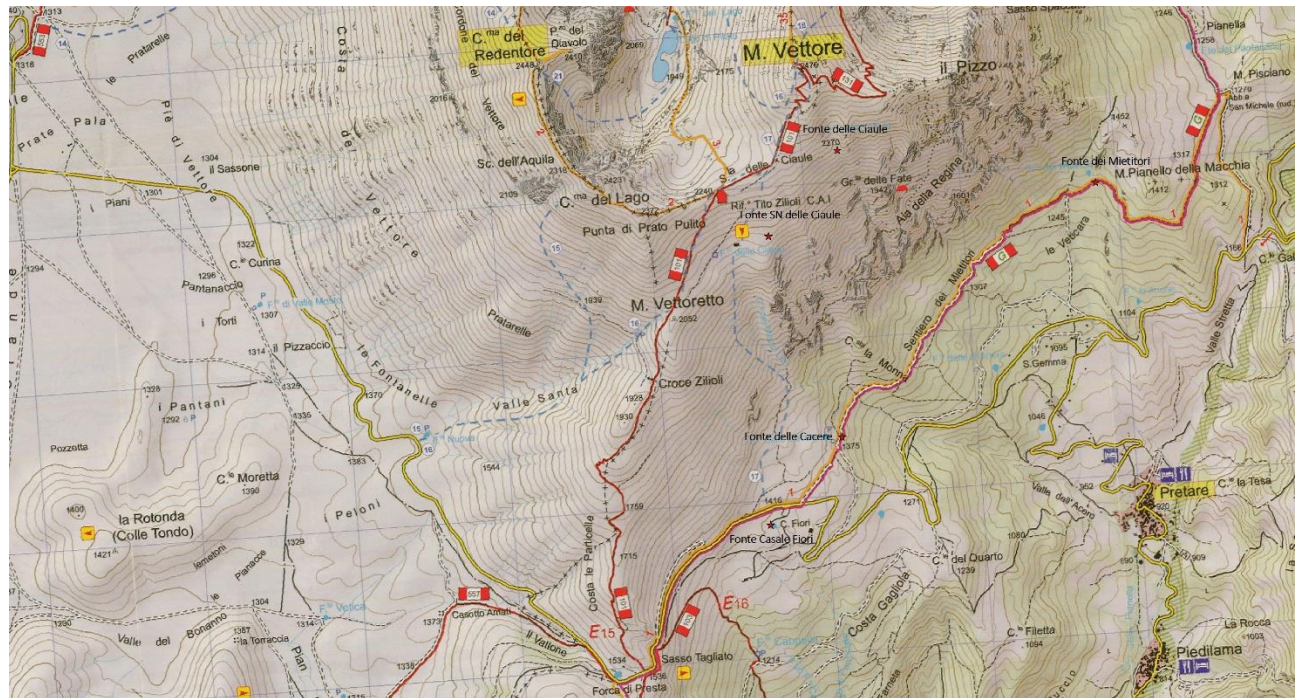


Fig. 7.3.1.3. Map of the southern side of Monte Vettore. CAI – Monti Sibillini – Carta dei Sentieri 1:25'000

**Geological setting.** The spring (group b) has a similar geological setting of the previous one (Fig. 7.3.1.4.). It emerges from *Corniola* (COI) beds dipping 30-35° ESE. The flow rate regime, because of the restricted supply basin, has the same characters of Fonte delle Ciaule, being fed by the most surficial rock beds.

## Cross section Fonte SN delle Ciaule

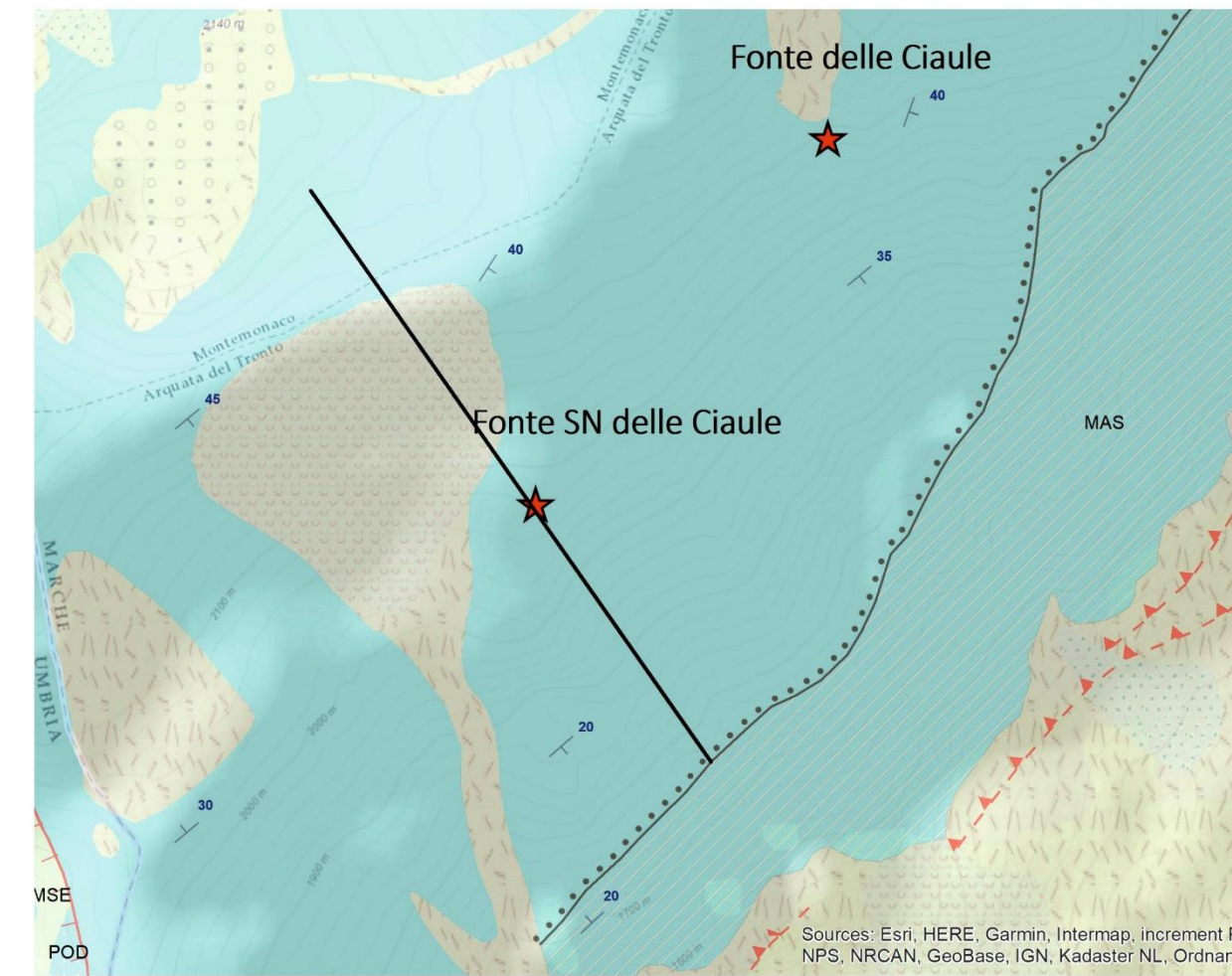
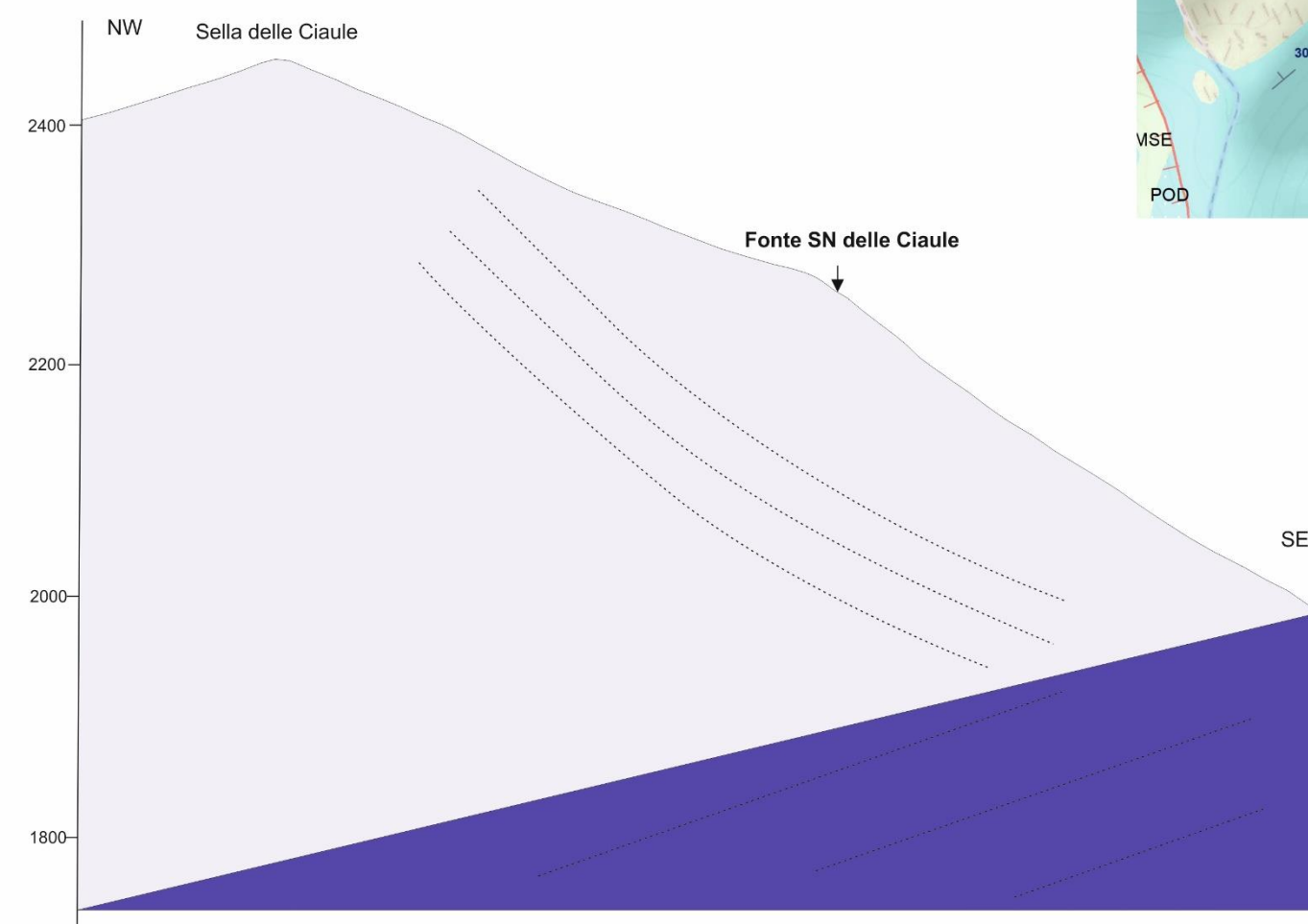


Fig. 7.3.1.4. Fonte SN delle Ciaule geologic cross section. ©CorelDraw 2018

### 7.3.2. Physical and chemical data

#### PRE-EARTHQUAKE STATE

Physical parameters

Data	Air Temperature	Water Temperature	Flow rate (l/min)	Annotations
30/6/2010	15.7	5.6	3.4	
23/6/2011	16.9	6.0	3.7	
15/11/2011	--	--	0	No water flowing. Ice into the tanks

Tab. 7.3.2.1. Pre-earthquake physical data

Chemical analysis

Data	pH	Conductivity ( $\mu\text{S}/\text{cm}$ )	Ca mg/l	Ca meq/l	Mg mg/l	Mg meq/l	HCO <sub>3</sub> mg/l	HCO <sub>3</sub> meq/l	Hardness (Ca+Mg) °F
30/6/2010	7	182.0	35.8	1.79	4.0	0.33	118.0	1.93	10.59
23/6/2011	7	188.0	37.0	1.85	5.9	0.49	107.8	0.42	11.67
15/11/2011	--								

Tab. 7.3.2.2. Pre-earthquake chemical data

#### POST-EARTHQUAKE STATE

Physical parameters

Data	Air Temperature	Water Temperature	Flow rate (l/min)	Annotations
1/8/2018			0.01	not sampled
10/10/2018	14.4	8.4	0.71	

Tab. 7.3.2.3. Post-earthquake physical data

Chemical analysis

Data	pH	Conductivity ( $\mu\text{S}/\text{cm}$ )	Ca mg/l	Ca meq/l	Mg mg/l	Mg meq/l	HCO <sub>3</sub> mg/l	HCO <sub>3</sub> meq/l	Hardness (Ca+Mg) °F
10/10/2018	8.64	210	44.80	2.24	5.16	0.42	140.95	2.31	13.31

Tab. 7.3.2.4. Post-earthquake chemical data

Here below the chemical analysis table (Tab. 7.3.2.1.) made by the Water Analysis Laboratory - UNICAM Chemical Division.

Spring		Fonte SN Ciaule		Data:	10/10/18		
pH at the emergence			8.64	Hydrogen ion activity at the spring			4.36E+08
spring temp			8.4				
lab temp		°C	21.9				
R.F. (180°C)	142	D.T.(G.F.)	13		Balance: cat		2.753615
K20 (μS/cm)	210	Alcal.Tot.	23.1	0.676	ani		2.768138
					-0.53% =Δ=		-0.014523
<b>Cationic Substances</b>		<b>mg/l</b>		<b>m.mol/l</b>	<b>m.equiv/l</b>		<b>m.eq/m.eq.tot</b>
Lithium		0.00189		0.000272749	0.000272749		0.000049
Sodium		1.39815		0.060815572	0.060815572		0.011014
Potassium		0.83493		0.021354801	0.021354801		0.003867
Calcium		44.79750		1.117702096	2.235404192		0.404836
Magnesium		5.15880		0.212252623	0.424505246		0.076879
Strontium		0.48047		0.005483508	0.010967017		0.001986
Aluminum		0.00000		0	0		0.000000
<b>Contaminants or cationic unwanted:</b>							
Barium		0.01268		0.000101944	0.000203888		0.000037
Selenium		0.00000		0	0		0.000000
Chromium		0.00003		6.53896E-06	3.92338E-05		0.000007
Nickel		0.00000		0	0		0.000000
<b>Anionic:</b>				<b>1.41801887</b>	<b>2.75361507</b>		
Fluoride		0.07120		0.003747763	0.003747763		0.000679
Chloride		1.17010		0.033004259	0.033004259		0.005977
Bromine		0.00000		0	0		0.000000
Bicarbonate		140.94696		2.310003786	2.310003786		0.418346
Carbonate		2.77329		0.046215299	0.092430598		0.016739
Sulfate		15.33807		0.159678417	0.319356834		0.057836
<b>Contaminants or anionic unwanted:</b>							
Nitrite		0.00000		0	0		0.000000
Nitrate		0.59490		0.009594542	0.009594542		0.001738
<b>Neutral:</b>				<b>2.56224407</b>	<b>2.76813778</b>		
<b>Contaminants or neutral unwanted:</b>							
Boron							
FIXED RESIDUE		mg/L	141.944809				
				TOTAL HARDNESS		°F	13
				PERMANENT HARDNESS		°F	1.80697152
				TOTAL CALCULATED ALCALINITY			23.1

Fig. 7.3.2.1. Chemical analysis table elaborated by UNICAM – Water Analysis Laboratory

### 7.3.3. Data analysis

Looking at the previous map and section (Fig. 7.2.1.5.), it is easy to understand the geological similarity between this and the previous emergence, however here it was possible to perform accurate **flow rate** measurements because the water came out from a pipe. It is crucial to take into account what has been reported before (paragraph 7.3.1.) about the pipe, coming from Fonte delle Ciaule, before and after the earthquake. Looking at the 2010/2011-2018 measurements (Fig. 7.3.3.2.) a sharp decrease (not related to rainfalls and/or snowfalls) catches to the eye. Probably, this is a sign that the supply setting is different between before and after the 2016 mainshocks. Therefore, a pre/post-seismic sequence flow rate comparison was not possible and, despite the geological similarity (i.e. both springs come out from widespread *Corniola* outcrops) there could be chemical differences.



Fig. 7.3.3.1 Fonte SN delle Ciaule (August, 1<sup>st</sup> 2018)

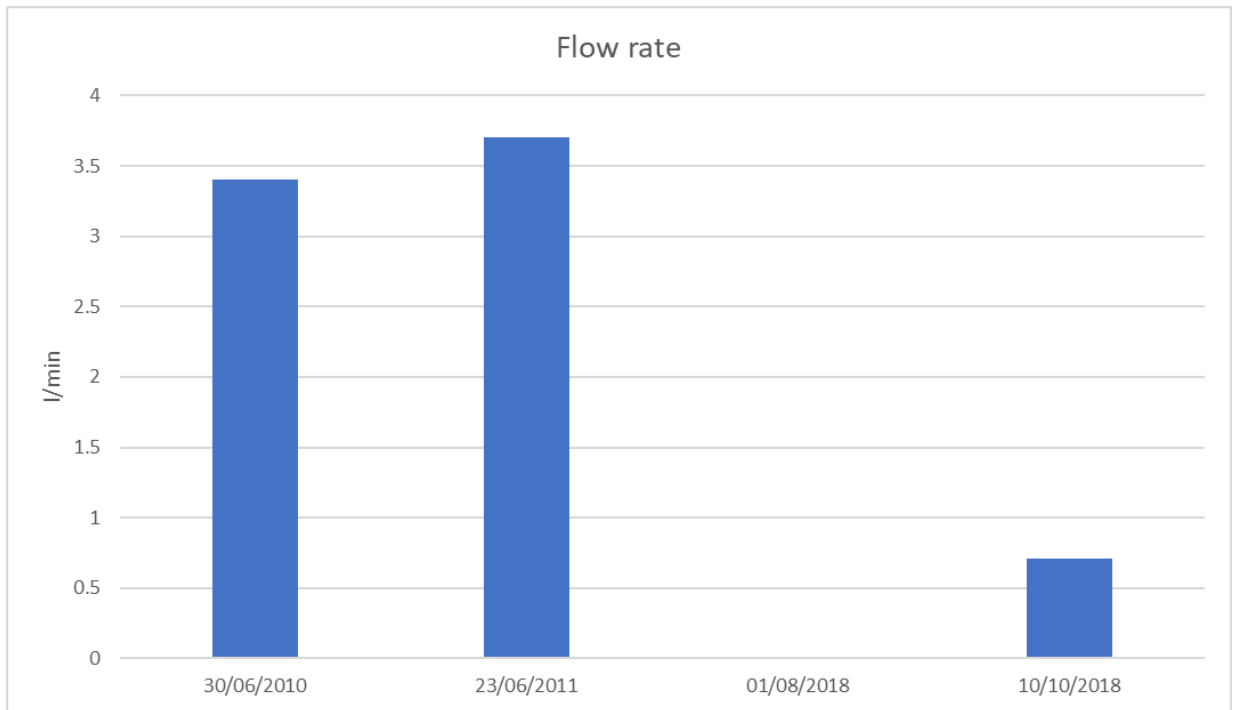


Fig.7.3.3.2. Flow rate data. ©Microsoft Excel

In the 2018 surveys the spring displayed an anomalous seasonal behavior: in August 2018 it was almost dry (estimated value of 0.01 l/min) while in October the flow was weak (0.71 l/min). The explanation could reside in the 2-3 days immediately preceding rainfalls, that in October were 6.8 mm respect to the 3.8 mm of the last July days. This confirms that the springs with a shallow hydrogeological basin have a flow rate-precipitations quick response.

The underlying graph (Fig. 7.3.3.3.), for the 2010-2011 data, shows a general average **water temperature** increase (+ 5°C), respect to Fonte delle Ciaule, due to the travel in the conduit. Instead, comparing the two water temperature October 2018 values (Fonte delle Ciaule: 8.1 °C, Fonte SN delle Ciaule 8.4°C) the same increment is not displayed (+ 0.3°C), confirming the supposed post-earthquake supply modifications.

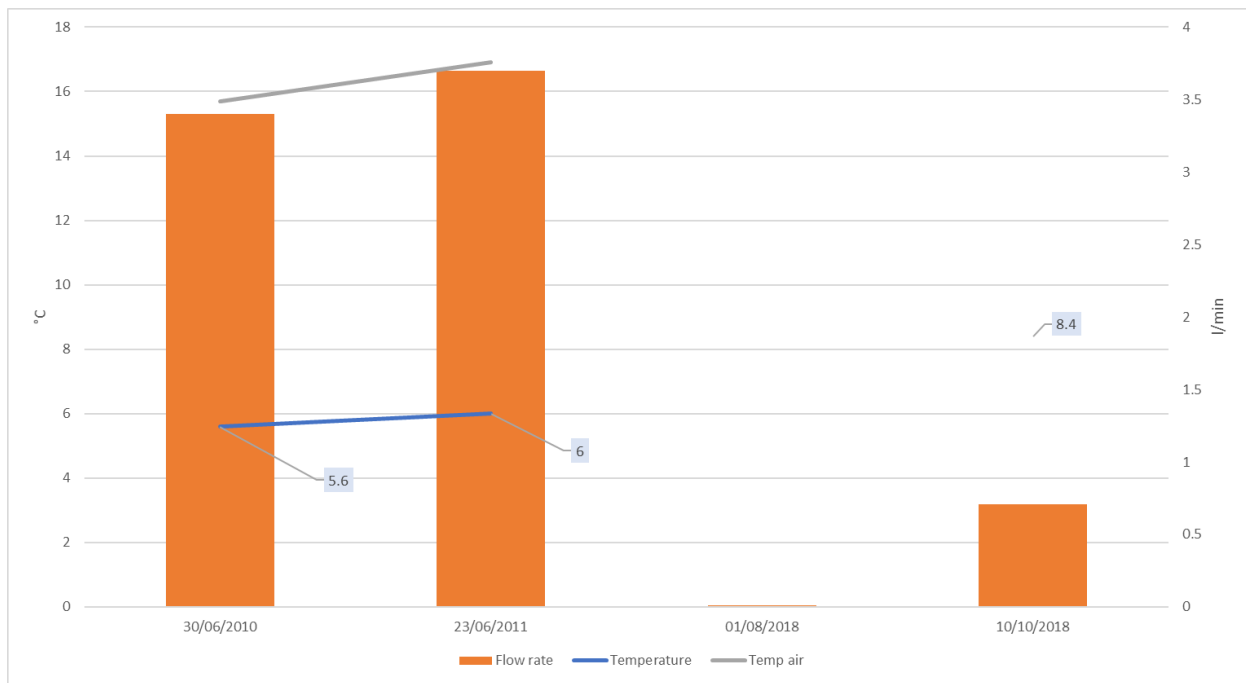
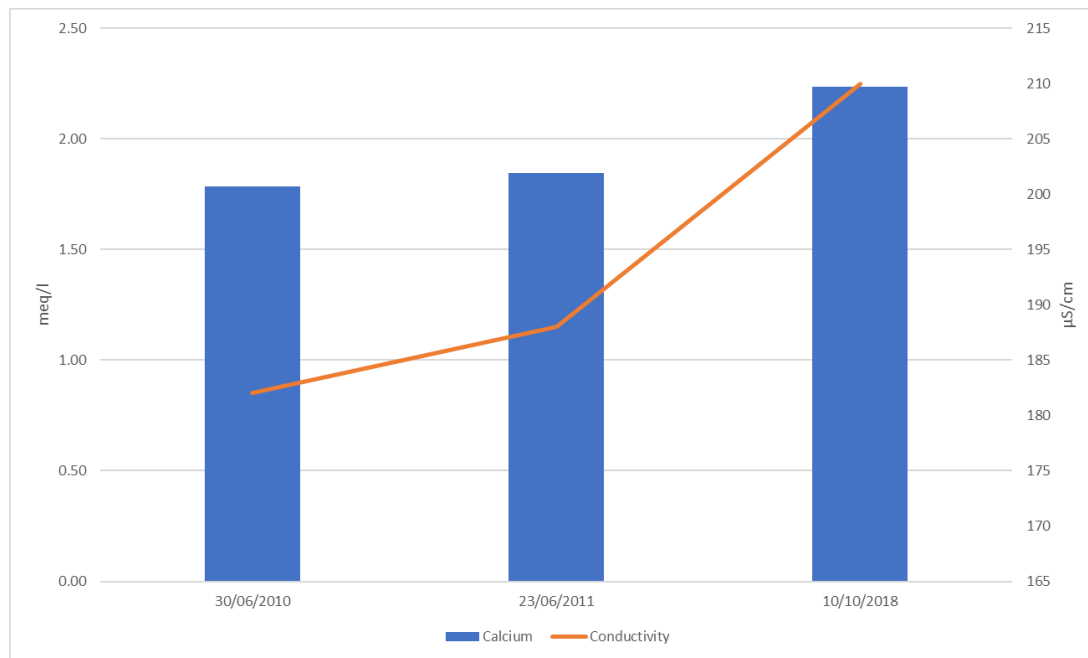


Fig. 7.3.3.3. Flow rate, water and air temperatures data. ©Microsoft Excel

The **conductivity** values are low because of the brief underground path travelled, and are similar to those of the Fonte delle Ciaule (Fig.7.3.3.4.).



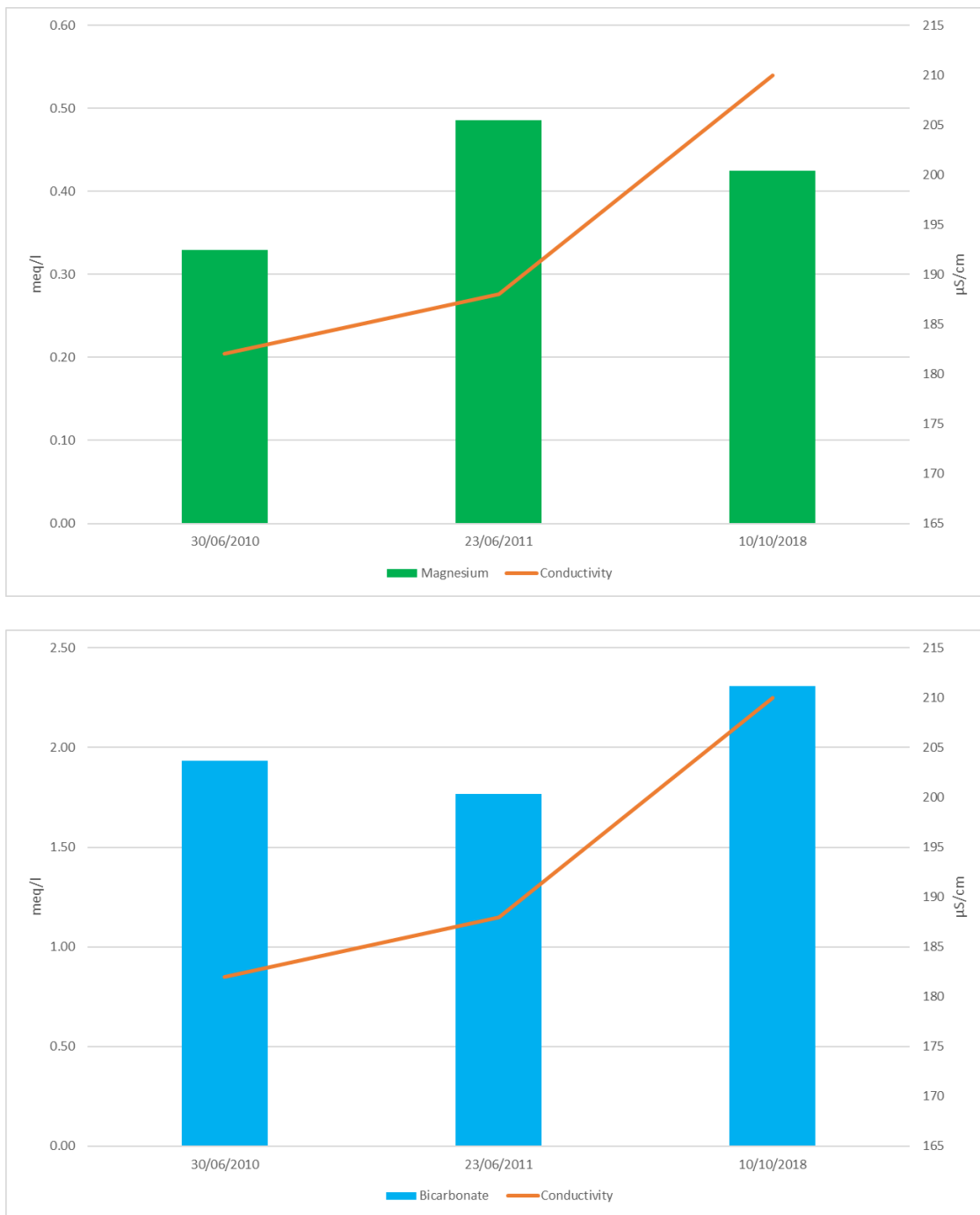


Fig. 7.3.3.4. Conductivity vs Calcium, Magnesium and Bicarbonate contents. ©Microsoft Excel

The values have slightly increased from 2010 to 2011 (+6  $\mu\text{S}/\text{cm}$ ), in contrast with the decreasing Fonte delle Ciaule ones. Also, the salinity values follow the same trend. The assumption is: the water coming out Fonte delle Ciaule openings may be shallower (probably it also flows under the scree) than those in the locked box on the right of the channel, which fed Fonte SN delle Ciaule. In this way, the former conductivity would be more affected by recent rainfalls than the latter.

On the contrary, an increment (between June 2010 and October 2018) has been observed after the earthquake in both emergences: + 22  $\mu\text{S}/\text{cm}$  here and + 42  $\mu\text{S}/\text{cm}$  in the previous one. It could depend both on the normal seasonal trend and on the increased ions solubilization. The difference in magnitude may be related to the water circulation depth, as previously mentioned.

Here below the Piper diagram (Fig. 7.3.3.5.), denoting the bicarbonate-calcium and/or magnesium facies, consonant with the limestone *Corniola* beds crossed by the water before emerging.

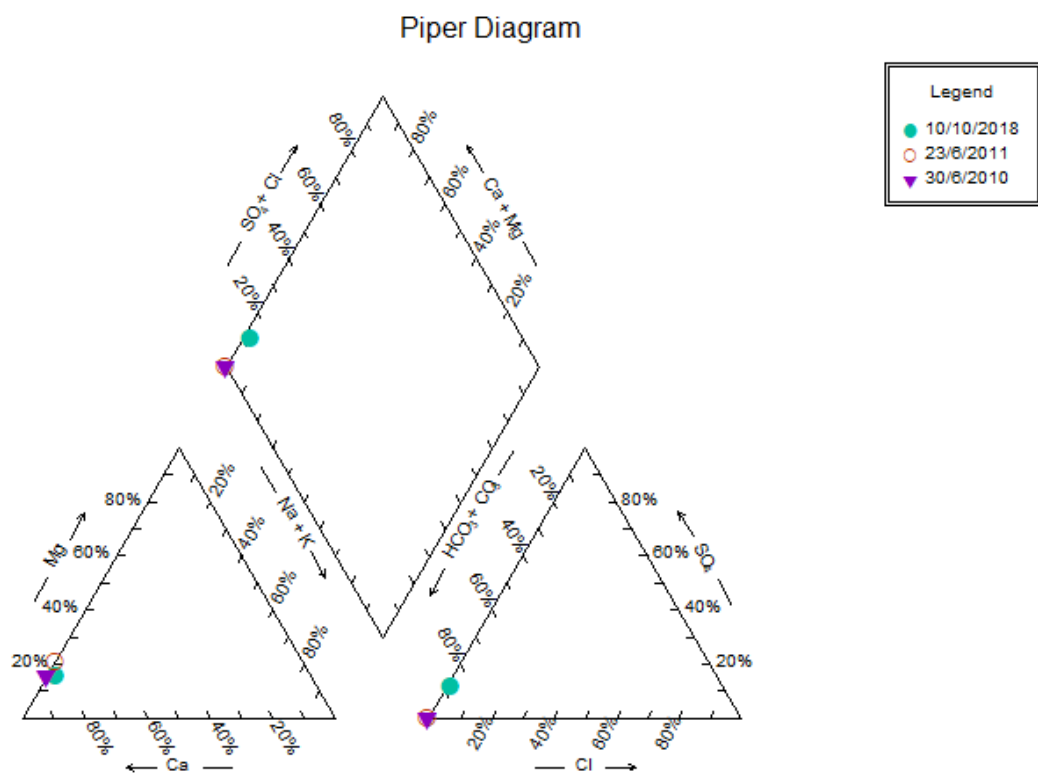


Fig. 7.3.3.5. The Piper diagram. ©RockWare - AqQa

Samples **chemical composition** have been correlated by means of a Calcium / Magnesium / Bicarbonate ternary diagram and a column graph.

The first (Fig. 7.3.3.6.) tries to evidence variations between June 2010 and June 2011.

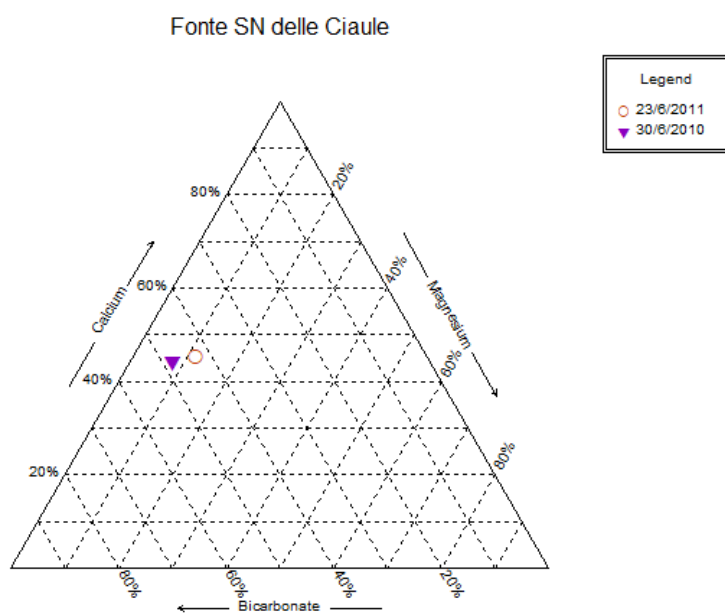


Fig. 7.3.3.6. Ca vs Mg vs  $\text{HCO}_3^-$  ternary diagram. ©RockWare - AqQa

It displays: Ca and Mg slight increase (+0.06 meq/l and +0.16 meq/l) and a negligible loss in HCO<sub>3</sub> (-0.16 meq/l). This reflects on the conductivity with the previously mentioned slight gain and it is justifiable because the 2011 winter was a little snowy compared to the 2010 one.

For the pre/post-earthquake comparison, a column graph (Fig. 7.3.3.7.) highlights better the discrepancies.

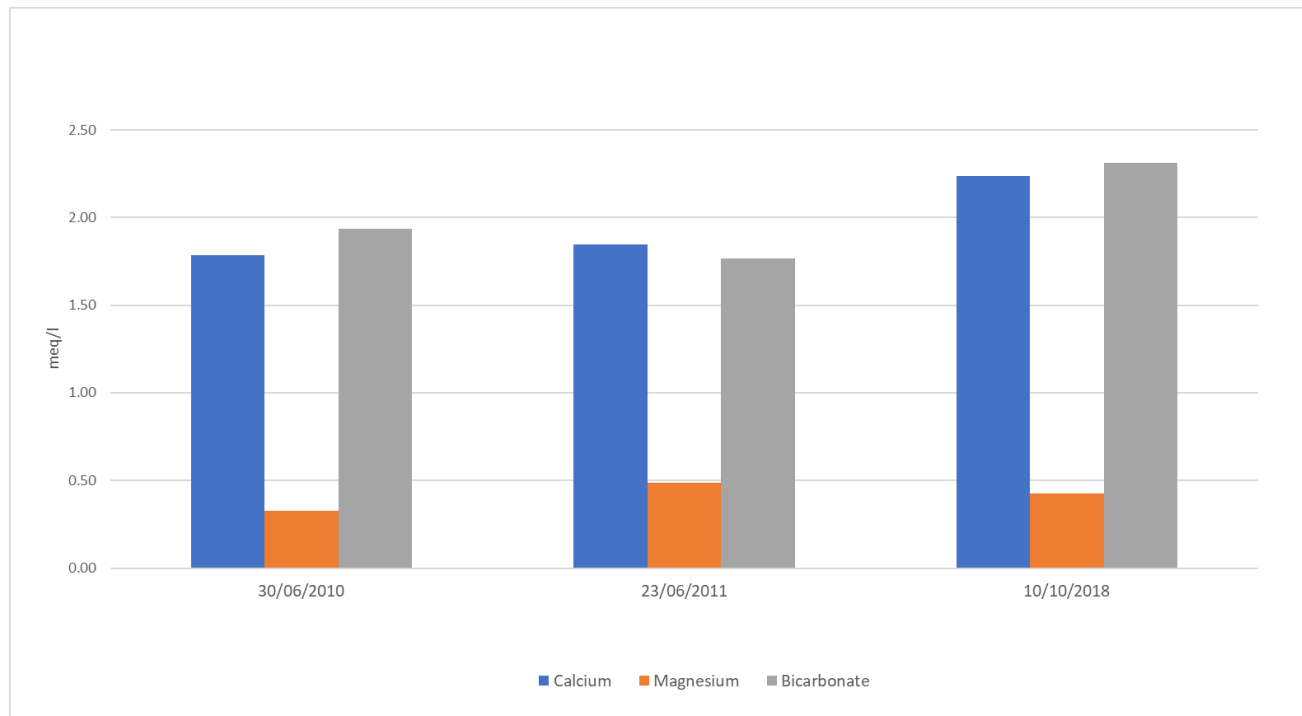


Fig. 7.3.3.7. Ca, Mg and HCO<sub>3</sub><sup>-</sup> column graph. ©Microsoft Excel

Not having data representative of the same period for 2010/2011 and 2018 and due to the pipe break, it is a quite complex to take conclusions on the earthquake-related effects. The diagram shows a marked increase in Calcium and Bicarbonate, while Magnesium is on the pre-earthquake levels. However, being changed the supply area, but not its unique outcropping lithology (*Corniola*), it is not possible to estimate how much the shaking has affected the ions solubilization. Because of the higher altitude difference between the emergence and the above ridge, which coincides with the hydrographic watershed, Fonte SN delle Ciaule water should have an underground residing time slightly lower than Fonte delle Ciaule and therefore a pre-earthquake minor salt content. On the base of the previous analysis, we can conclude that an increase in salinity is rather probable.

## 7.4. Fonte Casale Fiori

### 7.4.1. Detailed features and geological setting

Elevation: 1400 m a.s.l. – Hydrographic basin: Tronto

Coordinates: 33T 358618 4739837 UTM / 13°16'16,005" E 42°47'52,942" N

Description: it is a watering place with three tanks fed by an aqueduct (Fig. 7.4.1.1. and Fig. 7.4.1.2.) (Aringoli et al., 2017).



Fig. 7.4.1.1. Fonte Casale Fiori (September, 11<sup>st</sup> 2018)



Fig. 7.4.1.2. The spring on February, 28<sup>th</sup> 2019

Location: it is sited on the SE slope that originates between the base of the ridge Forca di Presta – Vettoretto and the Costa Gagliola, 200 m WNW of Casale Fiori (Fig. 7.4.1.3.). You can arrive here following the road from Forca di Presta to Pretare for about 1.6 km from the pass where, on the right, there is a large parking. The fountain is 100 m south.

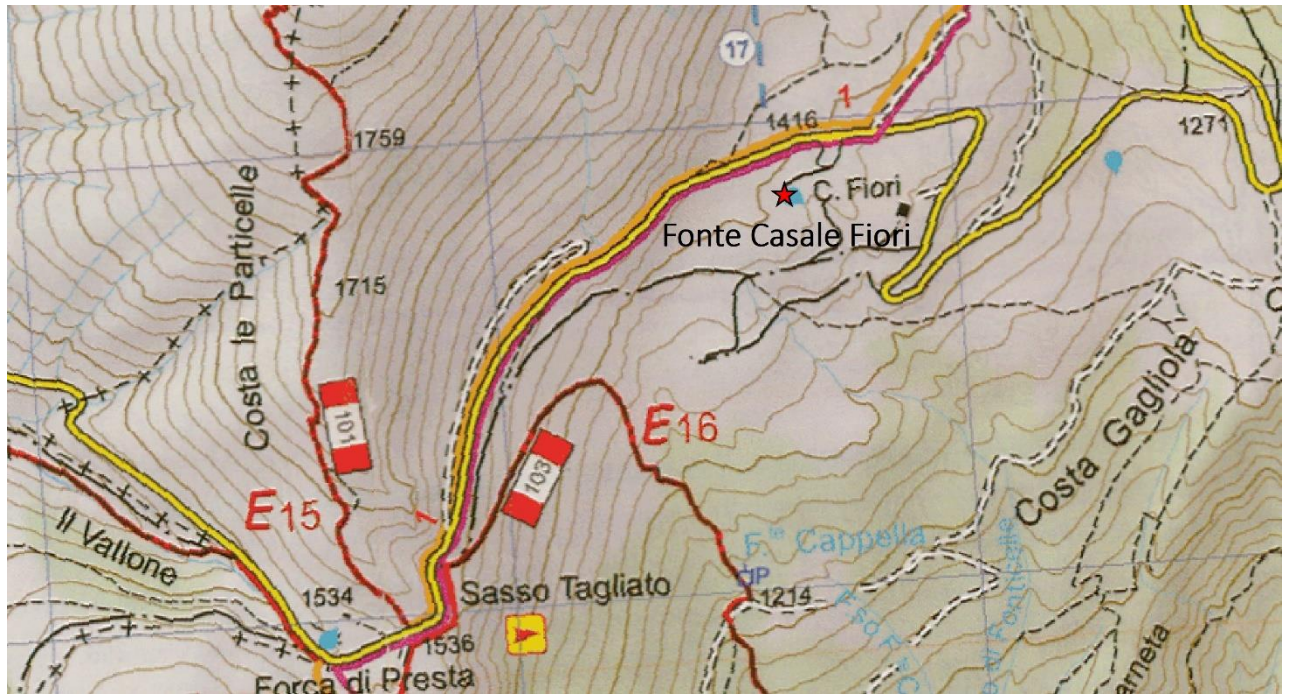


Fig. 7.4.1.3. Map of Forca di Presta – Costa Gagliola area. CAI – Monti Sibillini – Carta dei Sentieri 1:25'000

**Geological setting.** It is the southernmost of the springs lying onto landslide and slope deposits overlying the *Formazione della Laga* (LAG) (group a). However, the real (remember: it is only a watering place fed by a buried pipe) spring could probably come out from the *Calcare massiccio* (MAS) / *Corniola* (COI) cropping out in the road cut, few tens of meters above the tanks. Here, the thrust plane is the basal hydrogeological boundary, separating the calcareous-aquifer formations from the arenaceous/pelitic-aquiclude ones (Fig. 7.4.1.4.).

The complete succession is segmented by a series of W-dipping normal faults (belonging to the Monte Vettore – Monte Bove fault system). The E block is characterized by outcropping *Corniola*, resting discordantly onto *Calcare massiccio*: the former dips easternward while the latter dips towards NE. In the block included between the faults, the outcropping formations are *Calcaria a Posidonia* (POD) and *Marne del Monte Serrone* (MSE) overlying *Corniola*. The W block probably displays the whole complete succession, from *Corniola* to *Calcaria diasprigni* (CDU), whose beds are slightly WNW inclined.

The spring could be sustained:

- by a shallower flow (from W to E) inside *Maiolica* (MAI), *Calcaria diasprigni*, *Calcaria a Posidonia* (the last two only in case of pervasive fracturing) up to the contact with *Marne del Monte Serrone*, where it could emerge and infiltrate again in the Basal complex once *Corniola* outcrops are reached. *Calcaria diasprigni* and *Calcaria a Posidonia* can be aquifers only if characterized by

widespread pervasive fracturing because the former has a huge chert content filling the primary porosity and into the latter the marl content is not negligible.

- *Marne del Monte Serrone* could partially compartmentalize the shallower water route from the Basal complex (*Corniola* and *Calcare massiccio*), that conceivably emerges close to the contact with *Formazione della Laga*.

Therefore, Fonte Casale Fiori could be sustained by the Basal aquifer, through a permeability threshold emergence, and by a shallower contribution that combines with the former. In addition, the thick deposits, extending up to over the thrust line, might have a not too marginal contribution.

## Cross section Fonte Casale Fiori

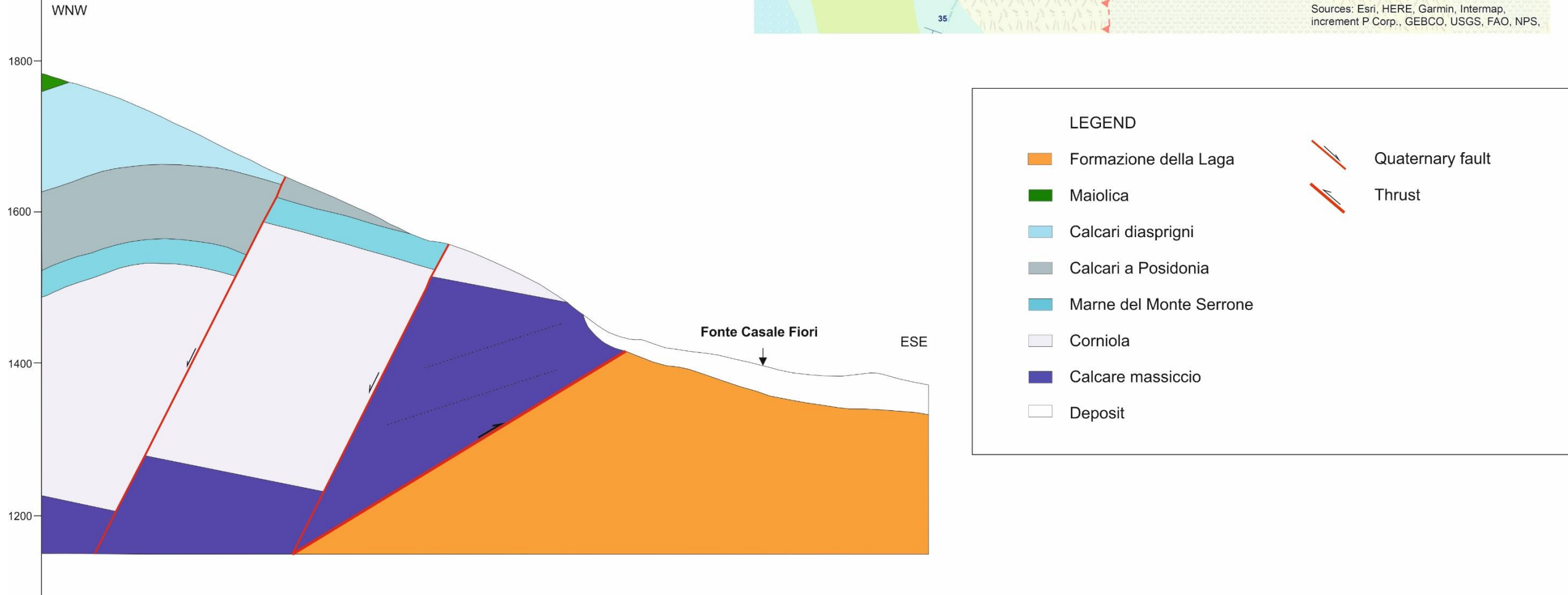


Fig. 7.4.1.4. Fonte Casale Fiori geologic cross section. ©CorelDraw 2018

#### 7.4.2. Physical and chemical data

##### PRE-EARTHQUAKE STATE

Physical parameters

Data	Air Temperature	Water Temperature	Flow rate (l/min)
7/5/2011	15.0	7.7	11.6
29/9/2011	14.7	12.5	0.35

Tab. 7.4.2.1. Pre-earthquake physical data

Chemical analysis

Data	pH	Conductivity ( $\mu\text{S}/\text{cm}$ )	Ca mg/l	Ca meq/l	Mg mg/l	Mg meq/l	HCO <sub>3</sub> mg/l	HCO <sub>3</sub> meq/l	Hardness (Ca+Mg) °F
7/5/2011	7.5	355.0	41.5	2.07	13.3	1.09	195.2	3.20	15.84
29/9/2011	7.5	411.0	66.2	3.30	19.3	1.59	209.8	3.44	24.48

Tab. 7.4.2.2. Pre-earthquake chemical data

##### POST-EARTHQUAKE STATE

Physical parameters

Data	Air Temperature	Water Temperature	Flow rate (l/min)
10/7/2018	--	10.6	12.1
11/9/2018	19.4	13.9	2.82
28/2/2018	13.3	8.6	23.0

Tab. 7.4.2.3. Post-earthquake physical data

Chemical analysis

Data	pH	Conductivity ( $\mu\text{S}/\text{cm}$ )	Ca mg/l	Ca meq/l	Mg mg/l	Mg meq/l	HCO <sub>3</sub> mg/l	HCO <sub>3</sub> meq/l	Hardness (Ca+Mg) °F
10/7/2018	8.08	458	66.16	3.30	23.31	1.92	285.62	4.68	26.12
11/9/2018	7.83	479	69.05	3.45	23.17	1.91	295.32	4.84	26.79
28/2/2018	7.83	386	65.77	3.28	17.01	1.40	257.85	4.23	23.43

Tab. 7.4.2.4. Post-earthquake chemical data

Here below the chemical analysis tables (from Fig. 7.4.2.1. to 7.4.2.3.) made by the Water Analysis Laboratory - UNICAM Chemical Division.

<b>Spring</b>		<b>Fonte Casale Fiori</b>			<b>Data:</b>	10/07/18	
pH at the emergence				8.08	Hydrogen ion activity at the spring		8.32E-09
spring temp				10.6			
lab temp			°C	21.4			
R.F. (180°C)	278	D.T.(G.F.)	29.3		Balance: cat		5.602625
K20 (µS/cm)	-	458 Alcal.Tot.	46.81	0.607	ani		5.540778
					1.10% =Δ=		0.061847
<b>Cationic Substances</b>		<b>mg/l</b>			<b>m.mol/l</b>	<b>mequiv/l</b>	<b>meq/meq.tot</b>
Lithium		<b>0.00443</b>			0.000638347	0.000638347	0.000057
Sodium		<b>7.76533</b>			0.337770045	0.337770045	0.030311
Potassium		<b>1.54280</b>			0.039459819	0.039459819	0.003541
Calcium		<b>66.15467</b>			1.650565536	3.301131071	0.296241
Magnesium		<b>23.31233</b>			0.959157924	1.918315847	0.172148
Strontium		<b>0.22300</b>			0.002545043	0.005090086	0.000457
Aluminum		<b>0.00000</b>			0	0	0.000000
Contaminants or cationic unwanted:							
Barium		<b>0.01298</b>			9.44804E-05	0.000188961	0.000017
Selenium		<b>0.00000</b>			0	0	0.000000
Chromium		<b>0.00026</b>			5.06802E-06	3.04081E-05	0.000003
Nickel		<b>0.00000</b>			0	0	0.000000
<b>Anionic:</b>					<b>2.99023626</b>	<b>5.60262458</b>	
Fluoride		<b>0.04580</b>			0.00241078	0.00241078	0.000216
Chloride		<b>4.92770</b>			0.138992469	0.138992469	0.012473
Bromine		<b>0.00000</b>			0	0	0.000000
Bicarbonate		<b>285.61590</b>			4.681007672	4.681007672	0.420070
Carbonate		<b>1.57060</b>			0.026173107	0.052346214	0.004698
Sulfate		<b>31.35814</b>			0.326456858	0.652913717	0.058592
Contaminants or anionic unwanted:							
Nitrite		<b>0.00000</b>			0	0	0.000000
Nitrate		<b>0.81270</b>			0.013107219	0.013107219	0.001176
<b>Neutral:</b>					<b>5.18814811</b>	<b>5.54077807</b>	
Contaminants or neutral unwanted:							
Boron		<b>0.01951</b>					
FIXED RESIDUE		mg/L	278.199202		TOTAL HARDNESS	°F	29.3
					TOTAL CALCULATED ALCALINITY		46.81

Spring			Fonte Casale Fiori		Data:	11/09/18	
pH at the emergence				7.83	Hydrogen ion activity at the spring		1.48E-08
spring temp				13.9			
lab temp			°C	22.2			
R.F. (180°C)	289	D.T.(G.F.)	29.5		Balance: cat	5.760184	
K20 (µS/cm)	-	479 Alcal.Tot.	48.4	0.603	ani	5.749100	
					0.19% =Δ=	0.011084	
<u>Cationic Substances</u>		<b>mg/l</b>		<b>m.mol/l</b>	<b>m.equiv/l</b>	<b>meq/meq.tot</b>	
Lithium		<b>0.00489</b>		0.000705143	0.000705143	0.000061	
Sodium		<b>8.51200</b>		0.370247934	0.370247934	0.032170	
Potassium		<b>1.24488</b>		0.031839992	0.031839992	0.002766	
Calcium		<b>69.04917</b>		1.722783599	3.445567199	0.299373	
Magnesium		<b>23.17082</b>		0.953335391	1.906670781	0.165664	
Strontium		<b>0.20586</b>		0.002349485	0.004698969	0.000408	
Aluminum		<b>0.00000</b>		0	0	0.000000	
Contaminants or cationic unwanted:							
Barium		<b>0.01919</b>		0.000139761	0.000279521	0.000024	
Selenium		<b>-0.00030</b>		-3.74641E-06	-3.74641E-06	0.000000	
Chromium		<b>0.00022</b>		4.28847E-06	2.57308E-05	0.000002	
Nickel		<b>0.00448</b>		7.62249E-05	0.00015245	0.000013	
<u>Anionic:</u>				<b>3.08147807</b>	<b>5.76018397</b>		
Fluoride		<b>0.04680</b>		0.002463417	0.002463417	0.000214	
Chloride		<b>6.01400</b>		0.169633035	0.169633035	0.014739	
Bromine		<b>0.00000</b>		0	0	0.000000	
Bicarbonate		<b>295.31744</b>		4.840007932	4.840007932	0.420531	
Carbonate		<b>0.91545</b>		0.015255475	0.03051095	0.002651	
Sulfate		<b>33.05357</b>		0.344107292	0.688214583	0.059796	
Contaminants or anionic unwanted:							
Nitrite		<b>0.00000</b>		0	0	0.000000	
Nitrate		<b>1.13280</b>		0.018269789	0.018269789	0.001587	
<u>Neutral:</u>				<b>5.38973694</b>	<b>5.74909971</b>		
Contaminants or neutral unwanted:							
Boron		<b>0.01929</b>					
FIXED RESIDUE		mg/L	288.612727				
				TOTAL HARDNESS		°F	29.5
				TOTAL CALCULATED ALCALINITY			48.4

<b>Spring</b>	Fonte Casale Fiori			<b>Data:</b>	28/02/19	
pH at the emergence			7.83	Hydrogen ion activity at the spring		1.48E-08
Air temperature on the field			13.3			
spring temp		°C	8.6			
R.F. (180°C)	242	D.T.(G.F.)	25.02		Balance: cat	4.898536
K20 (µS/cm)	386	Alcal.Tot.	42.26		ani	4.824172
A.T.(Carb)	211.3	D.T.(Carb)	234.4302568		1.52% =Δ=	0.074364
<b>Cationic</b>				<b>m.mol/l</b>	<b>m.equiv/l</b>	<b>m.eq/m.eq.tot</b>
<b>Substances</b>	<b>2019</b>					
Lithium		<b>0.00290</b>		0.000417807	0.000417807	0.000043
Sodium		<b>4.60620</b>		0.200356677	0.200356677	0.020607
Potassium		<b>0.51470</b>		0.013164356	0.013164356	0.001354
Calcium		<b>65.76497</b>		1.64084244	3.28168488	0.337528
Magnesium		<b>17.00475</b>		0.699639992	1.399279984	0.143919
Strontium		<b>0.14322</b>		0.001634558	0.003269117	0.000336
Aluminum		<b>0.00061</b>		2.24611E-05	6.73832E-05	0.000007
Contaminants or cationic unwanted:						
Barium		<b>0.01400</b>		0.000101944	0.000203888	0.000021
Selenium		<b>0.00045</b>		5.69909E-06	5.69909E-06	0.000001
Chromium		<b>0.00034</b>		6.53896E-06	3.92338E-05	0.000004
Nickel		<b>0.00137</b>		2.3335E-05	4.66701E-05	0.000005
<b>Anionic:</b>				<b>2.55621581</b>	<b>4.8985357</b>	
Fluoride		<b>0.04710</b>		0.002479208	0.002479208	0.000255
Chloride		<b>4.68530</b>		0.132155248	0.132155248	0.013592
Bromine		<b>0.00000</b>		0	0	0.000000
Bicarbonate		<b>257.85362</b>		4.226006926	4.226006926	0.434653
Carbonate		<b>0.79932</b>		0.013320173	0.026640346	0.002740
Sulfate		<b>20.28136</b>		0.211141001	0.422282002	0.043433
Contaminants or anionic unwanted:						
Nitrite		<b>0.00330</b>		7.17313E-05	7.17313E-05	0.000007
Nitrate		<b>0.90130</b>		0.014536159	0.014536159	0.001495
<b>Neutral:</b>				<b>4.59971045</b>	<b>4.82417162</b>	
Contaminants or neutral unwanted:				0 total milliequivalents	meq/L	9.72270732
Boron		<b>0.01260</b>		total mMol	mM/L	7.15592626
FIXED RESIDUE	mg/L	241.58089		TOTAL HARDNESS	°F	25.02
				TOTAL CALCULATED ALCALINITY		42.26

Fig. from 7.4.2.1. to 7.4.2.3. Chemical analysis tables elaborated by UNICAM – Water Analysis Laboratory

#### 7.4.3. Data analysis

As a result of the different geological setting, it is legitimate to expect values quite different from the previous springs. The good accessibility, the lower elevation and the S exposure have permitted to perform surveys in periods during which the upper springs were covered by the snow (Fig. 7.4.3.1.).



Fig. 7.4.3.1. The fountain on February, 28<sup>th</sup> 2019

The underlying **flow rate** diagram (Fig. 7.4.3.3.) displays larger values than those seen up to here and a regular seasonal trend with higher values in late-spring/early-summer, lower ones at the beginning of autumn and a maximum registered in winter 2019, during an exceptionally hot period (Fig. 7.4.3.2.) that led to a rapid snowmelt.

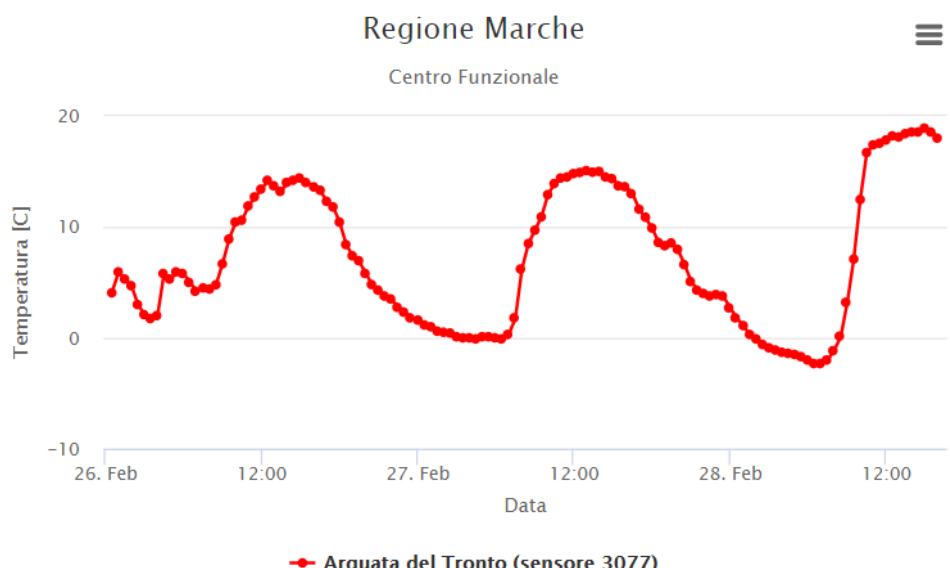


Fig. 7.4.3.2. Temperature since February 26<sup>th</sup> to 28<sup>th</sup> 2019 in Capodacqua. SIRMIP – Protezione Civile Regionale – Regione Marche

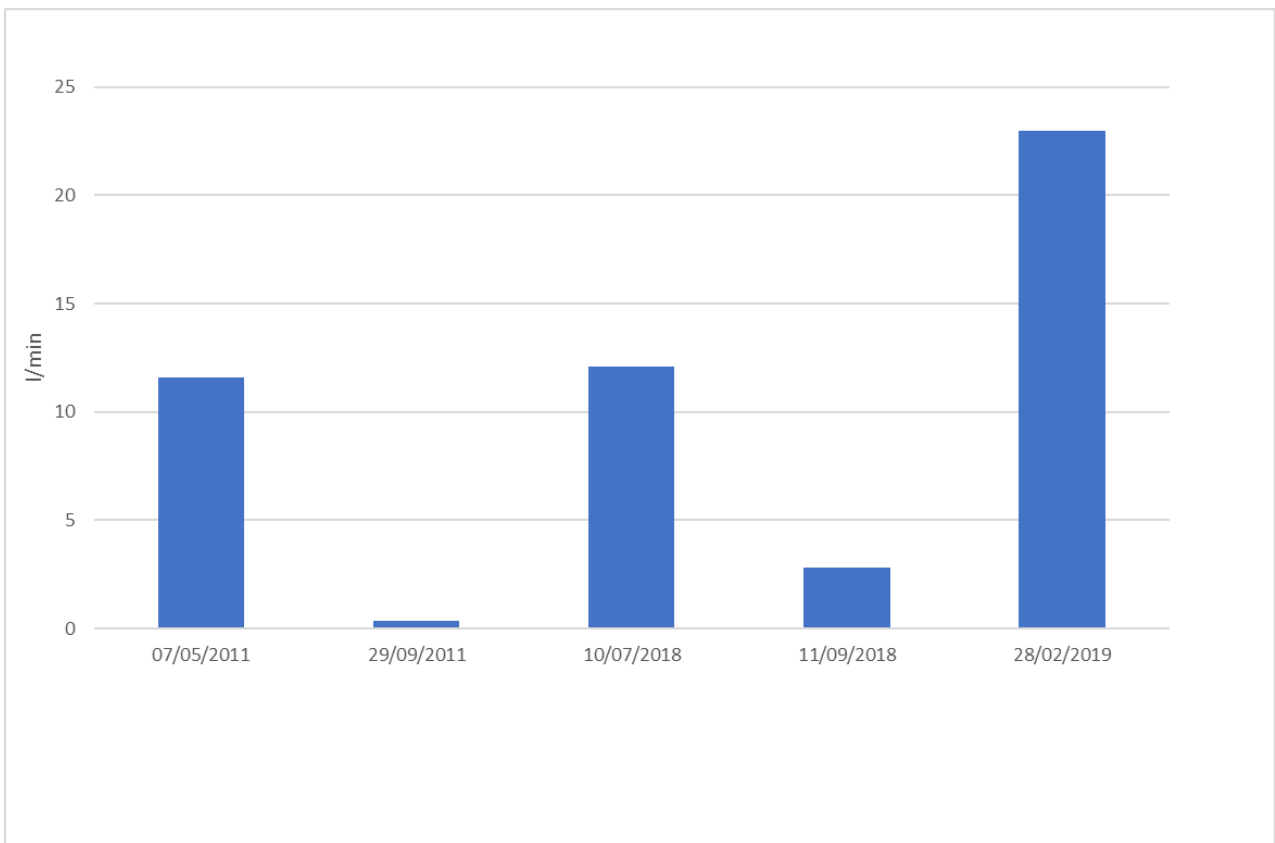


Fig.7.4.3.3. Flow rate data. ©Microsoft Excel

The May 2011 value is almost equal to the July 2018 one. Consequently, according to the typical seasonal regime, the May 2018 flow rate should be higher respect to the May 2011 one. If this were true, the 2018 winter should have been more snowy than the 2011 one, but this was not the case: since September to April in 2011 and 2018, in Capodacqua, fell respectively 875.4 mm and 650.4 mm of rain. Also, the September data are higher in 2018 (+2.47 l/min), not due to precipitations again. Therefore, excluding climatic factors, this change is to be assigned to the earthquake and, according to the hydrogeological model proposed in the geological description, it should be confined in the Basal aquifer.

The **water temperature** changes inversely with the flow rate (Fig. 7.4.3.4.), as one would expect for this type of springs.

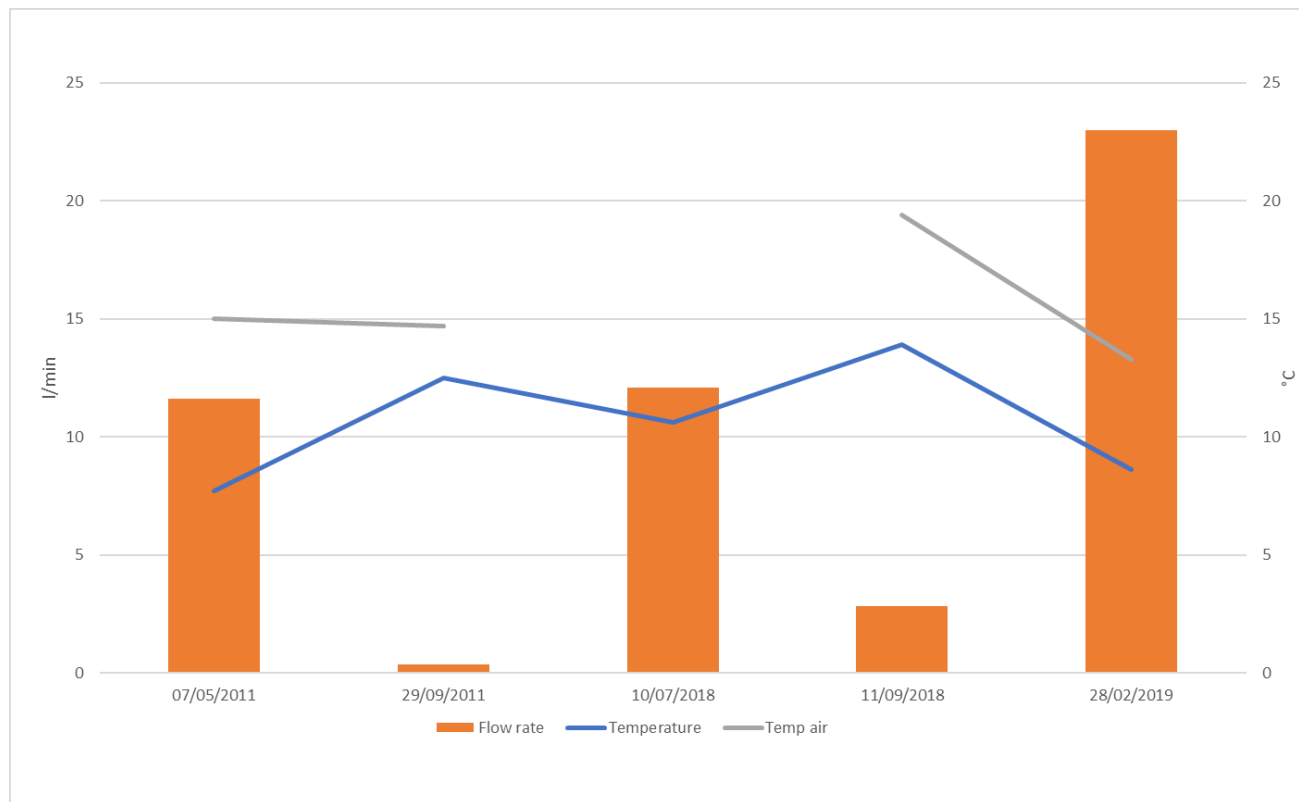


Fig. 7.4.3.4. Flow rate, water and air temperatures data. ©Microsoft Excel

During the snowmelt periods, lower water T values were collected: May 2011 and February 2019, but also July 2018. The reason could be linked to the shallower water path, bordered at the bottom by *Marne del Monte Serrone*, which would permit a rapid and shallow outflow. According this scenario, the water temperature is more stable during dry seasons, because the flow is sustained only by the Basal aquifer, and it decreases during the snowmelt feeding the shallow aquifer. Probably the snow melting rate plays a key role, as in case of higher air temperatures a less water amount could infiltrate in the Basal aquifer and a volume would rapidly reach the spring, decreasing the temperature.

The maximum water T value has been registered in September 2018 (13.9 °C) and it coincides with the higher air temperature data. Then, the water temperature fell to 8.6 °C in February 2019. Here they seem to be directly linked, but looking at the May-September 2011 values, this is denied and probably is the truth. Therefore, presumably a more complex mechanism, perhaps linked to the complex hydrogeological setting, relates water and air temperature.

The **conductivity** values (Fig. 7.4.3.5.) are much larger than the previous springs (+ 230 µS/cm in average), due to the higher water residence time and longer underground travelled path.



Fig. 7.4.3.5. Conductivity vs Calcium, Magnesium and Bicarbonate contents. ©Microsoft Excel

Comparing the 2011-2018/2019 data a general growth is noticeable. The seasonal trend, with higher values in correspondence of lower flow rates, is respected. Being able to exclude pre-earthquake dilution effects (the average discharge increases after the seismic sequence), as evidenced in the flow rate analysis, and looking at the ions concentrations, the conductivity increase should be related to the increased ions solubilization. The huge drop (-93  $\mu\text{S}/\text{cm}$ ) registered from September 2018 to February 2019 is attributable to dilution effects linked to a quick snowmelt.

**Chemical composition.** On the Piper diagram (Fig. 7.4.3.6.), Fonte Casale Fiori water falls in the bicarbonate-calcium and/or magnesium area, crossing limestone and marly lithologies.

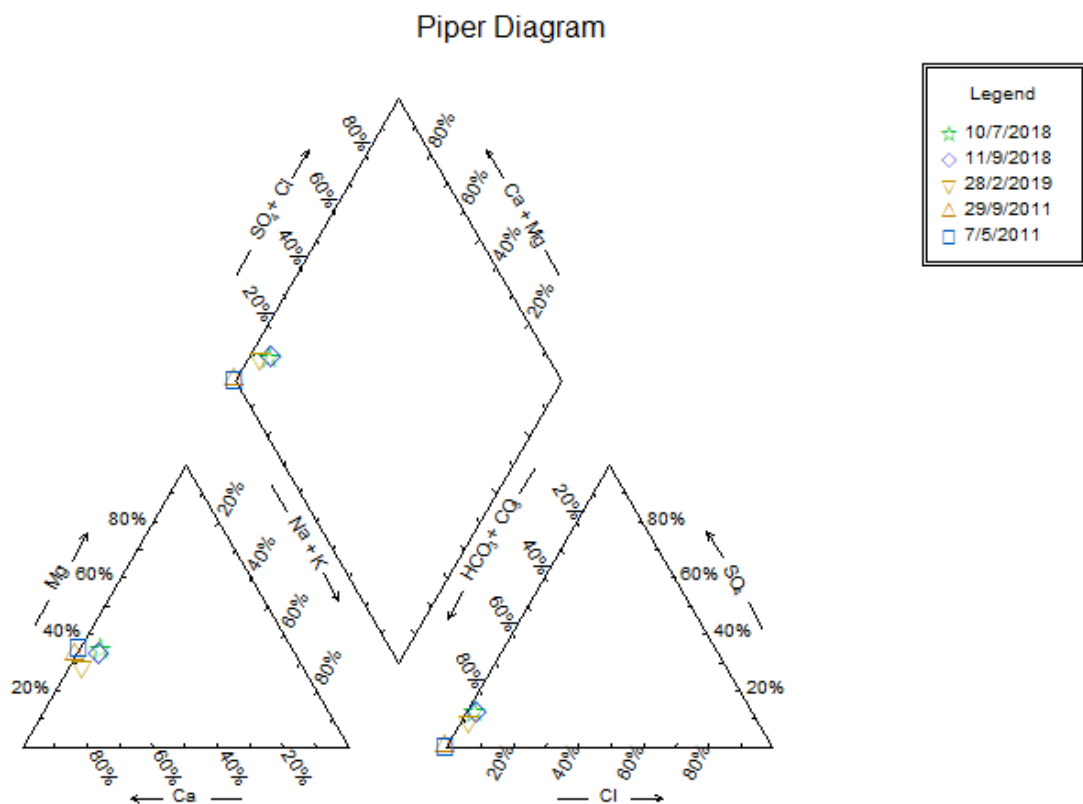


Fig. 7.4.3.6. The Piper chart. ©RockWare - AqQa

The reliable pre/post-seismic sequence correlation is between September 2011 and September 2018 values (Fig. 7.4.3.7.).

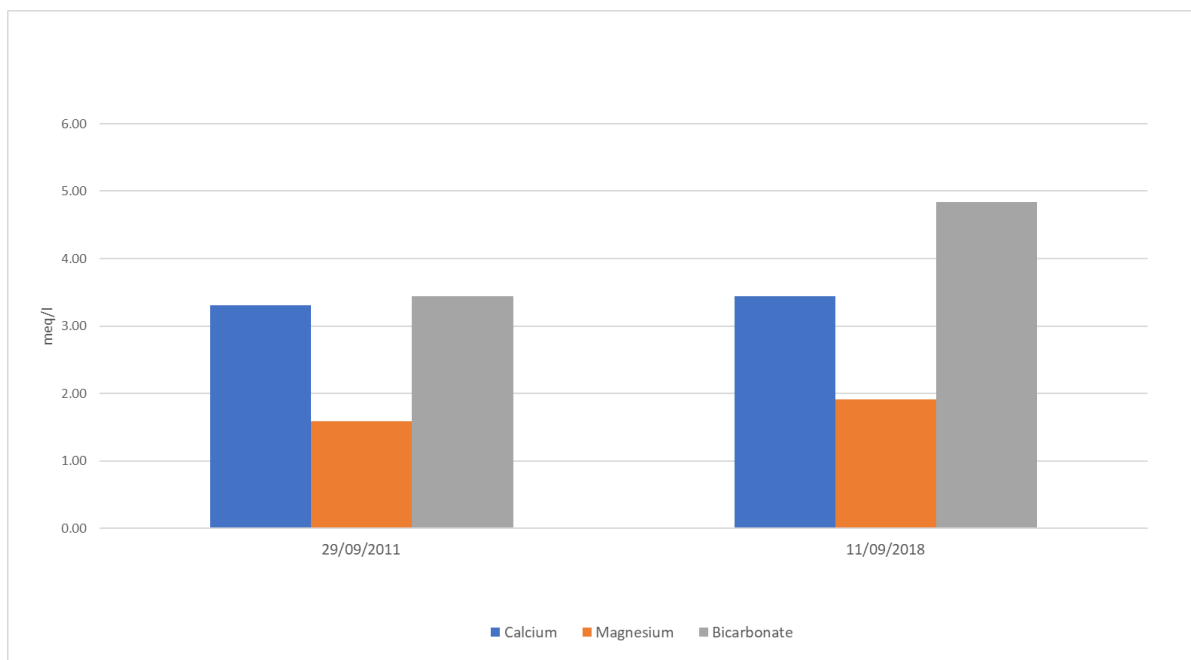


Fig. 7.4.3.7. Ca, Mg and  $\text{HCO}_3^-$  column graph. ©Microsoft Excel

Modest increments in Calcium and Magnesium (+ 0.14 and + 0.32 meq/l) and a higher one (+ 1.40 meq/l) in Bicarbonate have been noticed. Cumulative rainfalls, in Capodacqua, since September of the previous year, are 1008 mm in 2010/2011 and 1058 mm in 2017/2018. In the month prior to the 2011 sampling no precipitations occurred; instead, between August and September 2018, 36.6 mm have been registered. Therefore, a climatic factor could be excluded, due to the magnitude of the relative variations, it is easier to ascribe to the earthquake effects the Bicarbonate rise, respect to the Calcium and Magnesium ones. It is crucial to keep in mind that such a small change in concentrations (especially Ca and Mg) may be related to other more complex factors.

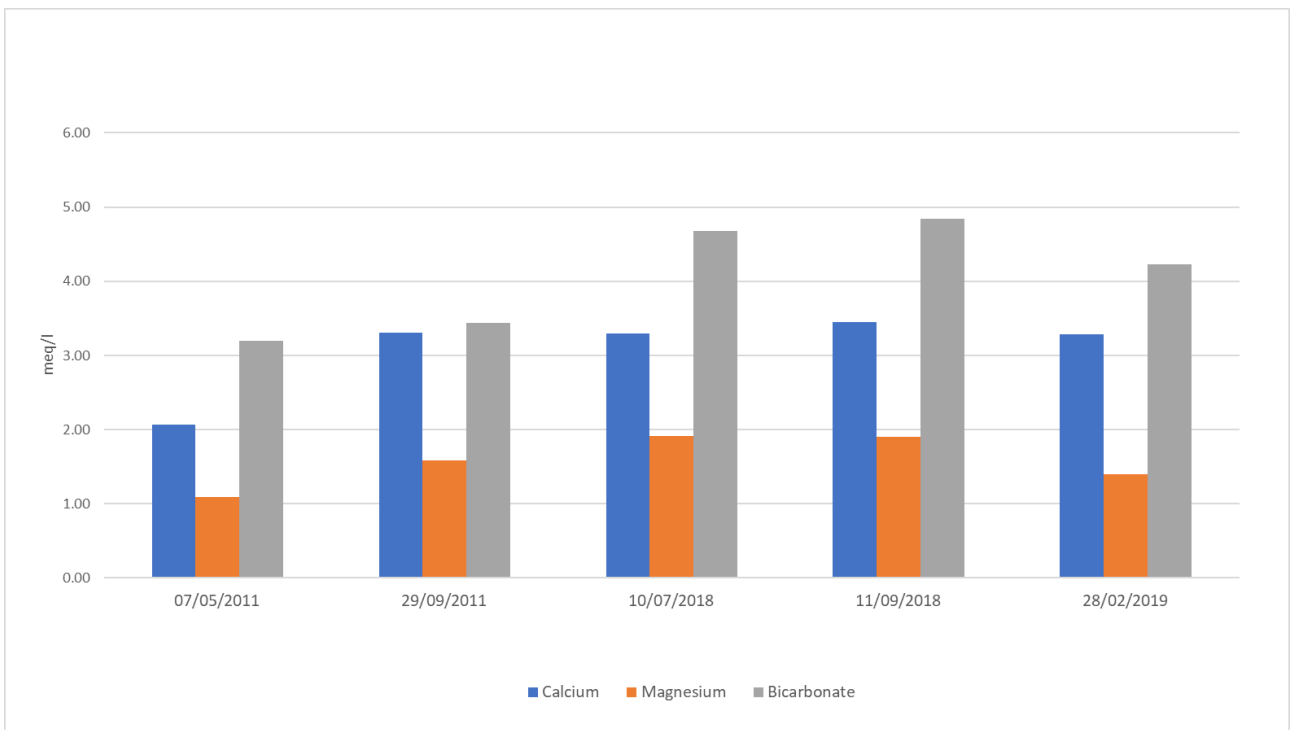


Fig. 7.4.3.8. Ca, Mg and  $\text{HCO}_3^-$  column graph. ©Microsoft Excel

From the above whole concentrations chart (Fig.7.4.3.8.), we can observe:

- a great Calcium increase (+1.20 meq/l) between May and September 2011 respect to other ions. Therefore, if it was characterized by a seasonal trend, a decrease in its concentration was probable expected for the 2012 spring/summer. After the earthquake no such a huge rise in Ca level was ever registered; it remains almost stable with values similar to that of September 2011.

The other hypothesis is that the anomalous May 2011 low value is due to a laboratory mistake which could have underestimated the data. Consequently, the Ca variation rate should be lower.

- Magnesium increases of 0.49 meq/l from May to September 2011 (+0.003 (meq/l)/day), remains stable during the 2018 summer and decreases of 0.51 meq/l from September 2018 to February 2019 (-0.003 (meq/l)/day). An explanation could be in the different solubility of Calcite ( $\text{CaCO}_3$ ) and Dolomite ( $(\text{Mg},\text{Ca})\text{CO}_3)_2$ ), both present in *Corniola* and *Calcare massiccio*. The  $\text{CaCO}_3$  has a solubility of 0.014 g/l while the Mg-carbonate of 0.106 g/l (at 293K or 20°C), therefore Magnesium enters in solution easier than Calcium, whose change rates are always lower (with the exception of May-September 2011).

Therefore, according to this model the melting water crosses Mg-rich lithologies carrying with it mostly Calcium ions (because Calcite is much more widespread in these rocks) but also Magnesium ones. Mg variation gradient, thanks to its higher solubility, is higher than that of Ca. This is the reason why, during spring/early summer and autumn/winter, Magnesium varies faster than Calcium, and in the dry seasons the former is almost constant.

- Bicarbonate levels show a more homogeneous behavior, characterized by a seasonal trend and a general huge increment after the earthquake, which is unreliable, for its magnitude, to climatic factors and so attributable to the shaking.

## 7.5. Fonte delle Cacere

### 7.5.1. Detailed features and geological setting

Elevation: 1359 m a.s.l. – Hydrographic basin: Tronto

Coordinates: 33T 359114 4740315 UTM / 13°16'37,387" E 42°48'8,759" N

Description: it is a watering place with three tanks (Fig. 7.5.1.) (Aringoli et al., 2017) fed by an intake (Fig. 7.5.3.) 50 m SW.



Fig. 7.5.1. Fonte delle Cacere (July, 7<sup>th</sup> 2018)



Fig. 7.5.2. The spring on February, 28<sup>th</sup> 2019



Fig. 7.5.3. The intake

Location: it is located at the bottom of the SE slope of the Forca di Presta – Vettoretto ridge (Fig. 7.5.4.), along the Mietitori path. You can get there following the road from Forca di Presta to Pretare, leaving your car on the right, 1.6 km after the pass. Soon after the track crosses the road; continuing on the path for about 500 m you will come to the fountain.



Fig. 7.5.4. Map of Forca di Presta – Costa Gagliola area. CAI – Monti Sibillini – Carta dei Sentieri 1:25'000

**Geological setting.** The tanks are connected to the main emergence through a conduit. The spring lies on coverages over *Formazione della Laga* (LAG). The carbonatic domain is segmented by one of the same normal faults displayed in the Fonte Casale Fiori section (Fig. 7.5.5.). The W block is characterized by complete succession from *Corniola* to outcropping *Calcare massiccio*, whose beds slightly dip NE. The E block holds the Basal aquifer: *Corniola* outcropping beds, E dipping, unconformably lies (on a Jurassic paleofault) onto *Calcare massiccio* NW dipping. The proposed hydrogeological setting supposes an alimentation mainly sustained by the Basal aquifer, emerging by permeability threshold near the thrust line, and to a lesser extent by the thick deposits above the emergence.

## Cross section Fonte delle Cacere

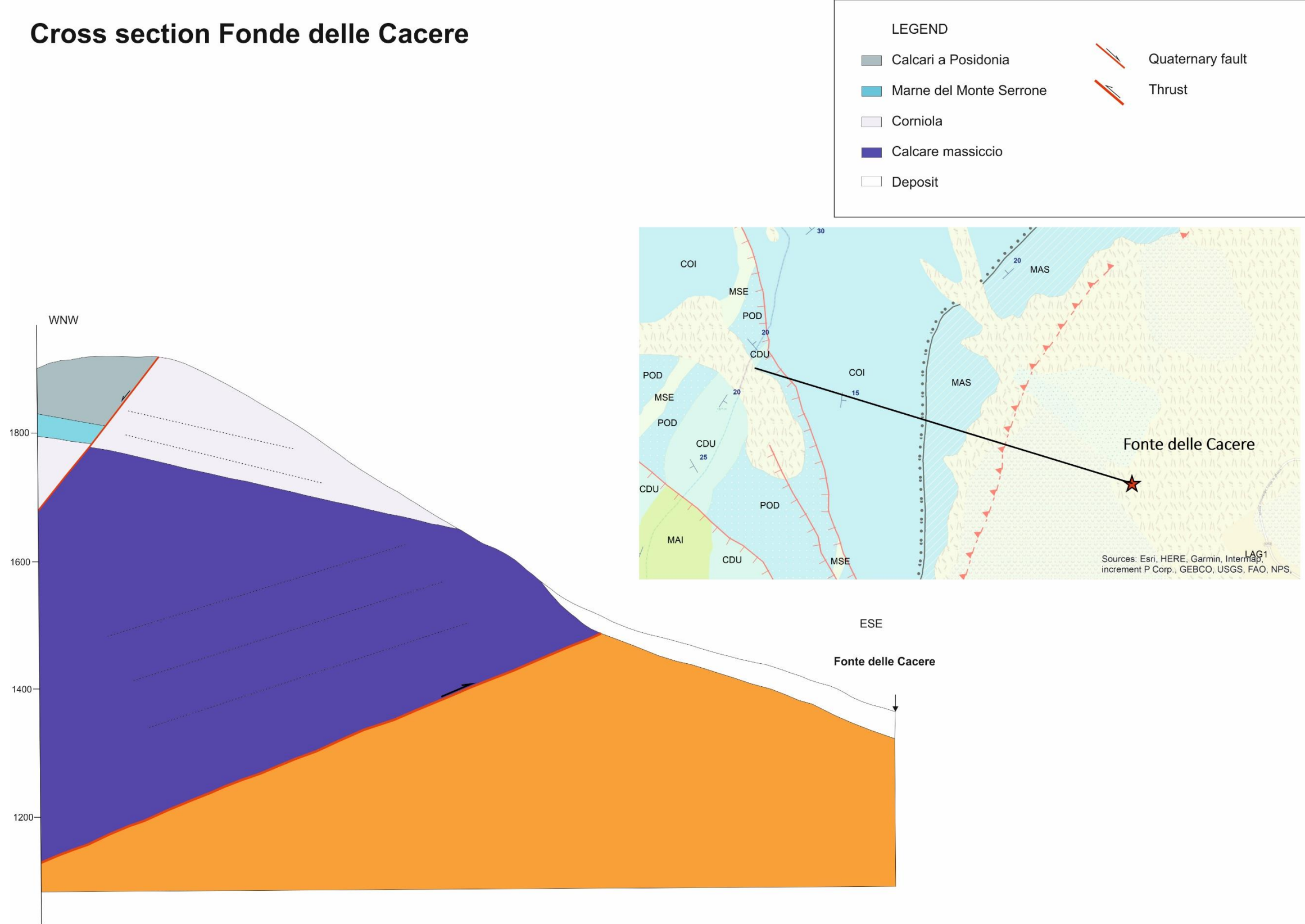


Fig. 7.5.5. Fonte delle Cacere geological cross section. ©CorelDraw 2018

### 7.5.2. Physical and chemical data

#### PRE-EARTHQUAKE STATE

Physical parameters

Data	Air Temperature	Water Temperature	Flow rate (l/min)
7/5/2011	17.2	8.5	4.6
29/9/2011	13.9	9.3	5.5

Tab. 7.5.2.1. Pre-earthquake physical data

Chemical analysis

Data	pH	Conductivity ( $\mu\text{S}/\text{cm}$ )	Ca mg/l	Ca meq/l	Mg mg/l	Mg meq/l	HCO <sub>3</sub> mg/l	HCO <sub>3</sub> meq/l	Hardness (Ca+Mg) °F
7/5/2011	7.5	197.0	30.6	1.53	9.4	0.77	134.2	2.20	11.51
29/9/2011	7.5	261.0	45.9	2.29	8.7	0.72	144.3	2.37	15.04

Tab. 7.5.2.2. Pre-earthquake chemical data

#### POST-EARTHQUAKE STATE

Physical parameters

Data	Air Temperature	Water Temperature	Flow rate (l/min)
10/7/2018	--	11.9	3.89
11/9/2018	20.6	11.4	3.96
28/2/2018	11.7	8.4	5.73

Tab. 7.5.2.3. Post-earthquake physical data

Chemical analysis

Data	pH	Conductivity ( $\mu\text{S}/\text{cm}$ )	Ca mg/l	Ca meq/l	Mg mg/l	Mg meq/l	HCO <sub>3</sub> mg/l	HCO <sub>3</sub> meq/l	Hardness (Ca+Mg) °F
10/7/2018	8.49	288	43.67	2.18	13.56	1.12	195.98	3.21	16.49
11/9/2018	8.31	289	47.83	2.39	14.74	1.21	214.17	3.51	18.02
28/2/2018	8.25	266	46.46	2.32	11.28	0.93	191.41	3.14	16.25

Tab. 7.5.2.4. Post-earthquake chemical data

Here below the chemical analysis tables (Fig. 7.5.2.1. to 7.5.2.3.) made by the Water Analysis Laboratory – UNICAM Chemical Division.

Spring		Fonte delle Cacere		Data:	02/07/18		
pH at the emergence			8.49	Hydrogen ion activity at the spring			3.24E-09
spring temp			11.9				
lab temp		°C	21.7				
R.F. (180°C)	166	D.T.(G.F.)	17.5		Balance: cat		3.431211
K20 (µS/cm)	-	288 Alcal.Tot.	32.12 <b>0.575</b>		ani		3.442578
					-0.33% =Δ=		-0.011367
<u>Cationic</u>				<u>m.mol/l</u>	<u>m.equiv/l</u>	<u>m.eq/m.eq.tot</u>	
<u>Substances</u>							
Lithium		<b>0.00055</b>		7.92439E-05	7.92439E-05		0.000012
Sodium		<b>2.65032</b>		0.115281427	0.115281427		0.016771
Potassium		<b>0.75528</b>		0.019317612	0.019317612		0.002810
Calcium		<b>43.66080</b>		1.089341317	2.178682635		0.316955
Magnesium		<b>13.55760</b>		0.55781115	1.1156223		0.162301
Strontium		<b>0.09574</b>		0.001092627	0.002185255		0.000318
Aluminum		<b>0.00000</b>		0	0		0.000000
Contaminants or cationic unwanted:							
Barium		<b>0.00166</b>		1.21095E-05	2.4219E-05		0.000004
Selenium		<b>0.00000</b>		0	0		0.000000
Chromium		<b>0.00016</b>		2.99478E-06	1.79687E-05		0.000003
Nickel		<b>0.00000</b>		0	0		0.000000
<u>Anionic:</u>				<b>1.78293848</b>	<b>3.43121066</b>		
Fluoride		<b>0.03840</b>		0.002021265	0.002021265		0.000294
Chloride		<b>2.60110</b>		0.073367557	0.073367557		0.010674
Bromine		<b>0.00000</b>		0	0		0.000000
Bicarbonate		<b>195.98339</b>		3.212005264	3.212005264		0.467283
Carbonate		<b>2.74602</b>		0.04576094	0.09152188		0.013315
Sulfate		<b>2.96461</b>		0.030863351	0.061726701		0.008980
Contaminants or anionic unwanted:							
Nitrite		<b>0.00000</b>		0	0		0.000000
Nitrate		<b>0.12000</b>		0.001935359	0.001935359		0.000282
<u>Neutral:</u>				<b>3.36595374</b>	<b>3.44257803</b>		
Contaminants or neutral unwanted:							
Boron		<b>0.00361</b>					
FIXED RESIDUE		mg/L	165.56885				
				TOTAL HARDNESS		°F	17.5
				TOTAL CALCULATED ALCALINITY			32.12



Spring		Fonte delle Cacere		Data:	28/02/19	
pH at the emergence			8.25	Hydrogen ion activity at the spring		5.62E-09
Air temperature on the field			11.7			
spring temp		°C	8.4			
R.F. (180°C)	161	D.T.(G.F.)	18.77	Balance: cat		3.337605
K20 ( $\mu\text{S}/\text{cm}$ )	-	266 Alcal.Tot.	31.37	ani		3.317771
A.T.(Carb)	0	D.T.(Carb)	162.5586917	0.59%	=Δ=	0.019835
Cationic		mg/l		m.mol/l	mequiv/l	meq/meq.tot
<u>Substances</u>						
Lithium		<b>0.00051</b>		7.27561E-05	7.27561E-05	0.000011
Sodium		<b>1.90708</b>		0.082952675	0.082952675	0.012464
Potassium		<b>0.23755</b>		0.00607581	0.00607581	0.000913
Calcium		<b>46.45725</b>		1.159113024	2.318226048	0.348324
Magnesium		<b>11.27879</b>		0.464052047	0.928104094	0.139452
Strontium		<b>0.06951</b>		0.000793312	0.001586624	0.000238
Aluminum		<b>0.00263</b>		9.73314E-05	0.000291994	0.000044
Contaminants or cationic unwanted:						
Barium		<b>0.01400</b>		0.000101944	0.000203888	0.000031
Selenium		<b>0.00045</b>		5.69909E-06	5.69909E-06	0.000001
Chromium		<b>0.00034</b>		6.53896E-06	3.92338E-05	0.000006
Nickel		<b>0.00137</b>		2.3335E-05	4.66701E-05	0.000007
<u>Anionic:</u>				<b>1.71329447</b>	<b>3.33760549</b>	
Fluoride		<b>0.04730</b>		0.002489736	0.002489736	0.000374
Chloride		<b>2.34580</b>		0.066166474	0.066166474	0.009942
Bromine		<b>0.00000</b>		0	0	0.000000
Bicarbonate		<b>191.40719</b>		3.137005141	3.137005141	0.471349
Carbonate		<b>1.55267</b>		0.025874339	0.051748677	0.007775
Sulfate		<b>2.63747</b>		0.027457629	0.054915258	0.008251
Contaminants or anionic unwanted:						
Nitrite		<b>0.00330</b>		7.17313E-05	7.17313E-05	0.000011
Nitrate		<b>0.33320</b>		0.005373847	0.005373847	0.000807
<u>Neutral:</u>				<b>3.2644389</b>	<b>3.31777086</b>	
		--		total milliequivalents	meq/L	<b>6.65537636</b>
Contaminants or neutral unwanted:				total mMol	mM/L	<b>4.97773337</b>
Boron		<b>0.00700</b>				
FIXED RESIDUE		mg/L	161.01891	TOTAL HARDNESS	°F	18.77
				TOTAL CALCULATED ALCALINITY		31.37

Fig. 7.5.2.1. to 7.5.2.3. Chemical analysis tables elaborated by UNICAM – Water Analysis Laboratory

### 7.5.3. Data analysis

Fonte delle Cacere, the second spring of the lower group, is fed by an aqueduct whose emergence is sited close to the fountain. The geological setting is quite similar to the previous spring, but only one fault has displaced the carbonatic domain, with almost certain hydrogeological differences that, as it will be seen later, could have an impact on the measured parameters. As for Fonte Casale Fiori, a winter post-earthquake measurement has been performed.



Fig. 7.5.3.1. Detail of the fountain (July, 7<sup>th</sup> 2018)

The first considered parameter is the **flow rate**. From the graph below (Fig. 7.5.3.2.) it appears an unusual trend, especially for the 2011 surveys, characterized by an increase from May to September.

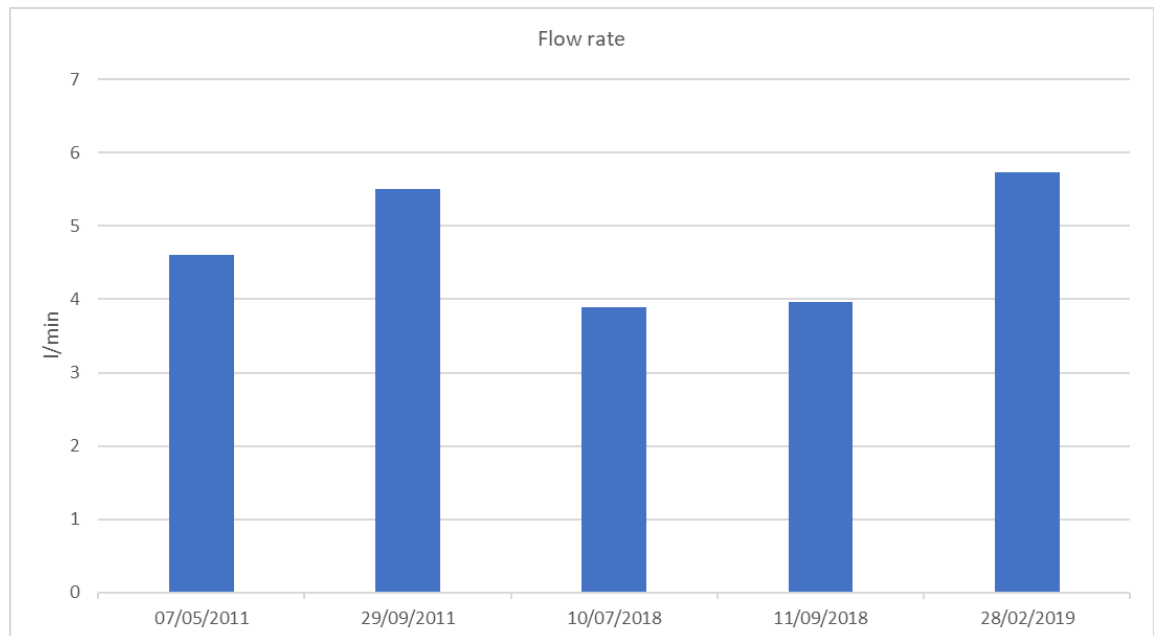


Fig.7.5.3.2. Flow rate data. ©Microsoft Excel

The natural behavior should be characterized by a maximum in the spring/early summer period, followed by a gradual decrease up to the late autumn/winter, at the net of sporadic rainfalls. The anomaly can be easily ascribed to the intake that allows to control the flow towards the fountain. Precipitations also support this hypothesis: in September 2011 in Capodacqua no rainfalls were registered. The flow was stable from July to September 2018, while in Fonte Casale Fiori it had dropped, despite the closeness between the emergences. The only interval displaying a seasonal trend is from September 2018 to February 2019. This presumably depends on the rapid snowmelt (water excess at the intake), which characterize the days before the 2019 sampling. Therefore, we can conclude that, in this case, a flow rate analysis is not suitable for the hydrogeologic reconstruction.

The **water temperature** is more stable compared to Fonte Casale Fiori (Fig. 7.5.3.3.), with a minimum registered in February 2019 ( $8.4^{\circ}\text{C}$ ) and a maximum in July 2018 ( $11.9^{\circ}\text{C}$ ). A lower temperature seasonal variation could mean that the spring is mainly sustained by a deeper circulation inside the Basal aquifer. Usually, flow rate and water temperature are inversely correlated and this is appreciable between September 2018 and February 2019, when the temperature has dropped because of the season. However, the hot days, in the end of February 2019, fast melted the snow causing great runoff which may have contributed to reduce the water temperature. It is possible that runoff concentrates over slope and landslide deposits, characterized by a lower permeability respect to *Calcare massiccio* and *Corniola* limestones that crop out above the deposits.

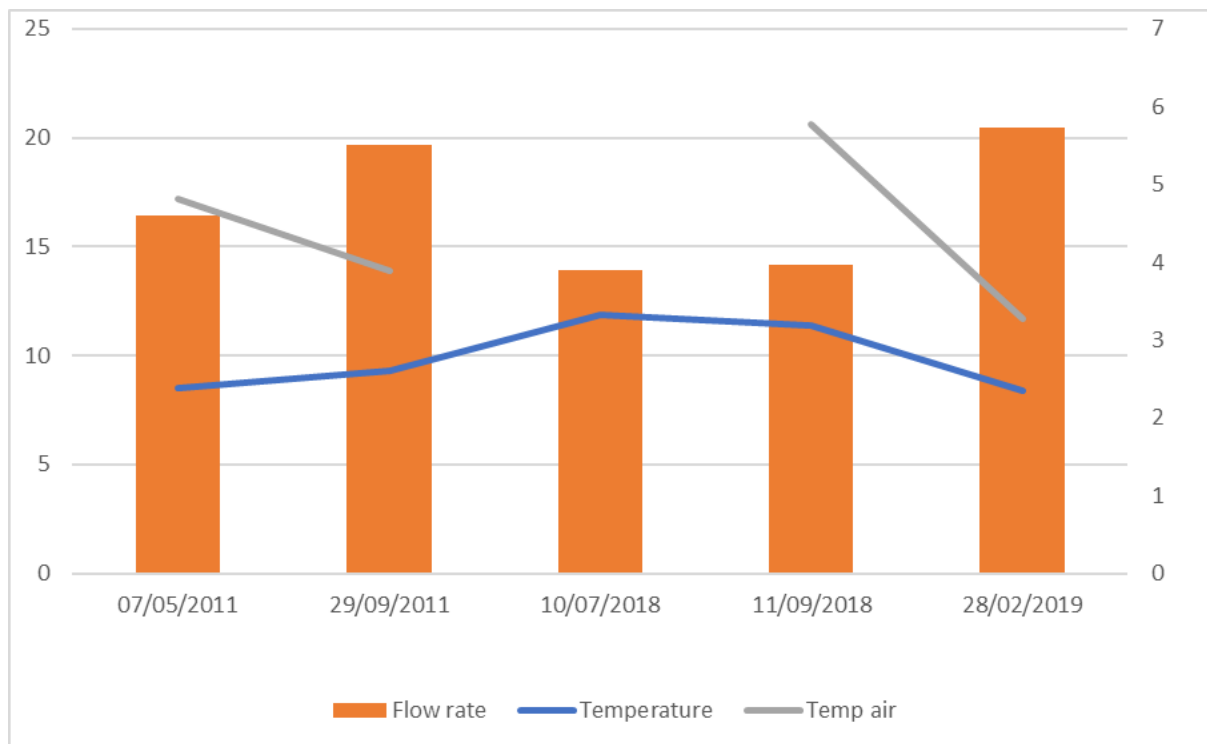


Fig. 7.5.3.3. Flow rate, water and air temperatures data. ©Microsoft Excel

The **conductivity** on average is higher respect to the upper springs but lower than that of Fonte Casale Fiori (Fig. 7.5.3.4.). Also, a post-earthquake increment is present. Anyhow, it seems to follow a quasi-typical seasonal trend after the seismic sequence.



Fig. 7.5.3.4. Conductivity vs Calcium, Magnesium and Bicarbonate contents. ©Microsoft Excel

An important increment is present between May and September 2011 with a variation gradient of 0.44 ( $\mu\text{S}/\text{cm}$ )/day. During the summer 2018, conductivity has remained stable and then decreases, from September 2018 to February 2019, of a magnitude much lower (gradient of -0.14 ( $\mu\text{S}/\text{cm}$ )/day) than the pre-earthquake summer gain. Substantially, the 2018-2019 measures are less affected by the seasonal signal respect to the 2011 ones. This could be a consequence of the shaking-induced ions solubilization that has reduced the influence of the flow rate on the conductivity. Before the earthquake, in dry periods the conductivity was high (water rich in salts), and with increasing flow rate (wet seasons), the salts became much more diluted, as one would expect. In 2018, considering the same flow rate behavior, in wet conditions the salts concentration did not decrease, as in 2011, due to the larger ions availability. In dry conditions the conductivity increases, but with a lower rate compared to 2011. Comparing the September values, a dilution phenomenon for 2011 can be excluded because of the slightly higher precipitations registered in 2017/2018 interval.

**Chemical composition.** Up to here all the springs fall to the bicarbonate-calcium and/or magnesium facies area and Fonte delle Cacere is no exception (Fig. 7.5.3.5.).

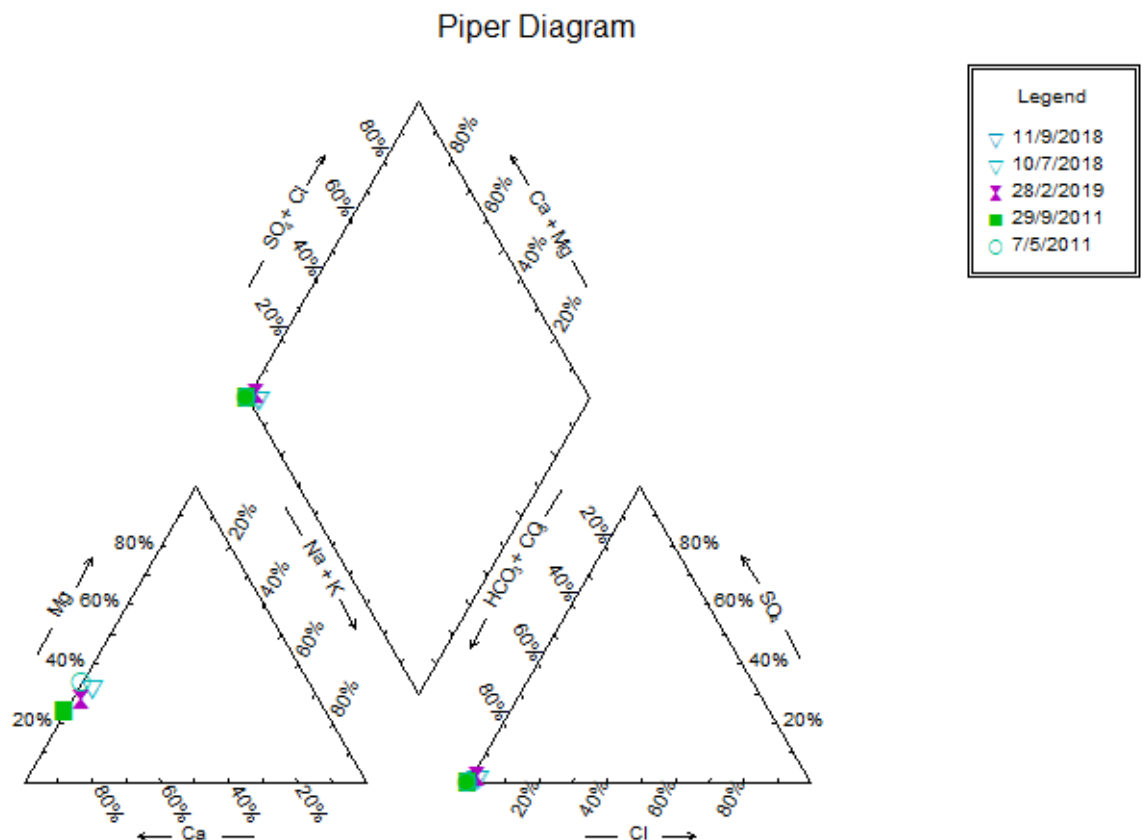


Fig. 7.5.3.5. The Piper chart. ©RockWare - AqQa

The chemical discussion is supported by a column graph (Fig. 7.5.3.6.) to visualize more clearly the data.

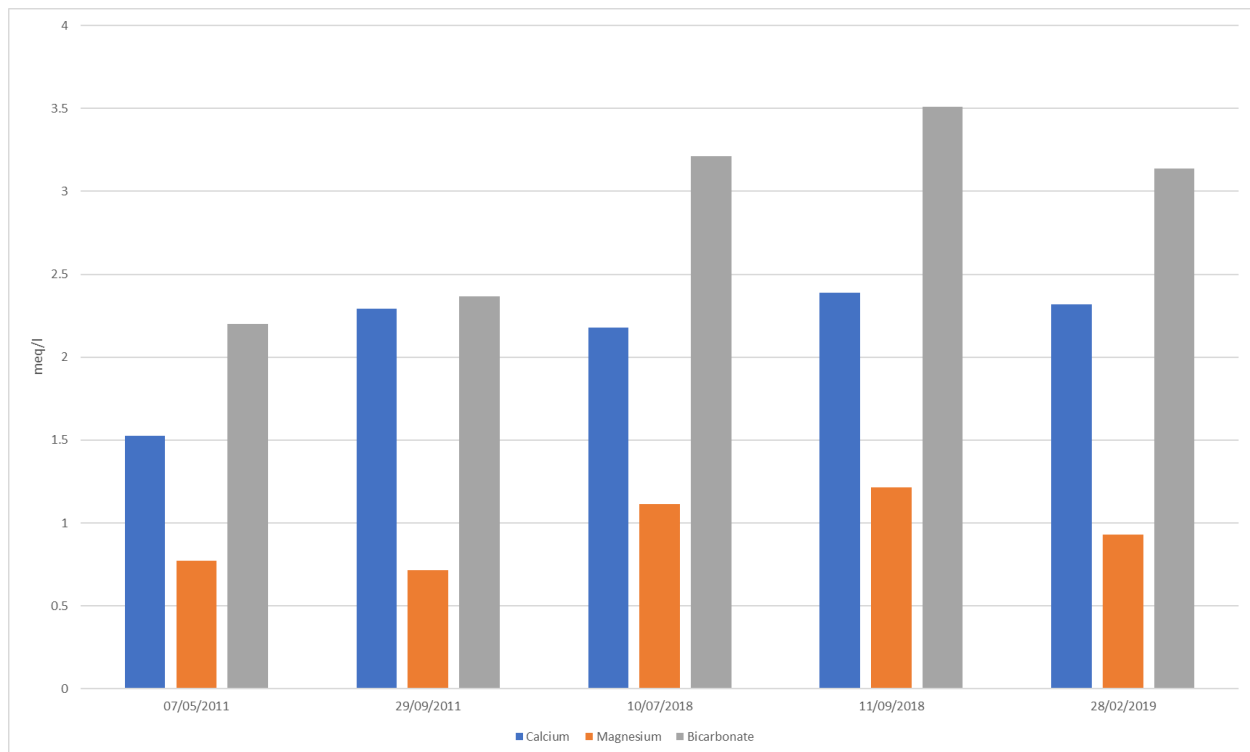


Fig. 7.5.3.6. Ca, Mg and  $\text{HCO}_3^-$  column graph. ©Microsoft Excel

The above chart shows the phenomenon already described in the conductivity paragraph, but in terms of ion concentrations. From May to September 2011 there is a sharp increase in Calcium (+0.76 meq/l) and a slighter one in Bicarbonate (+0.17 meq/l), while the Magnesium is almost stable (-0.06meq/l). The three post-earthquake samples display the same typical seasonal trend followed by the conductivity.

One of the first things that stands to the eye from the graph are the 2018 higher concentrations respect to the 2011. Going into detail and considering all the September values (both 2011 and 2018) we note that Bicarbonate (+1.15 meq/l), mainly, but also Magnesium (+0.50 meq/l) have experienced a greater increase respect to Calcium (+0.10 meq/l). The explanation probably lies, one more time, in the different solubility of the ions most abundant salts: Calcite solubility is 0.014 g/l, Magnesite 0.106 g/l, Na-bicarbonate 95.5 g/l and Ca-bicarbonate 166 g/l. These values help us to understand why Magnesium and specially Bicarbonate have raised more than Calcium.

## 7.6. Fonte dei Mietitori

### 7.6.1. Detailed features and geological setting

Elevation: 1309 m a.s.l. – Hydrographic basin: Tronto

Coordinates: 33T 360866 4741882 UTM / 13°17'53,103" E 42°49'0,701" N

Description: it is a fountain with tank included into an artifact used for rest (Fig. 7.6.1.1.). The intake was not identified but should be proximal, given the presence of other nearby emergences (Aringoli et al., 2017).



Fig. 7.6.1.1. Fonte dei Mietitori (February, 28<sup>th</sup> 2019)



Fig. 7.6.1.2. Detail of the fountain (July, 7<sup>th</sup> 2018)

Location: it is found at the base of the SE slope of Il Pizzo (Fig. 7.6.1.3.), ENE to Monte Pianello della Macchia in the bottom of the channel. You can arrive here following the Mietitori track (see Fonte delle Cacere description) for about 3.2 km.

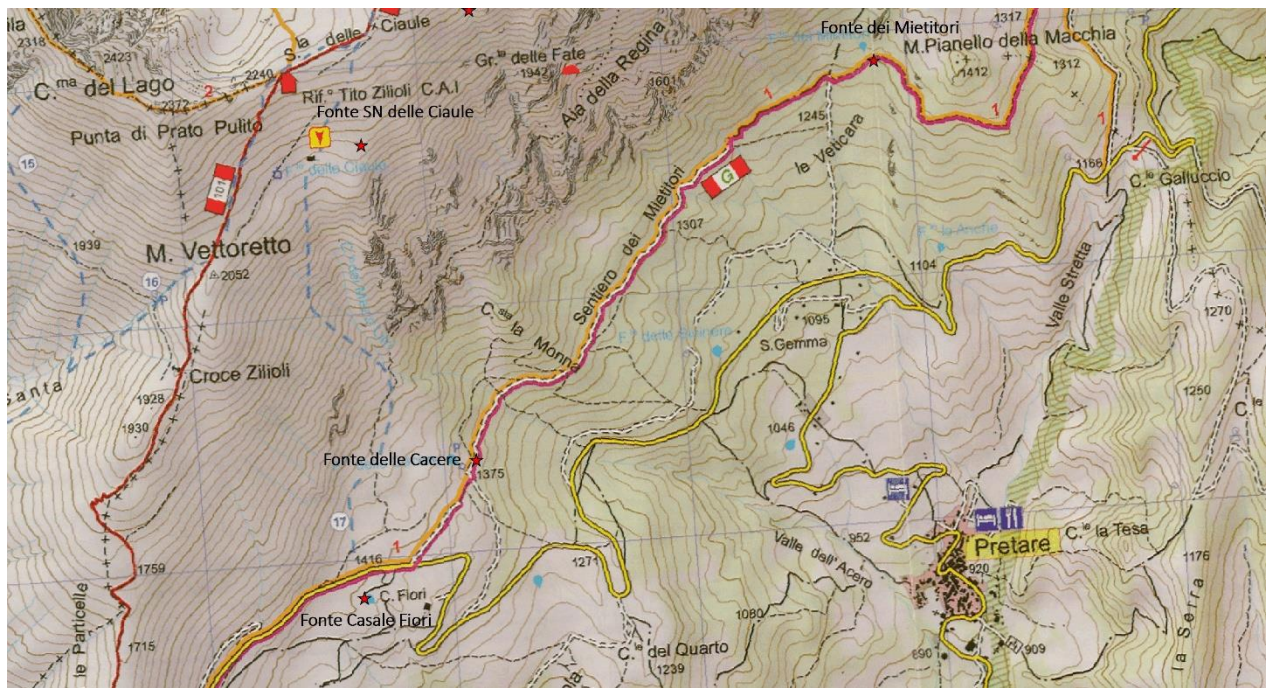


Fig. 7.6.1.3. Map of Pizzo southern slopes. CAI – Monti Sibillini – Carta dei Sentieri 1:25'000

**Geological setting.** The fountain is surrounded by the coverages overlying *Formazione della Laga* (LAG) (Fig. 7.6.1.4.) and the real emergence is thought to be close to the tank. The E sector, where Laga sandstones crop out, is characterized by a less pronounced morphology respect to the W carbonatic one. The Sibillini thrust and a splay-thrust (both NW dipping) separate the domains. The thrusts border a huge *Maiolica* (MAI) tectonic chip. *Corniola* beds, SE dipping, discordantly rest on the gently SE dipping *Calcare massiccio* beds by means of the already cited Jurassic unconformity. Given this framework, the spring may be sustained by the Basal aquifer that, because of the permeability threshold, at the tectonic contact among *Calcare massiccio* – *Calcari diasprigni* (CDU) – *Maiolica*, would feed the Maiolica tectonic-chip tilted aquifer. The latter, limited at the bottom by *Formazione della Laga* aquiclude and laterally by the aquitard/aquiclude formations of *Marne a Fucoidi* (FUC) and *Calcari diasprigni* – *Calcari a Posidonia* (POD), would emerge at the MAI – FUC contact. Then the flow would continue inside the quaternary deposits up to the spring area.

## Cross section Fonte dei Mietitori

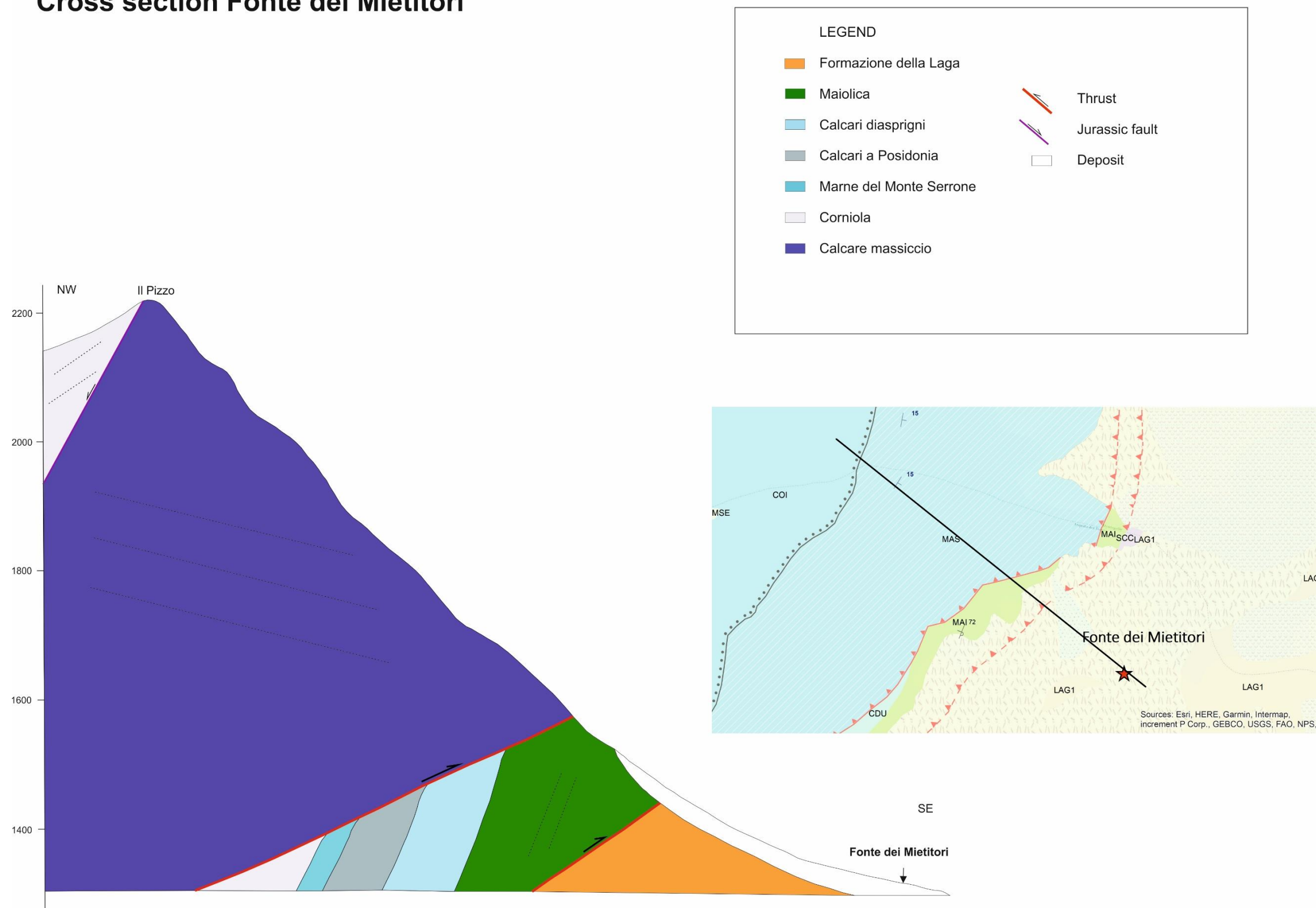


Fig. 7.6.1.4. Monte dei Mietitori geological cross section. ©CorelDraw 2018

### 7.6.2. Physical and chemical data

#### PRE-EARTHQUAKE STATE

##### Physical parameters

Data	Air Temperature	Water Temperature	Flow rate (l/min)
16/7/2011	18.4	7.8	2.3
29/9/2011	12	9	0.6

Tab. 7.6.2.1. Pre-earthquake physical data

##### Chemical analysis

Data	pH	Conductivity ( $\mu\text{S}/\text{cm}$ )	Ca mg/l	Ca meq/l	Mg mg/l	Mg meq/l	HCO <sub>3</sub> mg/l	HCO <sub>3</sub> meq/l	Hardness (Ca+Mg) °F
16/7/2011	7.3	347.5	51.2	2.56	1.7	0.14	323.3	5.30	13.48
29/9/2011	7.5						270.6	4.44	

Tab. 7.6.2.2. Pre-earthquake chemical data

#### POST-EARTHQUAKE STATE

##### Physical parameters

Data	Air Temperature	Water Temperature	Flow rate (l/min)
10/7/2018	--	9.4	3.13
11/9/2018	18.1	10.9	1.19
28/2/2018	14.9	8.2	3.63

Tab. 7.6.2.3. Post-earthquake physical data

##### Chemical analysis

Data	pH	Conductivity ( $\mu\text{S}/\text{cm}$ )	Ca mg/l	Ca meq/l	Mg mg/l	Mg meq/l	HCO <sub>3</sub> mg/l	HCO <sub>3</sub> meq/l	Hardness (Ca+Mg) °F
10/7/2018	7.99	547	78.91	3.94	21.76	1.79	309.05	5.07	28.67
11/9/2018	7.78	573	77.96	3.88	24.81	2.04	325.28	5.33	29.64
28/2/2018	7.43	540	89.39	4.46	17.54	1.44	321.80	5.27	29.55

Tab. 7.6.2.4. Post-earthquake chemical data

Here below the chemical analysis tables (from Fig. 7.6.2.1. to 7.6.2.3.) made by the Water Analysis Laboratory - UNICAM Chemical Division.

Spring	Fonte dei Mietitori			Data:	10/07/18	
pH at the emergence			7.99	Hydrogen ion activity at the spring		1.02E-08
spring temp			9.4			
lab temp		°C	21.5			
R.F. (180°C)	356	D.T.(G.F.)	31		Balance: cat	6.829424
K20 (µS/cm)	-	547 Alcal.Tot.	50.65	0.650	ani	6.729167
					1.47% =Δ=	0.100258
<u>Cationic Substances</u>	<b>mg/l</b>			<b>m.mol/l</b>	<b>m.equiv/l</b>	<b>m.eq/m.eq.tot</b>
Lithium	<b>0.01488</b>			0.002143351	0.002143351	0.000158
Sodium	<b>23.80950</b>			1.035645933	1.035645933	0.076383
Potassium	<b>1.86030</b>			0.047580439	0.047580439	0.003509
Calcium	<b>78.90750</b>			1.96875	3.9375	0.290406
Magnesium	<b>21.75975</b>			0.895278749	1.790557498	0.132061
Strontium	<b>0.65799</b>			0.007509587	0.015019174	0.001108
Aluminum	<b>0.00000</b>			0	0	0.000000
Contaminants or cationic unwanted:						
Barium	<b>0.05712</b>			0.000415908	0.000831816	0.000061
Selenium	<b>0.00000</b>			0	0	0.000000
Chromium	<b>0.00000</b>			0	0	0.000000
Nickel	<b>0.00429</b>			7.30966E-05	0.000146193	0.000011
<u>Anionic:</u>				<b>3.95739706</b>	<b>6.8294244</b>	
Fluoride	<b>0.13910</b>			0.007321823	0.007321823	0.000540
Chloride	<b>6.52950</b>			0.184173413	0.184173413	0.013584
Bromine	<b>0.00000</b>			0	0	0.000000
Bicarbonate	<b>309.04604</b>			5.065008301	5.065008301	0.373565
Carbonate	<b>1.38280</b>			0.023043623	0.046087247	0.003399
Sulfate	<b>68.27546</b>			0.710788082	1.421576164	0.104847
Contaminants or anionic unwanted:						
Nitrite	<b>0.00000</b>			0	0	0.000000
Nitrate	<b>0.31000</b>			0.004999677	0.004999677	0.000369
<u>Neutral:</u>				<b>5.99533492</b>	<b>6.72916663</b>	
Contaminants or neutral unwanted:						
Boron	<b>0.07277</b>					
FIXED RESIDUE	mg/L	355.751463		TOTAL HARDNESS	°F	31
				TOTAL CALCULATED ALCALINITY		50.65

Spring		Fonte dei Mietitori		Data:	11/09/18	
pH at the emergence			7.78	Attività ioni idrogeno alla sorgente		1.66E-08
spring temp			10.9			
lab temp		°C	21.8			
R.F. (180°C)	370	D.T.(G.F.)	33.5		Bilancio: cat	7.121340
K20 (µS/cm)	-	573 Alcal.Tot.	53.31	0.646	ani	7.025131
					1.35% =Δ=	0.096209
<u>Cationic</u>		mg/l		m.mol/l	mequiv/l	meq/meq.tot
<u>Substances</u>		-				
Lithium		0.03484		0.005019166	0.005019166	0.000355
Sodium		25.56673		1.112080615	1.112080615	0.078612
Potassium		1.88947		0.048326598	0.048326598	0.003416
Calcium		77.76587		1.940266134	3.880532269	0.274311
Magnesium		24.81150		1.020839333	2.041678667	0.144324
Strontium		1.43911		0.016424485	0.032848969	0.002322
Aluminum		0.00000		0	0	0.000000
Contaminants or cationic unwanted:						
Barium		0.05828		0.000424404	0.000848807	0.000060
Selenium		0.00000		0	0	0.000000
Chromium		0.00000		2.33351E-09	1.40011E-08	0.000000
Nickel		0.00016		2.64203E-06	5.28405E-06	0.000000
<u>Anionic:</u>				4.14338338	7.12134039	
Fluoride		0.13500		0.007106011	0.007106011	0.000502
Chloride		6.63870		0.187253547	0.187253547	0.013237
Bromine		0.00000		0	0	0.000000
Bicarbonate		325.27630		5.331008737	5.331008737	0.376844
Carbonate		0.89897		0.014980897	0.029961793	0.002118
Sulfate		70.53288		0.734289165	1.468578329	0.103812
Contaminants or anionic unwanted:						
Nitrite		0.00000		0	0	0.000000
Nitrate		0.07580		0.001222502	0.001222502	0.000086
<u>Neutral:</u>				6.27586086	7.02513092	
Contaminants or neutral unwanted:						
Boron		0.08422				
FIXED RESIDUE		mg/L	369.88312	TOTAL HARDNESS	°F	33.5
				TOTAL CALCULATED ALCALINITY		53.31

Spring		Fonte dei Mietitori		Data:	28/02/19	
pH at the emergence			7.43	Hydrogen ion activity at the spring		3.72E-08
Air temperature on the field			11.7			
spring temp		°C	8.2			
R.F. (180°C)	343			Balance: cat		6.603817
K20 (µS/cm)	-	540		ani		6.599874
A.T.(Carb)	263.7			0.06%	=Δ=	0.003944
<u>Cationic Substances</u>		<b>mg/l</b>		<b>m.mol/l</b>	<b>m.equiv/l</b>	<b>meq/meq.tot</b>
Lithium		<b>0.00950</b>		0.001368679	0.001368679	0.000104
Sodium		<b>15.27670</b>		0.664493258	0.664493258	0.050326
Potassium		<b>0.85450</b>		0.021855338	0.021855338	0.001655
Calcium		<b>89.38997</b>		2.230288548	4.460577096	0.337828
Magnesium		<b>17.53847</b>		0.721599054	1.443198107	0.109303
Strontium		<b>0.52406</b>		0.005980997	0.011961995	0.000906
Aluminum		<b>0.00061</b>		2.2461E-05	6.73832E-05	0.000005
Contaminants or cationic unwanted:						
Barium		<b>0.01400</b>		0.000101944	0.000203888	0.000015
Selenium		<b>0.00045</b>		5.69909E-06	5.69909E-06	0.000000
Chromium		<b>0.00034</b>		6.53896E-06	3.92338E-05	0.000003
Nickel		<b>0.00137</b>		2.3335E-05	4.66701E-05	0.000004
<u>Anionic:</u>				<b>3.64574585</b>	<b>6.60381735</b>	
Fluoride		<b>0.12390</b>		0.006521739	0.006521739	0.000494
Chloride		<b>5.42230</b>		0.152943333	0.152943333	0.011583
Bromine		<b>0.00000</b>		0	0	0.000000
Bicarbonate		<b>321.79838</b>		5.274008644	5.274008644	0.399434
Carbonate		<b>0.39788</b>		0.006630456	0.013260911	0.001004
Sulfate		<b>55.22460</b>		0.574920879	1.149841759	0.087085
Contaminants or anionic unwanted:						
Nitrite		<b>0.00330</b>		7.17313E-05	7.17313E-05	0.000005
Nitrate		<b>0.20000</b>		0.003225598	0.003225598	0.000244
<u>Neutral:</u>				<b>6.01832238</b>	<b>6.59987372</b>	
				total milliequivalents	meq/L	<b>13.2036911</b>
Contaminants or neutral unwanted:				total mMol	mM/L	<b>9.66406823</b>
Boron		<b>0.06760</b>				
FIXED RESIDUE		mg/L	343.290887	TOTAL HARDNESS	°F	31.8
				TOTAL CALCULATED ALCALINITY		52.74

Fig. from 7.6.2.1 to 7.6.2.3. Chemical analysis tables elaborated by UNICAM – Water Analysis Laboratory

### 7.6.3. Data analysis

The last of the analyzed springs, lying below the Monti Sibillini thrust, is probably characterized by the most complex hydrogeological setting where the Basal aquifer feeds the tectonic chip Maiolica complex. As the whole *group a*, it was analyzed in February 2019 (Fig. 7.6.3.1.).



Fig. 7.6.3.1. The fountain on February, 28<sup>th</sup> 2019

The underlying **flow rate** chart (Fig. 7.6.3.2.) displays a classic seasonal trend both in 2011 and 2018/2019 campaigns. For the comparison we have used July and September data. The variation gradient seems not have been subjected to earthquake effects: it is -0.02 (l/min)/day in 2011 and -0.03 (l/min)/day in 2018.

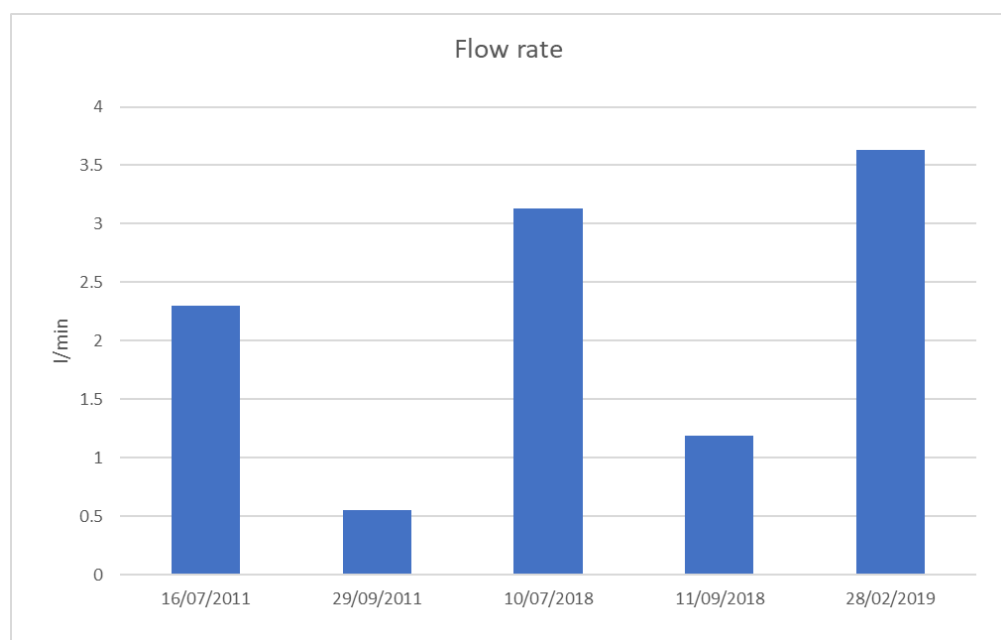


Fig. 7.6.3.2. Flow rate data. ©Microsoft Excel

A post-sequence flow gain is presumably present, and taking into account both the previous days and winter/spring precipitations (climatic station of Capodacqua), we can probably exclude that the 2018 flow rate gain is linked to the climate. Since September of the previous year to the sampling day:

- 951.6 mm in July 2011 and 1008.2 mm in September 2011;
- 916.6 mm in July 2018 and 1058.6 mm in September 2018.

The difference is exiguous, and therefore not sufficient to support a climatic factor. This probably confirms what has been already highlighted in Fonte Casale Fiori: an earthquake-related flow rate increase within the Basal aquifer in this S-E part of the S.M.

The peak value of February 2019 is a consequence, as for the previous springs, of the runoff linked to the rapid snowmelt.

Fonte dei Mietitori has the lowest **water temperature** variation (Fig. 7.6.3.3.), signal of a deep aquifer. The higher value is 10.9°C in September 2018 and the lower in July 2011 of 7.8°C, while the seasonal 2018/2019 difference is 2.7°C.

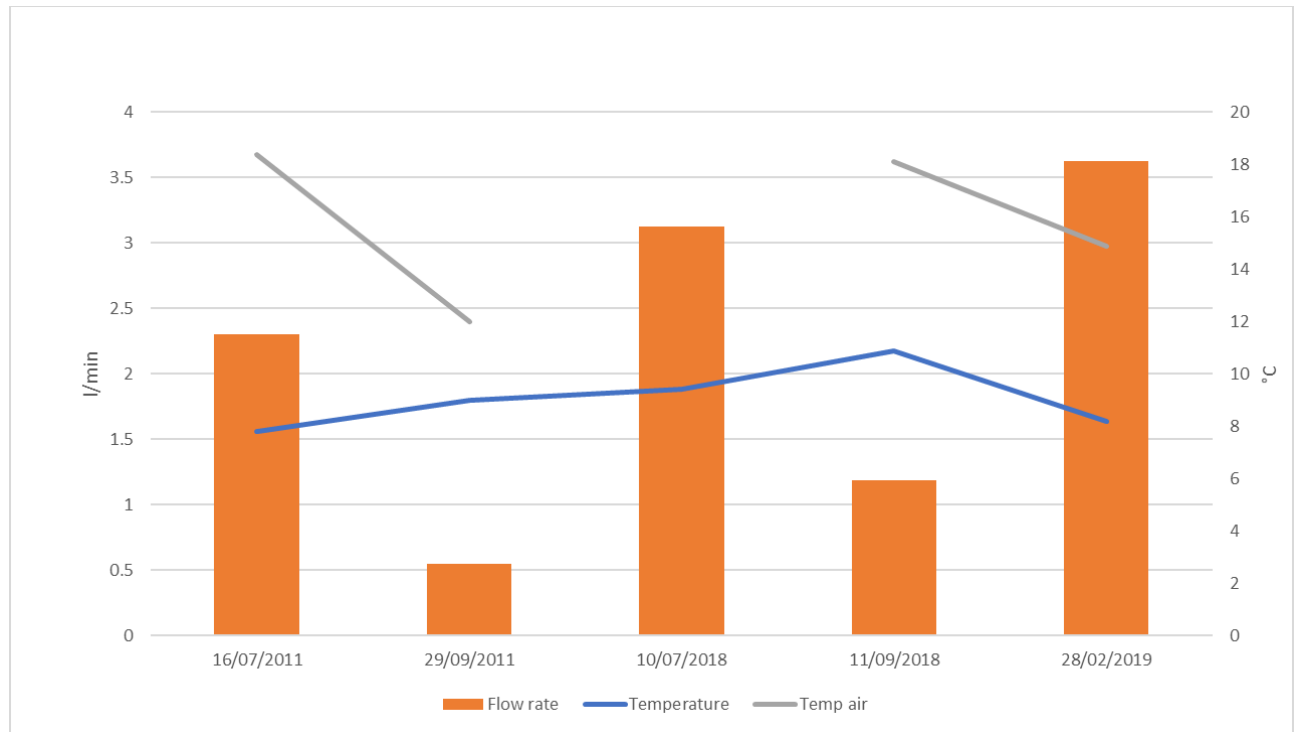


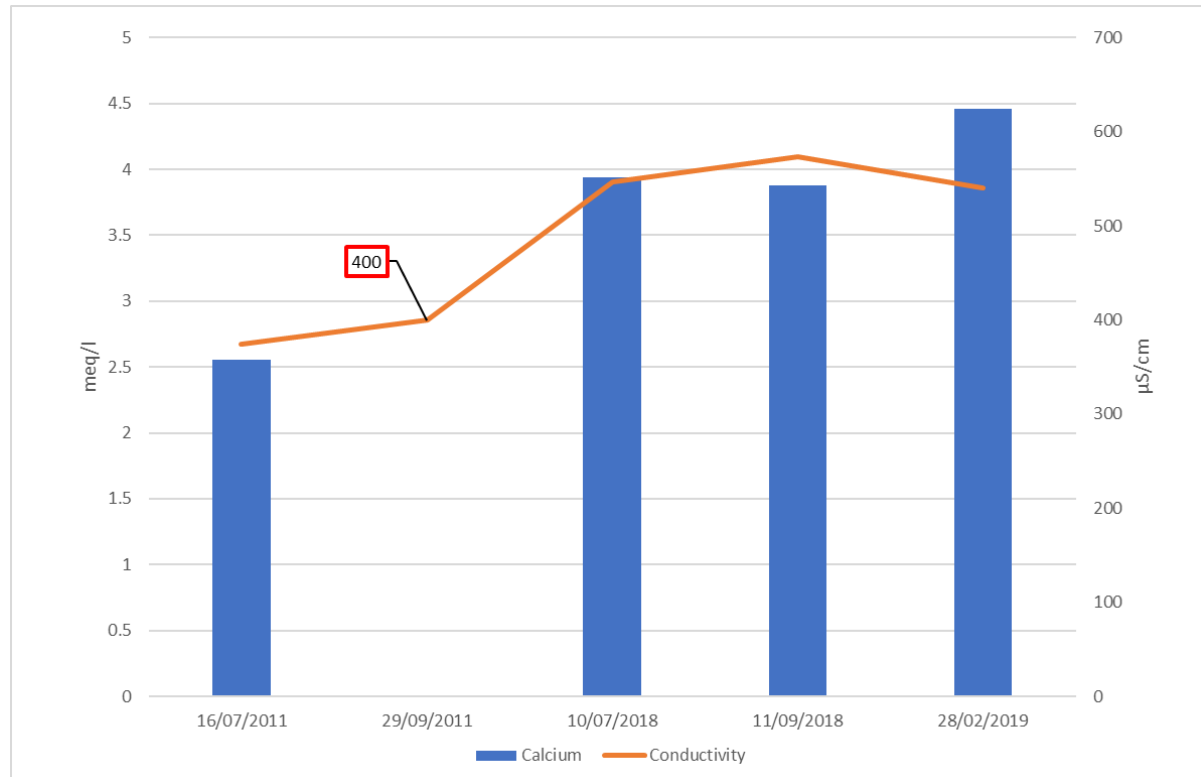
Fig. 7.6.3.3. Flow rate, water and air temperatures data. ©Microsoft Excel

Temperature increases from higher to lower flow rates, according to the normal behavior. The T gradient appears slightly more pronounced after the sequence, but we cannot understand the reason with the few available data. Comparing the air temperature with that of water, they behave irregularly and seem not to be related in anyway, supporting the deep circulation theory. The reduction from September 2018 to February 2019, as we have seen so far, is linked to the fast snowmelt.

Fonte dei Mietitori **conductivity** values are the highest (Fig. 7.6.3.4.), a further confirmation of the depth of water circulation. The conductivity has followed a predictable trend, as for Fonte delle Cacere and

Fonte Casale Fiori, during the post-earthquake campaign: increases from July to September and decreases up to February. The September 2011 value is missing for unknown reasons. We tried to estimate it through a regression-interpolation procedure with Fonte delle Cacere and Fonte dei Mietitori, ***however, considering the different geological settings, the outcome data has a low accuracy and the subsequent considerations could be affected by error.*** The procedure is the following:

- estimation of the conductivity gradient gain since May to September 2011 in both springs;
- average gain gradient calculation;
- as the linear regression starts from July and not from May, it needs a *correction factor* taking into account that the spring-to-summer conductivity gradient has to be higher than the summer-to-autumn one, because of the higher snowmelt impact of the salt concentrations. It has been calculated by the ratio between the July-September 2018 gradient and the May-September 2011 one. We obtain that the former is 16% lower than the latter.
- application of the correction factor to the average gain gradient; the outcome is (+0.35  $\mu\text{S}/\text{cm}$ )/day;
- regression procedure: since July, 16<sup>th</sup> 2011 to September, 29<sup>th</sup> 2011 75 days elapsed which have been multiplied for the gradient to obtain the conductivity increase. Then adding it to the July data we have obtained the September one (400  $\mu\text{S}/\text{cm}$ ), highlighted in red in the charts below.





- Fig. 7.6.3.4. Conductivity vs Calcium, Magnesium and Bicarbonate contents. The red value is the estimated missing data. ©Microsoft Excel

Also, Calcium and Magnesium values are absent for the same day, however, considering the variability of chemical parameters according to the geology, we have chosen not to estimate those data.

Comparing the pre/post-earthquake summer data, it is possible that the 2011 was characterized by a lower conductivity gradient with respect to the 2018.

Between the July values there is a difference of +172.5  $\mu\text{S}/\text{cm}$ . Remembering from the flow rate paragraph, that 2011 was only slightly less rainy than 2018, we can conclude that probably Fonte dei Mietitori has experienced the strongest seismic-related effects on conductivity, as also shown by Mg and Ca levels, greatly raised after the earthquake.

**Chemical composition.** Also, from the bottom-left triangle of Piper diagram (Fig. 7.6.3.5.) is well visible the great Magnesium increase after the seismic sequence, triggered by the ions shaking solubilization. The water facies is the same of the previous springs (bicarbonate-calcium and/or magnesium).

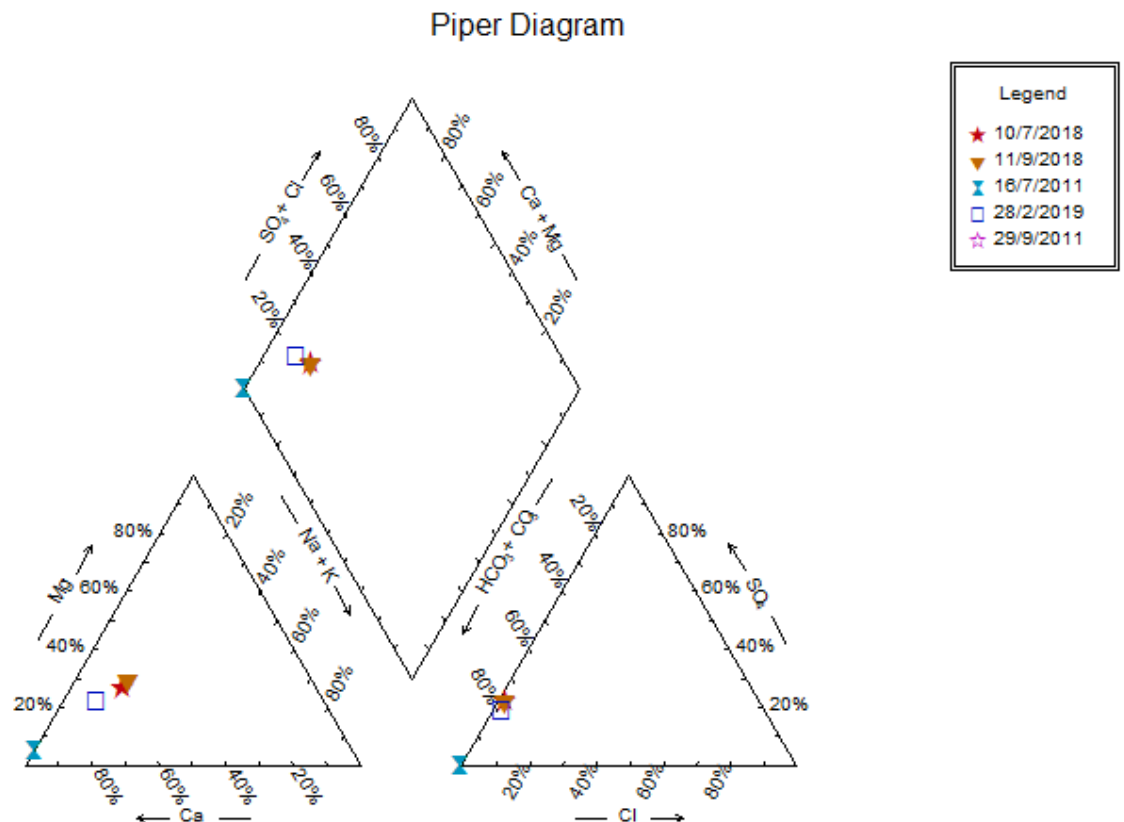


Fig. 7.6.3.5. The Piper chart. ©RockWare – AqQA

A column graph (Fig.7.6.3.6.) is the best way to evidence Calcium, Magnesium and Bicarbonate concentrations and their evolution in time.

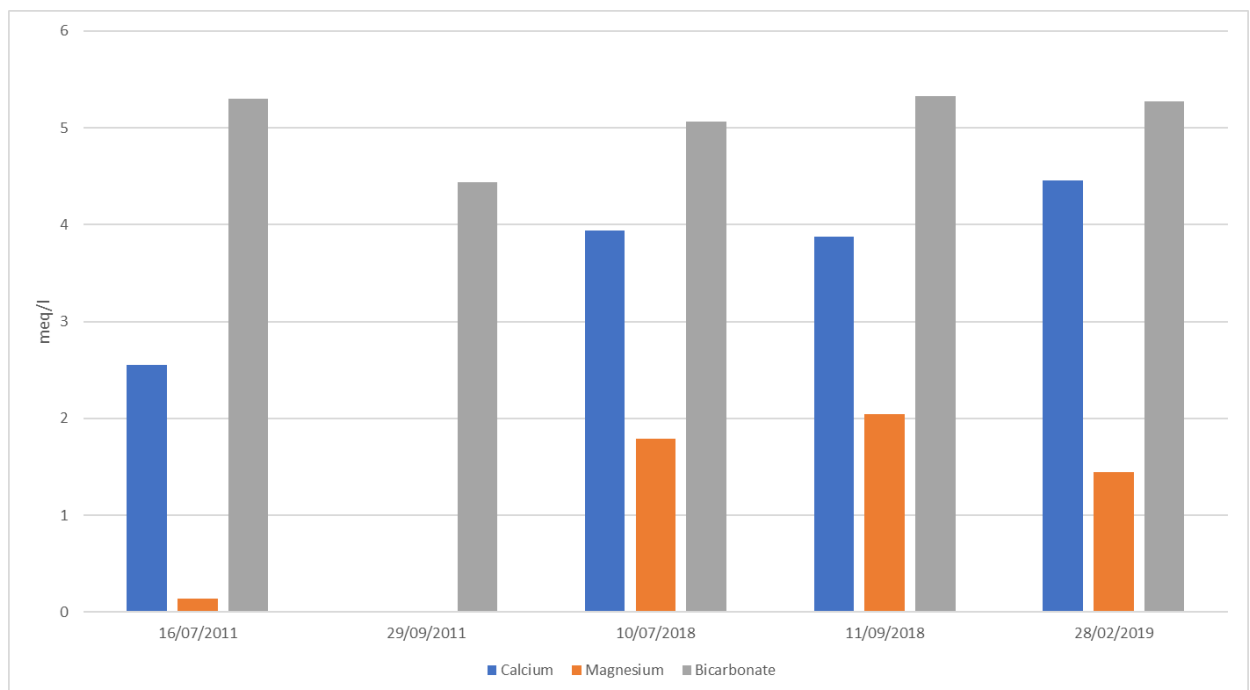


Fig. 7.6.3.6. Ca, Mg and HCO<sub>3</sub> column graph. ©Microsoft Excel

The above chart displays some interesting features not evidenced by the previous springs. The first is the Bicarbonate loss between July and September 2011, which may be caused by rainfalls in the days immediately before the sampling. However, at the Capodacqua station no precipitations have been recorded in the previous month and the Arquata del Tronto pluviometer (RM-2202) has recorded only 4.2 mm two days before. This is not enough to support the theory, that nevertheless could be anyway valid because of the higher climatic variability of the mountain areas. Another possibility, could be that the September 2011 value is affected by error.

Analyzing the three post-earthquake samples parameters we have noted that:

- from July to September: Ca is stable (-0.06 meq/l), Mg increases (+0.25 meq/l) and HCO<sub>3</sub> also rises (+0.27 meq/l). Considering also the other anions and cations the conductivity trend is consonant with their changes.
- The situation is more complex from September to February: Ca increases (+0.58 meq/l), Mg decreases (-0.60 meq/l) and HCO<sub>3</sub> is stable (-0.06 meq/l). Their ionic balance is -0.08 meq/l, therefore other ions could have contributed to decrease the conductivity; the major is the sulphate (-0.32 meq/l).

According to the hydrogeological model proposed before, it would be almost impossible to localize chemical changes within the Basal or in the tectonic chip Maiolica aquifers because both of them are characterized by the same prevalent lithology: micritic limestone. Anyhow, on the base of the foregoing springs (whose unique feeding complex was the Basal one) results, we can venture the hypothesis that

the main changes are confined in the Basal complex. Magnesium could confirm this: it has been subjected to the most elevated gain, probably because of the Magnesite higher solubility respect to Calcite. *Calcare massiccio* and *Corniola* in the Monte Vettore area are widespread dolomitized, becoming the main Mg-source, while in *Maiolica* the Dolomite is nearly absent. However, due to the Maiolica chip reduced dimensions, its contribution to the seismic-related effects could be present but anyway much limited.

## 7.7. Springs general observations

In the introduction of the Chapter 7 the springs have been separated into two groups: the 1<sup>st</sup> one (group a) characterized by deeper springs, located at a lower altitude on the SE slopes of Monte Vettore, respect to those of the 2<sup>nd</sup> group (group b), sited in the summit area of the massif. Even before this study a remarkable difference among the springs of the two groups, both in terms of water salinity and earthquake-induced variations, could be expected.

The analysis performed on the water samples have highlighted the following aspects:

- the overall conductivity of the group a (lower springs) is higher than that of the group b (higher springs), because of the deeper and longer underground water route, during which the water is enriched in salts present in the surrounding rock.  
After the seismic sequence the conductivity is raised in both groups, with a stronger signal for the deeper springs. For example, according to the suggested hydrogeological model, Fonte dei Mietitori is characterized by the deeper water circulation, confirmed by highest the pre/post-earthquake conductivity gain.
- the water temperature also, being linked to the depth of the route travelled and to the external air temperature (to a lesser extent), is characterized by a larger annual variation for the shallower emergences, even the available data do not clearly display this mainly because of the changes registered in the feeding system of Fonte SN delle Ciaule. The deeper springs, due to their longer response-time, that could exceed one year, present a lower annual temperature variation.
- take overall considerations about the seismic effects on the flow rate is doubtless inappropriate because each spring has its own different supply setting. In addition, the analyzed time periods are unavoidably interested by different precipitations (both in terms of nature and amount), making very difficult the estimation of the springs response-times. Given the geological similarity between Fonte delle Ciaule and Fonte SN delle Ciaule, a comparison would have been possible if the feeding system of the second spring had not been interrupted after the earthquake.

General considerations can be taken about the flow rate seasonal trend. In particular, on the base of the 2018/2019 data, the deeper springs display a decrease between summer and autumn, during which the minimum has been registered, and a steep increase between September and February.

- regarding the earthquake-induced consequences on the salinity, a general increase in Calcium, Magnesium and Bicarbonate levels have been observed (trying to exclude dilution and concentration phenomena related to the precipitations), probably due to the shaking-induced ions solubilization. As mentioned before, salinity and conductivity are strictly linked in a direct way, as reported in the previous chapters.

However, sometimes it happens that the conductivity is raised and not all of the analyzed ions behave as one would expect. This could be bounded to the not-considered cation and anions concentrations. Unfortunately, considering the scarcity of pre-earthquake chemical data it is almost impossible to go back to the other salt levels.

Hardness and conductivity display the same seasonal trend, with a peak corresponding to the minimum of flow rate (end of the summer/autumn beginning). The minimum has been registered in February 2018 (maximum of flow rate) for the lower springs and it is legitimate to expect almost the same trend for the group b.

In conclusion, the most relevant general observation is the possible salinity increase, proportional to the depth of the water circulation, after the 2016-2017 earthquake, probably due to the ionic solubilization mainly triggered by the friction inside the effective porosity. If the analysis had been performed closer to the earthquake (until few months after to the last important shocks), we might have expected that the salt content increase could be also due to the pressure gain inside the porosity that makes easier to solubilize the minerals. However, due to the uncertainty on this type of studies, this factor cannot be totally excluded.

The other analyzed parameters, such as pH, are too much related to the single emergences settings to be generalized to the whole area.

## **8. CONCLUSIONS**

The aim of the study was to evaluate the possible variations induced by the 2016-2017 seismic sequence on the hydrogeological setting of the S-E area of the Monti Sibillini National Park.

The analysis of the Basal aquifer was performed by a monitoring campaign in the uppermost part Aso river (close to the village of Foce), where it is directly fed by the aquifer, through a linear spring. The study led to conclude that the piezometric level has dropped of about 50/60 m, and then to the estimation of the lost water volumes in the considered months. In addition, we tried to rebuild the hydrogeological basin of the As45-As50 sector that, at the moment of the surveys, was the primary linear spring segment feeding the river.

The second part of the thesis focuses on 5 high-altitude springs, sited in the S-E slopes of Monte Vettore, characterized by different regimes compared to the Aso river linear spring. Here, by means of geological reconstructions, physical and chemical analysis we observed an increase in salinity that can be considered as a consequence of the increased ionic solubilization incremented by a shaking pressure-friction mechanism within the effective porosity of the aquifer. Other parameters, like water temperature and flow rate, being directly influenced by the single-spring hydrogeological settings, are not proper to take overall conclusions.

We tried to report all the sampled data and hopefully these will be used for further future studies.

## 9. BIBLIOGRAPHY

Aringoli D., Ferracuti P., Pierantoni P.P., Pistonesi D., Romagnoli A. (2017) – *Sorgenti e Fonti d'Alta Quota del Parco Nazionale dei Monti Sibillini*

Nanni T. & Petitta M. (2010) – *Studio del bacino idrogeologico carbonatico (Monti Sibillini) del Fiume Aso finalizzato alla caratterizzazione delle condizioni di alimentazione e di circolazione idrica, alla valutazione del bilancio idrogeologico e analisi della sorgente di Foce – prima (2010) e seconda fase (2012)*

Pierantoni P.P., Deiana G., Galdenzi S. (2013) – *Stratigraphic and structural features of the Sibillini Mountains (Umbria-Marche Apennines, Italy)*

Pierantoni P.P., Deiana G., Galdenzi S. (2013) – *Geological Map of the Sibillini Mountains (Umbria-Marche Apennines, Italy)*

Centamore E., Chiocchini M., Deiana G., Micarelli A., Pieruccini U. (1971) – *Contributo alla conoscenza del Giurassico dell'Appennino umbro-marchigiano*

Scisciani V., Tavarnelli E., Calamita E., Paltrinieri W. (2002) – *Pre-thrusting normal faults within syn-orogenetic basins of the Outer Central Apennines, Italy: implications for Apennine tectonics*

Materazzi M. & Pambianchi G. – *Individuazione delle Aree di Salvaguardia delle Captazioni Idriche – cap.4 – Il Territorio dell'AATO5 Marche Sud – Aspetti Geologici ed Idrogeologici Generali del Settore Montano*

Nanni T. (1991) – *L'Ambiente Fisico delle Marche – cap. Caratteri idrogeologici delle Marche*

Pierantoni P.P., Deiana G., Romano A., Paltrinieri W., Borracini F., Mazzoli S. (2005) – *Geometrie strutturali lungo la thrust zone del fronte montuoso umbro-marchigiano-sabino*

Boni C., Petita M. (2007) – *Studio idrogeologico per l'identificazione e la caratterizzazione degli acquiferi che alimentano le sorgenti dei corsi "acqua perenni dei monti Sibillini, esteso all'intera area del Parco Nazionale. Rapporto definitivo. Contratto di studio e ricerca Autorità di Bacino del Fiume Tevere – Parco Nazionale dei Monti Sibillini – Dipartimento di Scienze della Terra Università di Roma "La Sapienza".*

Gruppo di Lavoro INGV sul Terremoto in centro Italia. *Relazione sullo stato delle conoscenze sulla sequenza sismica in centro Italia 2016-2017 (aggiornamento al 2 febbraio 2017), doi: 10.5281/zenodo.267984*

Shuhan Zhong, Caijun Xu, Lei Yi & Yanyan Li (2018) - *Focal Mechanisms of the 2016 Central Italy Earthquake Sequence Inferred from High-Rate GPS and Broadband Seismic Waveforms*

Chiaraluce L., Di Stefano R., Tinti E. et alii. (2017) – *The 2016 Central Italy Seismic Sequence: A First Look at the Mainshocks, Aftershocks, and Source Models*

R. Civico, S. Pucci, L. Pizzimenti, P.M. De Martini, R. Nappi & the Open EMERGE Working Group (2018) – *Surface ruptures following the 30 October 2016 Mw 6.5 Norcia earthquake, central Italy, Journal Maps, 14:2, 151-160, DOI:10.1080/17445647.2018.1441756*

Serpelloni E., Anzidei M., Baldi P., Casula G., Galvani A. (2005) – *Crustal velocity and strain-rate fields in Italy and surrounding regions: New results from the analysis of permanent and non-permanent GPS networks*

Club Alpino Italiano - *Monti Sibillini – Carta dei Sentieri 1:25'000*

M. Civita (2005) – *Idrogeologia applicate e ambientale* – CEA Editore

## ACKNOWLEDGMENTS

I wish to express my gratitude to the Prof. Marco Materazzi and Prof. Pietro Paolo Pierantoni for giving me the opportunity to participate in this wonderful project and for the provided support during the whole thesis period.

A special thank to Prof. Rita Giovannetti, Prof. Laura Petetta and Prof. Stefano Ferraro (Chemistry Department of University of Camerino) for the assistance with the water chemical analysis.

I would thank my friends and workmates Leonardo, Alessio and Irene for the awesome days spent in mountain during the sampling periods, but also for the less exiting ones in the laboratories.

Finally, I want to show my gratitude to my parents, my friends and to all the other people having encouraged me through this unforgettable experience which was the university in Camerino.